Title
Many-body Ground State Preparation in Jaynes-Cummings Lattices

Author
Parajuli, Prabin

Publication Date
2022

Peer reviewed|Thesis/dissertation

UNIVERSITY OF CALIFORNIA, MERCED

Many-body Ground State Preparation in Jaynes-Cummings Lattices

A dissertation submitted in partial fulfillment of the requirements
for the degree of Doctor of Philosophy
in

Physics

by

Prabin Parajuli

Committee in charge:

Prof.Kevin Mitchell,Chair
Prof. Michael Scheibner
Prof. Lin Tian

2022

The dissertation of Prabin Parajuli, titled Many-body Ground State Preparation in Jaynes-Cummings Lattices, is approved, and it is acceptable in quality and form for publication.

(Prof. Lin Tian) Principal Advisor	Date
(Prof.Kevin Mitchell) Committee Chair	Date
(Prof. Michael Scheibner) Committee Member	Date

University of California, Merced

2022

Dedication

Dedicated to my Parents and Brother.

Acknowledgments

Life of a graduate student is filled with ups and downs but people surrounding them give them reasons to stay positive and smile. The guidance and support from advisor, unconditional love and support from family, relatives, and friends, and collaboration from peers always has great value in their life. All these people have a significant contribution in the successful dissertation. Acknowledgments section in the dissertation provides an opportunity to remember those individuals whose contribution is an integral part of the dissertation output.

I would like to begin an acknowledgments by acknowledging my advisor Prof. Lin Tian, without her guidance and support this dissertation is impossible. Here incessant faith in my abilities, help to troubleshoot obstacles, freedom to learn different skills, challenge to think deep in research questions has helped me to grow as a physicist and an independent researcher. She taught me how to formulate research questions and how to do research. These skills are precious to me. I would like to acknowledge Kang Cai, who taught me how to do research in theoretical physics. He also taught me numerical simulation skills patiently and motivate me to dig deep into research questions. I learned from him how to become calm and focus in research in difficult circumstances.

I was extremely lucky to be in a small department where I found helpful and talented people. I am grateful to hours of freewheeling discussions and trouble shooting with my lab mates Alessandro Monteros, Kevin Collins, Siddharth Pillai, Anuvetha Govindarajan, Mitch Mazzei, Ruixia Wang. I am grateful to my house mates Nabin Kumar Raut, Yogesh Bhusal and Samrajya Bikram Thapa with whom I spent significant amount of time laughing, chatting, exploring new places, cooking, and playing

ping pong. You guys are like my brothers. Nabin, Yogesh and I came to the USA in a same flight and we are staying together since then. Samrajya joined us after two years. Thank you guys, You helped me to grow as a person. I am also greatful to Jibanath Dahal, Gita Adhikari, Deepak Sapkota and Seema Adhikari who helped me to settle in Merced in initial days. I still remember accommodation you had provided to us in difficult time. Thank you Bishal Parajuli, Rijan Karki, Sneha Ghimire, Srijana Uprety, Nabin Pokharel, Uday Panta, Saurav Gautam, Binod Bhattarai, Pragya Dhungel, Mamata Pokharel, Renu Sitaula for being such awesome friends. I also like to thank Imtiaz Ali, and Palak Dugar for a fruitful discussion and help. Similarly, thank you, Prabin Baral, Uttam Pyakurel, Gyan Bahadur Khatri, Jayaram Paudel, Debendra Timilsina, Upendra Rijal, Dipesh Kumar Das for being best friends from B.Sc. and M.Sc. days. At last but not the least, I would like to thank Achyut Koirala for being an amazing friend from childhood and encourage me to pursue my career in physics.

Finally, I would like to thank my parents and brother for their love and support in all of my endeavors; without their support, I would not have been at this position. I am forever deeply indebted to you. I also like to thank my grand parents and relatives for their support, love and encouragement in every ups and downs in my life.

Gratefully,
Prabin

Prabin Parajuli

pparajuli@ucmerced.edu | (209)-421-1654 |
www.linkedin.com/in/pparajuli

EDUCATION

University of California, Merced, Department of Physics
Merced, CA

- Ph.D., Physics
  Expected May 2022

Thesis: "Many-body Ground State Preparation in Jaynes-Cummings Lattices"

University of California, Merced, Department of Physics
Merced, CA

- M.S., Physics
  May 2020

Tribhuvan University, Central Department of Physics
Kathmandu, Nepal

- M.Sc., Physics
  June 2016

Thesis: "A First Principle Study of Adsorption of Halogens on a Monolayer MoS_2"

RESEARCH EXPERIENCE

University of California, Merced
Merced, CA

Graduate researcher with Prof. Lin Tian
2016-present

- In the first project, collaborated with 1 graduate student to develop a new method to prepare quantum many-body ground state in quantum simulators/quantum computers

- In the second project, collaborated with 1 graduate student to explore possibility of using symmetric subspace to make state preparation task fast and efficient
- In the third project, used quantum optimal control technique to prepare quantum many-body ground state in optimal time. This work is the thesis of my Ph.D.
- Developed scientific code using MATLAB to perform numerical simulation such as: computing occupation number basis states in particle number conserved subspace of Hilbert space, evolving an initial state to the target state passing through quantum critical region using quantum adiabatic algorithm
- Developed code to perform optimization, analyzed energy gap, studied effect of gaussian noise in optimized parameters
- Research finding helped PI to land new NSF grant

Tribhuvan University
Kathmandu, Nepal
Graduate researcher
2015 - 2016

- Collaborated with 1 graduate student and Principal Investigator to study electronic and magnetic properties of Ni adsorbed 2D material MoS_2
- Used QUANTUM ESPRESSO software package to perform optimization and to calculate band structure, density of state and charge density
- Thesis "A first principle study of adsorption of halogens on a monolayer MoS_2" submitted to the Central Department of Physics, Tribhuvan University, Nepal

SKILLS

Numerical skills

- Matrix product representation of quantum many-body system
- Exact diagonalization method, DMRG calculation, Mean field calculation, DFT calculation, Quantum dynamics, Lindblad Master Equation
- Non-equilibrium quantum phase transition

- Shortcut to adiabaticity
- Quantum Optimal Control

Quantum algorithms & optimization

- Adiabatic quantum algorithms
- Variational quantum algorithms
- Quantum approximate optimization algorithms
- GRAPE optimization, Krotov optimization, CRAB optimization, GROUP/GOAT optimization, ML based optimization
- Classical optimization methods like genetic algorithm, differential programming

Coding/Programming skills

- MATLAB
- PYTHON
- Mathematica
- Basics of C and C++

TEACHING EXPERIENCE

University of California, Merced
Merced, CA
Teaching Assistant, Physics

Fall 2016, Spring 2017, Fall 2017, Spring 2018, Fall 2018, Spring 2019, Fall 2019, Spring 2020, Fall 2020, Spring 2021, Fall 2021

- Assisted in preparation and execution of weekly laboratory section
- Lead discussion sessions

PUBLICATIONS

- Cai, K., Parajuli, P., Long, G. *et al.* Robust preparation of many-body ground states in Jaynes–Cummings lattices. *npj Quantum Inf* **7,** 96 (2021). https://doi.org/10.1038/s41534-021-00433-y

Co-first author. We have developed a method for a robust preparation of quantum many-body ground state in Jaynes-cummings lattices using nonlinear adiabatic ramping.

- Parajuli, P. A first principle study of adsorption of halogens on a monolayer MoS_2. M. Sc. Thesis, Department of physics, Tribhuvan University, Nepal (2016).
- Parajuli, P., and Tian, L. Quantum optimal control on Jaynes-Cummings lattices. (To be submitted soon)
- Kai, C., Parajuli, P., and Tian, L. Shortcut to adiabaticity for the ground state preparation in Jaynes-Cummings lattices. (Co-first author, To be submitted soon)

CONFERENCES AND PRESENTATIONS

- Quantum optimal control on many-body ground state preparation in Jaynes-Cummings lattices, APS March Meeting (2022)
- Quantum optimal control on Jaynes-Cummings lattices, 23rd SQuInT Workshop. (Oct 14-Oct 15, 2021) (Poster presentation)
- Quantum optimal control on many-body states in Jaynes-Cummings lattice, APS March Meeting (2021)
- Many-body state preparation: Jaynes-Cummings lattices, 22nd SQuInT Workshop, Eugene, Oregon. (Feb 8-10, 2020) (Poster presentation)
- Quantum computing with superconducting qubit and quantum supremacy, Department of physics, Tribhuvan University, Nepal. (Dec 2019) (invited talk)
- Mesoscopic two-dimensional materials: from many-body interaction to device applications. Los Alamos National Laboratory, NM, USA. (Dec 2018)
- A first principle study of Adsorption of halogens on a monolayer MoS_2, Department of Physics, Tribhuvan University, Nepal. (June 2016)

PROFESSIONAL ASSOCIATIONS

- American Physical Society (APS)

- Nepal Physical Society (NPS)
- Association of Nepali Physicist in America (ANPA)

AWARDS

- Graduate student academic excellence, Tribhuvan University (May 2014)
- Physics Graduate Group Graduate Student Summer Fellowship (Summer 2020, Summer 2021)

ONLINE CERTIFICATES/BADGES

- Quantum Machine Learning (edx)
- IBM Quantum Challenges-2021 (IBM Qiskit)
- Open-Source Software Development Methods (Coursera)
- Deep learning specialization (Coursera)
- IBM Data Science Professional Certificate (edx)
- AWS Machine Learning Foundation Course (Udacity)

REFERENCES

- Lin Tian, Professor of Physics,
  Ph.D. Advisor
  Rm. ACS 247, UC Merced, Merced CA, 95343
  Tel: (209)386-3196, Email: ltian@ucmerced.edu

- Kevin Mitchell, Professor of Physics,
  Ph.D. Committee Chair
  Rm. ACS 249, UC Merced, Merced, CA, 95343
  Tel: (209)201-3471, Email: kmitchell@ucmerced.edu

- Michael Scheibner, Associate Professor of Physics,
  Ph.D. Committee Member
  Rm. SE1 378, UC Merced, Merced, CA, 95343
  Tel: (209)230-5509, Email: mscheibner@ucmerced.edu

Abstract

In recent years, due to unprecedented success in controlling and manipulating an individual quantum system, simulation of quantum systems using quantum simulators or quantum computer is becoming reality. In this thesis, the main goal is to study many-body correlations in quantum simulators and their impact in quantum information science. In particular, we focus on high fidelity many-body ground state preparation in Jaynes-cummings lattices in coupled cavity arrays. In the first work, we show that combining quantum engineering and nonlinear adiabatic ramping, high fidelity many-body ground state can be prepared in a targeted region either in the Mott insulating phase or in the Superfluid phase. In the second project, we use the shortcuts to adiabaticity (STA) method for the fast and efficient many-body state preparation. We compare the fidelity obtained by using the simple adiabatic method and the STA method to show the advantage of STA method over the adiabatic method. In the third project, we apply the quantum optimal control (QOC) technique with chopped random basis (CRAB) algorithm to prepare high fidelity many-body ground states in minimal time in the Jaynes-Cummings lattices. The methods we used are general and can be used for state preparation in other quantum simulators or quantum computers.

Contents

List of Tables

List of Figures

Chapter 1

Introduction

1.1 Background

Quantum mechanics has been established as the most successful theoretical framework to predict and explain different phenomena occurring in the microscopic world [1]. The unusual characteristics of sub-atomic particles in the microscopic world makes it harder to understand different physical phenomena associated with motion of these particles. Understanding these phenomena and emergent behavior from them has been a subject of interest for many years due to its relevance in areas ranging from nuclear physics to design and characterization of materials. Major parts of the last century had been invested to advance our understanding of quantum mechanics and develop theoretical frameworks to explain these phenomena. Quantum mechanics is based on a counter-intuitive prediction of the microscopic world based on the notion of superposition, interference and entanglement which are impossible to observe in normal settings. The reason behind this is that when many particles interact with each other via quantum mechanics, they becomes correlated in uncontrolled ways, which on average behave just as our intuition would predict. Exotic conditions like ultra-cold temperatures, ultra-cold vacuum environments are required to observe these phenomena in the microscopic world. Early experimental success in measurement of quantum interference, superposition and entanglement of multi-particles system validate that those phenomena do exist in nature [2, 3].

The difficulty in the interpretation of the behavior of quantum system makes an experimental observation of quantum effects extremely challenging. In such scenario, simulation of a quantum system before doing an experiment is extremely important to get insight into how to control the system, and predict and analyze the possible outcome. However, accurate simulation of a quantum mechanical system using classical resources is impossible once the number of particles exceeds 50. This is due to the way how quantum mechanical system interact with each other. For example, suppose there is a non-trivial quantum system with N qubits. For a single qubit, the state is described by a state vector $|\psi\rangle = c_0|0\rangle + c_1|1\rangle$, where c_0 and c_1 are complex number with $|c_0|^2 + |c_1|^2 = 1$. In the classical world, we can describe the state of N qubits in terms of state of N individual qubits. We assume qubits are separable and non-entangled. Thus, for N qubits systems, since 2 coefficients are required to describe the state of a single qubit, 2N complex number is sufficient to describe the state of the system.

The story is different when we follow the quantum mechanical description. In quantum world, the most generic way to describe the state of a system of N qubits is to express the state of the system as a superposition of all possible N-qubit states: $|\psi\rangle = c_{000...}|000...\rangle + c_{100...}|100...\rangle + ... + c_{111...}|111...\rangle$. The state is described by coefficients $c_{000...}$,$c_{100...}$,...,$c_{111...}$, and there are 2^N coefficients. This shows that an enormous amount of computational resources is required to store possible quantum states even for a small sized system. For a reference, even the most powerful supercomputer can store all possible quantum states for the system with only 50-60 particles [4].

From the above discussion, a fundamental question would arise: How can we computationally study different behaviors of a quantum system? In 1982, Richard Feynman came up with an answer to this question. His answer was to simulate complex quantum mechanical systems using another programmable quantum system build in a laboratory i.e. quantum computer/simulator. This notion gives rise to a birth of the field quantum simulation. His insight was that quantum computer would have the capacity to store exponentially large amounts of information without using an exponentially large amount of physical resources [5]. However, Feynman was not specific about how those quantum computers would functioned. Later, Seth Lloyd showed

that an ensemble of well-defined qubits which can be initialized, measured, and on which a universal set of quantum gates can be performed can act as a quantum computer. However, to perform quantum simulations, a simpler device which can mimic the evolution of other quantum system is sufficient [6].

From experimental prospective, past few decades have been very fruitful as people are being able to isolate individual quantum objects from the environment and control them. The latest advancement in the coherent manipulation of quantum systems ranging from ion trapped with electric field, electrons in metal cooled down to become superconductor to realization of optical lattices has opened up a door to perform quantum simulation in quantum devices. One of the challenges in building such quantum devices is to be able to isolate individual particles and control interaction between them. As the size of the device increases, due to the many-body correlations between particles, it becomes harder to isolate and control individual particles. Devices with few number of qubits in different platforms have already been demonstrated as a controllable quantum system. Nevertheless, these devices are in their early stages, and still key scientific and engineering challenges have to be overcome in order to scale up such devices to gain quantum advantage in computation. Some early glimpse include realization of topological order states in a Sycamore processor [7], probing topological states in spin liquid [8].

The computational challenges in simulating quantum systems motivates us to think about a question: can we program quantum devices such that the evolution of such devices results in the solution of some specific computational problem? This question leads to the introduction of quantum information and quantum computing.

In recent years, people have been using quantum information theoretic insight to answer various questions associated to quantum many-body systems. Answers to these questions help to understand emergent phenomena in different areas of physics ranging from condensed matter physics to quantum gravity. As classical simulation of quantum systems is limited to few particles, quantum devices working under principle like superposition, entanglement and interference would be a new tool to observe quantum mechanical phenomena based on a theory of quantum information.

1.2 Overview of thesis

This thesis is primarily composed of three projects in the context of quantum state preparation. The main objective of this thesis is to study the effects of many-body correlations in quantum simulators and their impact in quantum information science. We start chapter 2 by introducing quantum simulation. We discuss the concept of analog quantum simulation, digital quantum simulation and hybrid quantum simulation. We briefly mention different quantum simulation platforms.

In chapter 3, we discuss new algorithm to prepare many-body ground states in JC lattice using nonlinear adiabatic ramping. We start the chapter by briefly introducing a recent progress and limitations in many-body state preparation. It is followed by the results section. In the result section, we focus on how to prepare with high fidelity many-body ground states in different phases of the system far from the critical region by combining quantum engineering and adiabatic ramping. Specifically, we discuss methods of improving fidelity of state preparation based on initial state selection, optimization of ramping trajectory and ramping indices. The results section is followed by the discussion section. In the discussion section, we compare simulation parameters with experimentally accessible parameter range.

In chapter 4, we discuss a new approach for the high fidelity state preparation, called shortcuts to adiabaticity(STA) method. STA is an alternative approach to the adiabatic method which gives the same output as the adiabatic process gives but in much shorter evolution time [9]. We follow the method discussed in [10–12], [13], and develop the many-body ground state preparation protocol in the JC lattices. The chapter begins with a brief introduction of the STA method. After the introduction, we discuss Berry formulation of the transitionless tracking method. The main challenging part is to derive the counterdiabatic (CD) Hamiltonian which requires knowledge of the instantaneous energy spectrum. We consider a cavity coupled array of JC model and derive an analytical and numerical form of the CD Hamiltonian. In CD Hamiltonian, there involves product of operators operating on different lattice sites which give rise to non local term in the Hamiltonian. The non-local term can not be implemented in experiments. We use parity symmetry to convert the

non-local Hamiltonian to the local Hamiltonian. We also compare the fidelity of the state preparation between the adiabatic protocol and the shortcuts to adiabaticity protocol.

In chapter 5, we focus on quantum optimal control (QOC) method for the many-body ground state preparation in the JC lattice. Optimal control theory is extensively used in robotics, machine learning, and control engineering. Recently, its quantum analogue, QOC theory has also been used to optimize the single qubit gates, two qubit gates, quantum many-body dynamics. This chapter begins with a brief introduction of QOC theory. The introduction is followed by the definition of controllability in quantum system. The next section is the formulation of QOC problems. We discuss four types of optimization problems . After that, we discuss a few most popular QOC algorithms i.e. Gradient Ascent Pulse Engineering (GRAPE) algorithm, Krotov algorithm and Chopped basis algorithms. We give references for machine learning inspired QOC algorithms. In section 5, we discuss the application of chopped random basis (CRAB) algorithm to prepare many-body ground states in the JC lattices. We present our results, analysis and conclusion in this section. The chapter ends with a brief summary of the chapter.

In chapter 6, we conclude this thesis and give the outlook for future.

Chapter 2

Quantum simulation

2.1 Overview of the chapter

In this chapter, we present a basic idea of quantum simulation. We discuss different steps in quantum simulation. The idea of quantum simulation was proposed by Richard Feynman in 1982 [5]. Later, in 1996 Seth Lloyd showed that quantum simulation can be performed by implementing a complicated many-qubit unitary transformation U through the application of a sequence of single and two qubit gates [6]. I. M. Gerogescu publised a review of the main theoretical and experimental aspects of quantum simulation *et al.* [4]. We briefly discuss three types of quantum simulation: analog quantum simulation, digital quantum simulation, and hybrid quantum simulation. After the discussion about quantum simulation, we briefly introduce a few popular quantum simulation platforms. We briefly discuss superconducting circuits, trapped ion systems, photonic systems, Rydberg atoms system, coupled cavity-qubit arrays. Names of other promising platforms are mentioned under the 'other platforms' subsection with relevant references. The chapter ends with a brief summary of the chapter.

2.2 What is quantum simulation

Quantum simulation is a process of mimicking a complex quantum system using a controllable quantum systems [16]. For the controllable quantum system to be a quantum simulator, we should be able to (i) engineer different Hamiltonians exactly, (ii) control the dynamics and (iii) make sufficiently precise measurements in such devices [17]. The simulator would be useful only when it can solve 'hard' problems i.e. problems which can not be solved either analytically or numerically with a classical computer due to the large amount of resources required to store the state of the system and the exponentially large amount of resources required to study the dynamics of the system. Quantum simulators functioned based on quantum mechanical principles. Hence, the dynamics of a quantum system can be studied using such simulators. The dynamics of the quantum system, in the absence of interaction with the environment, is governed by the unitary evolution of the system. Based on how we implement the unitary evolution in quantum simulators, quantum simulation can be divided into:

- Analog quantum simulation
- Digital quantum simulation
- Hybrid quantum simulation

2.2.1 Analog quantum simulation

In analog quantum simulation, the Hamiltonian of a complex quantum system H_{sys} is directly mapped onto the Hamiltonian of a simulator H_{sim} using different kinds of mappings f :

$$H_{sim} \Leftrightarrow f H_{sys} f^{-1} \tag{2.1}$$

This kind of simulation is possible only if the mapping between the system Hamiltonian and the simulator Hamiltonian exists [18]. Though finding the mapping seems simpler at first sight, this would not be the case always. In most of the cases clever mapping techniques need to be figure out which might involve addition of ancillary

systems or external fields to mediate interactions. The advantages of analog simulation are that they are much easier to a build and the results could be useful even with errors up to certain tolerance [19]. Examples of successful implementation of the analog quantum simulation can be found in this reference [20].

2.2.2 Digital quantum simulation

In digital quantum simulation, the complicated unitary transformation is implemented using a sequence of single- and two-qubit gates. Some example of single qubit gates are X, Y and Z rotation gates, and an example of two qubit gate is a CNOT gate.The different set of quantum gates and their operations is explained in detail by Michael A. Nielsen and Isaac Chuang [21]. In most of the cases, due to the non-commuting nature of the Hamiltonian corresponding to local interactions, the decomposition of unitary operation into a sets of local gates is not straightforward and we need to implement some kind of approximations. An important step is to breakup the evolution time into a large number of small time steps and decompose each small time step into local gates. Different approximations have been used to decompose the small time steps into local gates. An example is trotterization [6, 16, 21]

$$U = (e^{-i\hbar H \Delta t})^{t/\Delta t} \tag{2.2}$$

$$U(\Delta t) = e^{-i\hbar \sum_j H_j \Delta t} = \Pi_j e^{-i\hbar H_j \Delta t} + \mathcal{O}((\Delta t)^2) \tag{2.3}$$

when $\Delta t \to 0$, unitary operator $U(\Delta t)$ can be written as

$$U(\Delta t) \approx \Pi_j e^{-i\hbar H_j \Delta t} \tag{2.4}$$

This implies that a large number of quantum gates is required in order to get high accuracy. The in-depth review of how to improve the accuracy of digital quantum simulation can be found in these references [22, 23].

2.2.3 Hybrid quantum simulation

In recent years, different hybrid methods have been developed to study the ground state properties of quantum systems. An example is variational quantum eigensolver. In such a method the quantum processsor is assigned only to perform a computationally expensive task and the classical processor is used to perform all other tasks. These methods are based on the variational principle. Different optimization methods, both gradient based and gradient free methods, have been developed to perform the optimization. People believe quantum advantage can be achieved using hybrid method in the Noisy Intermediate State Quantum (NISQ) era. The review of different hybrid methods and their platform based implementation can be found in these references [20, 22, 24].

2.3 Physical Implementation

In recent years, with an unprecedented success in controlling and manipulating dynamics of individual quantum system, different architectures have been emerging as quantum simulating platforms [16, 20]. Each of them has their own advantages and disadvantages. We will mention some of the leading platforms in this thesis.

2.3.1 Superconducting circuits

Superconducting circuits are the leading candidate in the quantum information processing field. In such systems quantum information is encoded either in the superconducting electrons on a small island, in the direction of a current loop or the oscillatory states of the circuit. The control and manipulation of a quantum system i.e. qubit, is performed by applying voltages and currents. The superconducting circuit can also be coupled to electromagnetic cavities [16]. Advantages of superconducting qubits are that they have long coherence. Similarly, they are fast and high fidelity one-qubit and two-qubit gates can be implemented within coherence time. A thorough review of superconducting qubits can be found in these references [25, 26].

2.3.2 Trapped ion systems

In this type of simulators, ions trapped in a radio frequency (RF) trap serve as qubits and quantum entanglement is achieved by using the shared motional mode of the ions. Different types of RF traps like Paul traps have been developed to control and manipulate the motion of ions. Using trapped ions single qubit and two quibt gates have also been performed [16, 27, 28]. Due to long coherence time and great promise of scalability, this platform has been a leading candidate for large-scale quantum computing. An extensive review of trapped ion quantum computation can be found in this reference [29].

2.3.3 Photonic systems

In photonic simulators, qubits are encoded in two photon occupation modes of some degree of freedom of the optical field. Examples of such modes are orthogonal polarizations, frequency modes, temporal modes, transversal spatial and other [16, 30]. This method of encoding is also called dual-rail encoding. Different sets of single qubit and two qubit gates have been realized in photonic simulators. The advantages of photonic simulators are that several degrees of freedom of the same photon can be used simultaneously, quantum states can be maintained without vacuum or cooling systems, and the large bandwidth of the photon provides high-speed operation. Reviews of photonic simulators can be found in these references [31, 32].

2.3.4 Rydberg atoms

In Rydberg atoms, valance electrons are placed in a higher excited states. Hence they have large electric dipole moments which facilitates a strong interaction between the atom and the external electromagnetic field. This strong interaction due to dipole-dipole interaction can be controlled and manipulated by external fields like electric field, magnetic field, laser field and microwave field [16, 33, 34]. Thus, Rydberg atoms based quantum many-body simulators have been emerging as an ideal candidate to perform quantum information processing tasks. The Rydberg atom based qubits have properties like long coherence time, are easy to scale up, they posses tunable

connectivity, and they can mapped onto photons. These properties are essential to perform deterministic quantum simulation and quantum communication. The recent progress in this field can be found in these references [35–37].

2.3.5 Coupled cavity arrays

Coupled qubit-cavity arrays has been emerging as a promising platform to study hybrids of many-body states of light and matter in a controlled way. The intriguing scenario emerging from these systems is based on the interaction of light-matter within the cavity and photon hopping across the cavity [14, 16]. Coherent light-matter interaction generates polaritonic excitations with physical properties that are similar to those of bosonic particles. The finite life time of polaritonic excitation in coupled cavity-qubit arrays make this an ideal system to study non-equilibrium dynamics resulting from the interplay between losses and external driving. Thus, this artificial many-body system has gained a lot of interests in recent years for exploring it as quantum simulators [38]. In this thesis, we consider coupled cavity-qubit arrays to study many-body correlations in quantum simulators and their impact in quantum information science.

2.3.6 Other platforms

Besides the above mentioned platforms, there are other promising platforms to perform quantum simulation. These include, Cold atom systems, nitrogen vacancy (NV) centers, arrays of quantum dots, polar molecules, nuclear magnetic resonance based systems, optomechanical systems. [4, 39–48].

2.4 Summary

In this chapter, we introduced quantum simulation. We discussed three types of quantum simulation - analog quantum simulation, digitial quantum simulation and hybrid quantum simulation. After that, we discussed different quantum simulating

platforms and their advantages. In the next chapter, we study robust high fidelity many-body ground state preparation in coupled cavity-qubit arrays.

Chapter 3

Optimal nonlinear ramping

This chapter was published in npj Quantum Information (Cai, K., Parajuli, P. et al. 2021)(https://doi.org/10.1038/s41534-021-00433-y).

3.1 Introduction

The Jaynes-Cummings (JC) model is a prototype for studying light-matter interaction, where a quantum two-level system is coupled to a cavity mode [15]. This model has been utilized to study cavity or circuit quantum electrodynamics (QED) in a wide range of systems, from individual particles on the atomic scale to collective modes in mesoscopic devices [49–51]. More recently, advances in device fabrication and quantum technology enabled the exploration of many-body physics in arrays of JC models, i.e., JC lattices, which can be realized with optical cavities coupled to defects in semiconductors [52–56] and superconducting circuit QED systems [57–62]. The light-matter coupling in a JC model induces intrinsic nonlinearity in the energy spectrum, which can be mapped to an onsite repulsive interaction between polariton excitations. The competition between this onsite interaction and polariton hopping between neighboring sites gives rise to rich many-body physics for strongly-correlated polaritons in JC lattices, such as quantum or dissipative phase transitions and photon blockade effects [63–65]. Moreover, when the counter-rotating terms in the qubit-cavity interaction cannot be neglected, the system becomes a quantum Rabi lattice,

where distinctively different many-body phase transitions have been studied [66, 67]. One effect of particular interest is the quantum phase transitions between the Mott-insulating (MI) and superfluid (SF) phases for polaritons in JC lattices at integer fillings, featured by the occurrence of off-diagonal long-range order in the correlation functions. It was shown that such phase transitions can be observed in coupled cavity arrays [52–54] and multi-connected JC lattices [60–62].

The prerequisite to observe the MI-SF phase transitions is to pump polariton excitations into a JC lattice and prepare them into appropriate ground states. However, preparing many-body ground states is a challenging task in engineered systems such as quantum simulators [5, 6, 68] and adiabatic quantum computers [69, 70]. A number of approaches have been studied to tackle this problem, including adiabatic quantum evolution [71–73], quantum shortcut method by applying counter-diabatic interactions [74, 75], quantum phase estimation via quantum Fourier transformation [76, 77], variational quantum eigensolver [78, 79], full quantum eigensolver [80], and engineered dissipative environment for the preparation and stabilization of entangled states [81–84]. Despite these efforts, it is still hard to generate desired many-body states with high fidelity in the noisy intermediate-scale quantum (NISQ) era [85], in particular, for systems working with excitations such as the JC lattices. The barriers to generating desired many-body states efficiently and accurately include the lack of a priori knowledge of the energy spectrum, the difficulty in engineering complicated counter-diabatic interactions, the rapid decrease of the energy gap and quick increase of the dimension of the Hilbert space with the size of the quantum simulators, and the finite decoherence times in NISQ devices. Furthermore, many-body states in strongly-correlated systems can be highly entangled, unknown, and hence, often impossible to be generated with pre-programed quantum logic gates.

Here we study the robust generation of many-body ground states in finite-sized JC lattices at unit filling using optimized nonlinear ramping. In previous works [86–88], it was shown that nonlinear ramping can reduce diabatic transitions to excited states or the production of domain walls when a many-body system in the thermodynamic limit evolves across a quantum critical point due to the scaling of the phase transition. We apply nonlinear ramping to a finite-sized system, where the energy gap between

the ground and the excited states remains finite. By exploiting a Landau-Zener type of estimation [95, 96] and the spectral feature along a selected ramping trajectory, we derive the optimal ramping index for the trajectory, which can significantly improve the fidelity of the prepared state. Our estimation agrees well with the result from our numerical simulation of the ramping process. Moreover, we show that by selecting an appropriate trajectory for a given set of target parameters in combination with the optimal ramping index, the fidelity can remain close to unity in almost the entire parameter space. The ramping trajectory can be adjusted by varying the initial parameters or the ratios between the ramping indices for different parameters. The initial states of this nonlinear ramping process can be prepared with high accuracy by applying engineered pulse sequences [89] when tuning the system parameters to either the deep MI regime with no hopping between adjacent unit cells or the deep SF regime with diminishing light-matter coupling.

JC lattices have been implemented with superconducting quantum devices in recent experiments [65,90,91], and the ramping process studied here is within reach of current technology [92–94]. Using practical parameters from the experiments, we show that high fidelity can be achieved for the prepared states on a time scale much shorter than the observed decoherence times of these devices. Meanwhile, the approach of optimized nonlinear ramping for finite-sized systems is general and can be applied to many other models. The study of state generation in finite-sized systems with this approach can provide insights to the problem of preparing complex quantum states in quantum computers. Our result can hence shed light on the high-fidelity preparation of many-body states in engineered quantum systems such as quantum simulators, and advance the implementation of quantum simulation with NISQ devices.

3.2 Results

3.2.1 Model and quantum phase transition

Consider the JC lattice depicted in Fig 3.1a. Here each unit cell contains a qubit coupled to a cavity mode with coupling strength g, and adjacent unit cells are connected via photon hopping with hopping rate J. The total Hamiltonian of this model is $H_{\rm t} = H_0 + H_{\rm int}$ ($\hbar = 1$), where

$$H_0 = \omega_{\rm c} \sum_j a_j^\dagger a_j + \omega_z \sum_j \frac{\sigma_{jz}+1}{2} + g \sum_j \left(a_j^\dagger \sigma_{j-} + \sigma_{j+} a_j \right) \tag{3.1}$$

is the Hamiltonian of uncoupled JC models with $\omega_{\rm c}$ the frequency of cavity modes, ω_z the level splitting of the qubits, a_j ($a_j^\dagger$) the annihilation (creation) operator of the j-th cavity mode, and $\sigma_{j\pm}$, σ_{jz} the Pauli operators of the j-th qubit, and

$$H_{\rm int} = -J \sum_j \left(a_j^\dagger a_{j+1} + a_{j+1}^\dagger a_j \right) \tag{3.2}$$

is the photon hopping between neighboring unit cells. Let $\{|n,s\rangle\}$ be the basis set of an individual JC model with the cavity in the Fock state of photon number n and the qubit in the state $s = \uparrow, \downarrow$. The eigenstates of the JC model include the ground state $|g_0\rangle = |0,\downarrow\rangle$ with no excitation and the polariton doublets $|n,\pm\rangle$ with n excitations:

$$|n,+\rangle = \cos(\theta/2)\,|n,\downarrow\rangle + \sin(\theta/2)\,|n-1,\uparrow\rangle, \tag{3.3}$$

$$|n,-\rangle = \sin(\theta/2)\,|n,\downarrow\rangle - \cos(\theta/2)\,|n-1,\uparrow\rangle, \tag{3.4}$$

where $\theta = 2\arcsin\sqrt{[1-\Delta/\chi(n)]/2}$, $\chi(n) = \sqrt{\Delta^2 + 4ng^2}$, and $\Delta = \omega_{\rm c} - \omega_z$ is the detuning between the cavity mode and the qubit. The corresponding eigenenergies are $E_{g_0} = 0$ and $E_{n,\pm} = (n-1/2)\,\Delta \pm \chi(n)/2$. When the coupling g is nonzero, the energy spacings between these eigenstates are unequal with $(E_{n+1,-} - E_{n,-}) > (E_{n,-} - E_{n-1,-})$. Specifically, $E_{2,-} > 2E_{1,-}$ for $n = 1$, which indicates that the energy to add two polaritons to the JC model is more than twice the energy to add a single polariton. The extra energy to add a second polariton can be viewed as an effective

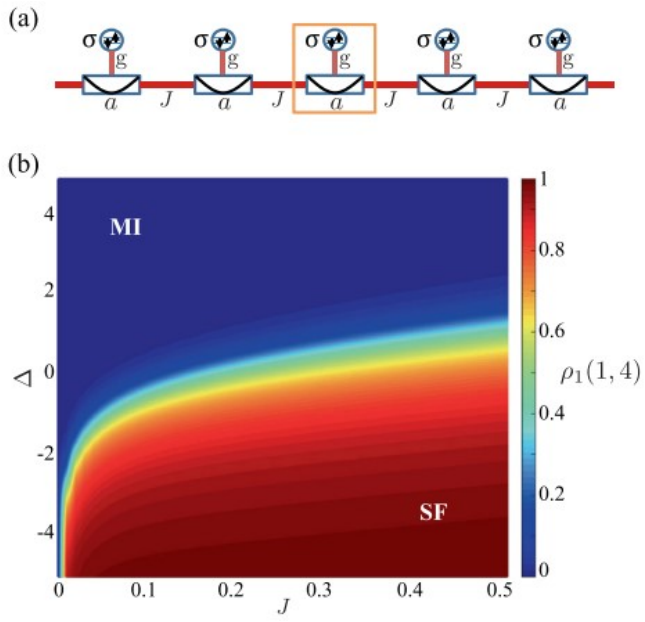

Figure 3.1: **Quantum phase transition in a JC lattice.** **a** Schematic of a 1D JC lattice. Circles (rectangles) represent qubits (cavity modes) with light-matter coupling g and hopping rate J. **b** Single-particle density matrix $\rho_1(1,4)$ vs hopping rate J and detuning Δ for a finite-sized lattice at unit filling with $N = L = 6$. Here we let g be the energy unit with $g \equiv 1$.

onsite interaction or nonlinearity for the polaritons, which is at the root of many interesting phenomena in JC models or JC lattices, such as the photon blockade effect [52–54] and electron-phonon-like effects [97].

In the limit of $J = 0$, the JC lattice is composed of isolated JC models. The ground state at unit filling, where the number of polaritons N is equal to the number of lattice sites L, is

$$|G\rangle_{J=0} = \prod_j |1,-\rangle_j \tag{3.5}$$

with one polariton excitation occupying the state $|1,-\rangle$ per site, which is in the deep MI regime. States with more than one excitation at the same site are energetically unfavorable due to the effective onsite interaction. In the opposite limit of $g = 0$ at finite hopping rate J, the cavity modes are decoupled from the qubits. The hopping Hamiltonian (3.2), now the dominant term, can be transformed to the momentum

space under the periodic boundary condition with $H_{\rm int} = -2J\sum_k \cos(k)\, a_k^\dagger a_k$, where a_k ($a_k^\dagger$) is the annihilation (creation) operator of a collective cavity mode at the quasi-momentum $k = \pi m/N$ with integer $m \in [-(N-1), N]$ and $a_k = \sum_j a_j e^{i k\cdot j}/\sqrt{N}$. At $\Delta < 0$ with the cavity frequency below the qubit energy splitting, the ground state at unit filling is

$$|G\rangle_{g=0} = \frac{1}{\sqrt{N!}}\left(a_{k=0}^\dagger\right)^N \prod_j |0,\downarrow\rangle_j \tag{3.6}$$

with all polaritons occupying the $k = 0$ mode, which is a nonlocal state in the deep SF regime.

With the mean-field approximation [52–54] and numerical methods [55, 56, 60–62], it was shown that quantum phase transitions between the MI and SF phases due to the competition between the onsite interaction and the photon hopping can occur in the intermediate regimes of the parameter space in JC lattices. For a finite-sized lattice with $N = L = 6$, we numerically calculate the many-body ground states using the exact diagonalization method. In this finite-sized system, the energy separation between the ground and the excited states decreases as the parameters approach the intermediate regimes, but maintains a finite energy gap. The spatial correlation in the many-body ground state $|G\rangle$ can be characterized by the normalized single-particle density matrix defined as [98, 99]

$$\rho_1(i,j) = \langle G|a_i^\dagger a_j|G\rangle / \langle G|a_i^\dagger a_i|G\rangle, \tag{3.7}$$

which reveals the off-diagonal long-range order of the state. The single-particle density matrix decreases algebraically with the spatial separation $|i-j|$ in the SF phase and decreases exponentially in the MI phase [60–62]. For a finite $|i-j|$, $\rho_1(i,j)$ of the SF phase is much larger than that of the MI phase. In Fig. 3.1b, we plot our numerical result of $\rho_1(1,4)$ as functions of the hopping rate J and the detuning Δ, with the coupling g as the energy unit ($g \equiv 1$). It can be seen that $\rho_1(1,4)$ increases with J at arbitrary detuning. In the deep MI regime with $J = 0$, $\rho_1(1,4) = 0$ with the polaritons localized in the lattice. In the deep SF regime, $\rho_1(1,4)$ can approach unity. This result clearly indicates the occurrence of the MI-SF phase transition in

the thermodynamic limit.

3.2.2 State initialization

We present methods to pump $N = L$ polaritons to the JC lattice in the limiting cases of $J = 0$ and $g = 0$, respectively, by applying engineered pulses. The polaritons are pumped into the many-body ground states at the corresponding parameters. These states will be used as the initial state of the nonlinear ramping approach.

In the deep MI limit of $J = 0$ and finite g, the ground state is given by Eq. (3.5) with each unit cell in the polariton state $|1, -\rangle$. Because the unit cells are decoupled, we can perform a Rabi rotation between the states $|g_0\rangle$ and $|1, -\rangle$ on each JC model, as illustrated in Fig. 3.2a. The driving Hamiltonian can have the form $H_{\mathrm{d1}}(t) = \sum_j [\varepsilon e^{i\omega_L t}\sigma_{j-} + h.c.]$ with driving amplitude ε and driving frequency $\omega_L = E_{1,-} - E_{g_0}$. The corresponding Rabi frequency can be derived as $\Omega_{\mathrm{d1}} = |\varepsilon \cos(\theta/2)|$ following Eq. (3.4). The duration of the Rabi flip from the initial state $|g_0\rangle$ to the final state $|1, -\rangle$ is $\tau_{\mathrm{d1}} = \pi/2\Omega_{\mathrm{d1}}$. To prevent the driving pulse from inducing unwanted transitions to higher states such as $|1, +\rangle$, it requires that $|\varepsilon| \ll g$.

In the deep SF limit of $g = 0$ and finite J, the ground state is given by Eq. (3.6) with all polaritons occupying the collective (nonlocal) mode $a_{k=0}$. To generate this state, we introduce an auxiliary qubit with Pauli operators $\sigma_{0\pm}$, σ_{0z}. This qubit has the Hamiltonian

$$H_{\mathrm{d2}}(t) = \frac{\omega_0}{2}\sigma_{0z} + \varepsilon(t)\, e^{i\omega_L t}\sigma_{0-} + g_{\mathrm{d}}(t) \sum_j a_j^\dagger \sigma_{0-} + h.c., \tag{3.8}$$

which includes the qubit energy splitting ω_0, a driving on the qubit with amplitude $\varepsilon(t)$ and frequency ω_L, and a tunable coupling between the qubit and the cavity modes with coupling strength $g_{\mathrm{d}}(t)$. By choosing ω_L, ω_0 to be both in resonance with the mode $a_{k=0}$, we have $H_{\mathrm{d2,r}}(t) = \varepsilon(t)\,\sigma_{0-} + \sqrt{N} g_{\mathrm{d}}(t)\, a_{k=0}^\dagger \sigma_{0-} + h.c.$ in the rotating frame. The first term of $H_{\mathrm{d2,r}}$ generates a Rabi rotation on the auxiliary qubit, and the second term is the coupling between the auxiliary qubit and the mode $a_{k=0}$. Both terms can be turned on and off within nanoseconds, as has been demonstrated in

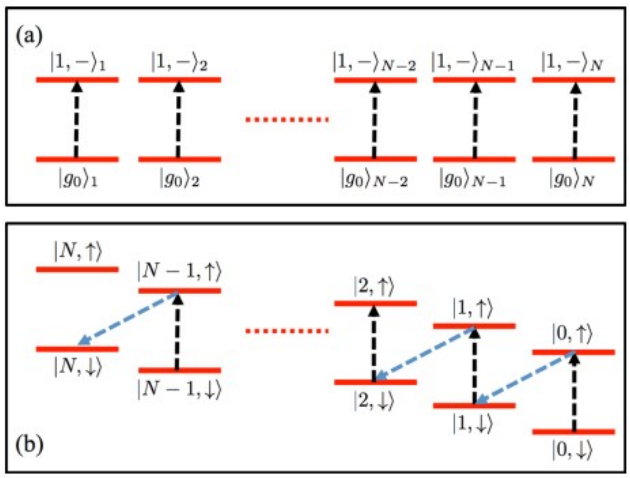

Figure 3.2: **Pulse sequence for state initialization. a** Pulses for MI initial state at $J = 0$ and finite g. The vertical arrows are Rabi flips between the states $|g_0\rangle$ and $|1,-\rangle$ in each JC model. **b** Pulses for SF initial state at $g = 0$ and finite J. The vertical (slanted) arrows are the operations C_l (Q_l) with $l \in [1, N]$ on the coupled system of the auxiliary qubit and mode $a_{k=0}$.

recent experiments on superconducting transmon qubits [90,91]. As the qubits in the JC lattice are decoupled from the cavities, the state of mode $a_{k=0}$ is only affected by its coupling to the auxiliary qubit. Let the initial state of the coupled system of mode $a_{k=0}$ and the auxiliary qubit be $|0,\downarrow\rangle$. To generate the state Eq. (3.6), we utilize the approach in [89] to design a pulse sequence, which can be implemented by switching on $\varepsilon(t)$ and $g_{\rm d}(t)$ alternately. The unitary operator for this pulse sequence is

$$U = Q_N C_N Q_{N-1} C_{N-1} \cdots Q_2 C_2 Q_1 C_1, \tag{3.9}$$

where the unitary operator C_l ($l \in [1, N]$) incurs a Rabi flip on the auxiliary qubit by applying a driving pulse with amplitude ε for a duration of $\tau_{\rm cl} = \pi/2|\varepsilon|$, and the unitary operator Q_l enables the exchange of excitations between the auxiliary qubit and the mode $a_{k=0}$ by turning on the coupling $g_{\rm d}$ for a duration of $\tau_{\rm ql} = \pi/2\sqrt{Nl}|g_{\rm d}|$. Following this pulse sequence, the state evolves as $|0,\downarrow\rangle \to |0,\uparrow\rangle \to |1,\downarrow\rangle \cdots \to |N,\downarrow\rangle$, as shown in Fig. 3.2b. The total duration of this pulse sequence is $\tau_{\rm d2} = \sum_l (\tau_{\rm cl} + \tau_{\rm ql})$. Assuming that the magnitudes of ε and $g_{\rm d}$ are the fixed for all l's, we find $\tau_{\rm d2} =$

$N\pi/2|\varepsilon| + \sum_l \pi/2\sqrt{Nl}|g_{\rm d}|$, which increases with the total number of polaritons as $\tau_{\rm d2} = {\rm O}(N)$. Meanwhile, it requires that $|\varepsilon|, \sqrt{N}|g_{\rm d}| \ll \omega_{\rm L}$ to achieve high fidelity for the generated state. Note that the other collective modes $a_{k\neq 0}$ of the cavities are not coupled to the auxiliary qubit due to the symmetry of the Hamiltonian $H_{\rm d2}$. The excitation of these modes will not occur during this pulse sequence.

3.2.3 Optimized nonlinear ramping

Many-body ground states in the intermediate regimes of the parameter space cannot be calculated analytically, and we cannot design quantum logic operations to generate such states, in contrast to the ground states in the deep MI or SF regimes. We employ optimized nonlinear ramping to reach such states via adiabatic evolution. In this approach, a parameter p has the time dependence:

$$p(t) = p(0)\left[1 - (t/T)^{r_p}\right] + p(T)\,(t/T)^{r_p}\,, \tag{3.10}$$

where $p = g, J, \Delta$ is a tunable parameter of the JC lattice, $p(0)$ is the initial value of the parameter at time $t = 0$, $p(T)$ is the target value at the final time T, and r_p is the ramping index of parameter p. For $r_p = 1$, it is the linear ramping studied in [69,70]; and $r_p \neq 1$ corresponds to nonlinear ramping [86–88]. It can be shown that for any parameter p at an arbitrary time t,

$$\left(\frac{p(t) - p(0)}{p(T) - p(0)}\right)^{1/r_p} \equiv \left(\frac{J(t) - J(0)}{J(T) - J(0)}\right)^{1/r_J}. \tag{3.11}$$

Hence when the initial and target parameters are given, the ramping trajectory in the parameter space is only determined by the ratios of the ramping indices r_g/r_J and r_Δ/r_J and is independent of the specific value of an individual ramping index (see Supplementary Notes). On the other hand, the value of an individual ramping index can strongly affect the sweeping rate of the Hamiltonian along a given trajectory. The sweeping rate of the Hamiltonian at parameters $\{p\}$ can be written as $\langle dH/dt\rangle = \sum_p \langle \partial H/\partial p\rangle p'(p)$, where $p'(p)$ is the time derivative $p' = dp(t)/dt$ at $p = p(t)$, with $\langle . \rangle$ denoting the operator average at the ground state of parameters $\{p\}$. Using (3.10),

we obtain:

$$p'(p) = \frac{r_p \left[p - p(0)\right]^{(r_p-1)/r_p}}{T \left[p(T) - p(0)\right]^{-1/r_p}}. \tag{3.12}$$

By varying the ramping index r_p, $p'(p)$, and hence $\langle dH/dt \rangle$, can be tuned in a large range. We also find that $p'(p) = J'(J)(r_p/r_J)[p - p(0)]/[J - J(0)]$, which reveals that $p'(p)/J'(J)$ at a given position only depends on the trajectory, i.e., it only depends on the ratios r_g/r_J and r_Δ/r_J that define the trajectory.

Let $|\psi(T)\rangle$ be the wave function of the final state of the evolution at time T. The fidelity of the final state can be defined as $F = |\langle\psi(T)|G_T\rangle|^2$ with $|G_T\rangle$ the many-body ground state at the target parameters $\{p(T)\} = \{g(T), J(T), \Delta(T)\}$. During a continuous evolution, the probability of diabatic transitions can be approximated by the Landau-Zener formula $\sim \mathrm{e}^{-\pi E_{\rm gp}^2/2H'_{\rm gp}}$ [95, 96], where the energy gap $E_{\rm gp}$ is defined as the minimal energy separation between the ground and the excited states along the evolution trajectory, and $H'_{\rm gp} = \langle dH/dt \rangle_{\rm gp}$ denotes the sweeping rate of the Hamiltonian at the position of the energy gap. To reach the desired state with high fidelity, the adiabatic criterion, commonly expressed as $H'_{\rm gp} \ll E_{\rm gp}^2$, needs to be satisfied so that diabatic transitions are negligible. For a given trajectory, we can optimize the ramping indices r_p to minimize $H'_{\rm gp}$ so as to suppress diabatic transitions in the most vulnerable region of the evolution and improve the fidelity of the final state. With the relation between different $p'(p)$'s, we find that $H'_{\rm gp} = c_p p'(p_{\rm gp})$ for any parameter p, with $p_{\rm gp}$ the value of the parameter p at the position of the energy gap. Here c_p only depends on the ratios r_g/r_J and r_Δ/r_J, not the individual ramping indices; whereas $p'(p_{\rm gp})$ depends on the ramping index r_p as shown in Eq.(3.12). At the optimal ramping index $r_p^{(\min)}$, $\partial H'_{\rm gp}/\partial r_p = 0$. This leads to

$$r_p^{(\min)} = \log\left[\frac{p(T) - p(0)}{p_{\rm gp} - p(0)}\right], \tag{3.13}$$

which only depends on the position of the energy gap for a given trajectory.

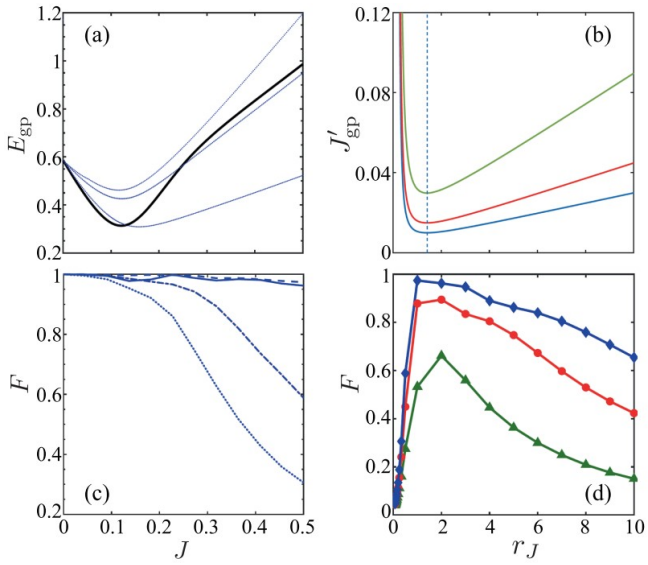

Figure 3.3: **Ramping from MI to SF phase.** **a** Energy spectrum of the lowest excited states vs hopping rate J. Solid (dotted) curve is for the symmetric (asymmetric) state with the ground-state energy set to zero. **b** Time derivative $J'_{\rm gp}$ vs ramping index r_J at $J(T) = 0.5$ and $T = 5\pi/g, 10\pi/g, 15\pi/g$ from top to bottom. **c** Fidelity F vs $J(T) = J$ for $r_J = 2$ (solid), 1 (dashed), 1/2 (dot-dashed), and 1/3 (dotted) at $T = 15\pi/g$. **d** Fidelity F vs r_J at $J(T) = 0.5$ and $T = 5\pi/g, 10\pi/g, 15\pi/g$ from bottom to top. In all plots, $g(t) \equiv 1$, $J(0) = 0$, and $\Delta(t) \equiv 0$.

3.2.4 Numerical simulation

Below we conduct numerical simulation to calculate the fidelity of the final states via nonlinear ramping with selected trajectories and compare the numerical result with the above estimation. In the simulation, we employ an algorithm developed in our previous work [60], which only involves basis states with the total excitation number $N = L$. This algorithm greatly speeds up the calculation of the eigenstates and dynamics of JC lattices. We first consider a trajectory following Eq.(3.10) with $g(t) \equiv 1$, $J(0) = 0$, $J(T) = 0.5$, and $\Delta(t) \equiv 0$, where the photon hopping rate is continuously increased from zero to a finite value. The initial state is the deep MI phase in Eq.(3.5). Using the exact diagonalization method, we can calculate the eigenstates and eigenenergies of the JC lattice along this trajectory. The energy spectrum of several lowest excited states is plotted as a function of the hopping rate

J in Fig. 3.3a. The solid curve corresponds to the energy of the lowest state that is symmetric with regard to all lattice sites, and the dotted curves are for asymmetric states. As both the initial state and the Hamiltonian $H(t)$ are symmetric with regard to lattice sites, the wave function $|\psi(t)\rangle$ at any time t during the evolution must remain symmetric. Hence diabatic transitions can only happen between the ground state and symmetric states, and the energy gap related to the adiabatic criterion is determined by the energy separation between the ground state and the lowest symmetric state. From our numerical result, we find that the gap position is at $J_{\rm gp} = 0.122$ with the energy gap $E_{\rm gp} = 0.31$.

The sweeping rate of the Hamiltonian can be written as $H'_{\rm gp} = c_J J'_{\rm gp}$ with $J'_{\rm gp}$ the time derivative of the hopping rate J at the gap position. Using Eq.(3.12), we plot $J'_{\rm gp}$ as a function of r_J in Fig. 3.3b, where $J'_{\rm gp}$ has a local minimum at the optimal ramping index $r_J^{(\rm min)} = \log\left[J(T)/J_{\rm gp}\right]$. For the selected trajectory, $r_J^{(\rm min)} = 1.41$, which indicates that the best fidelity for the final state can be achieved with a ramping index in-between the linear and the quadratic forms. At a total evolution time $T = 15\pi/g$, the optimal ramping index gives $J'_{\rm gp} = 0.01$. With $E_{\rm gp} = 0.31$, the adiabatic criterion is well satisfied. We numerically simulate this ramping process and calculate the fidelity of the final state. In Fig. 3.3c, the fidelity vs $J(T) = J$ is plotted for several values of r_J at $T = 15\pi/g$. The fidelity decreases quickly with $J(T)$, as $J'_{\rm gp}$ increases with $J(T)$. It can also be seen that for $J(T)$ sufficiently far away from $J_{\rm gp}$, where the Landau-Zener estimation becomes valid, the fidelity is much higher for $r_J = 1$, 2 than that for $r_J = 1/3$, $1/2$. As shown in Fig. 3.3d, the best fidelity for $J(T) = 0.5$ is achieved when $r_J \in (1,\, 2)$. These results agree well with our derivation of the optimal ramping index.

We also obtain the fidelity of the final states for a wide range of target parameters $J(T)$, $\Delta(T)$ following the trajectory Eq.(3.10) with $g(t) \equiv 1$, $J(0) = \Delta(0) = 0$, $r_\Delta/r_J = 1$, and the MI initial state Eq.(3.5). The fidelity is presented in Fig. 3.4a-d for $r_J = 1/3$, $1/2$, 1, 2, respectively. It can be seen that the fidelity decreases as the target parameters move further towards the SF phase. In particular, the fidelity exhibits a sharp decrease when the parameters cross the gap positions into the SF phase. Meanwhile, the fidelity demonstrates strong dependence on the ramping

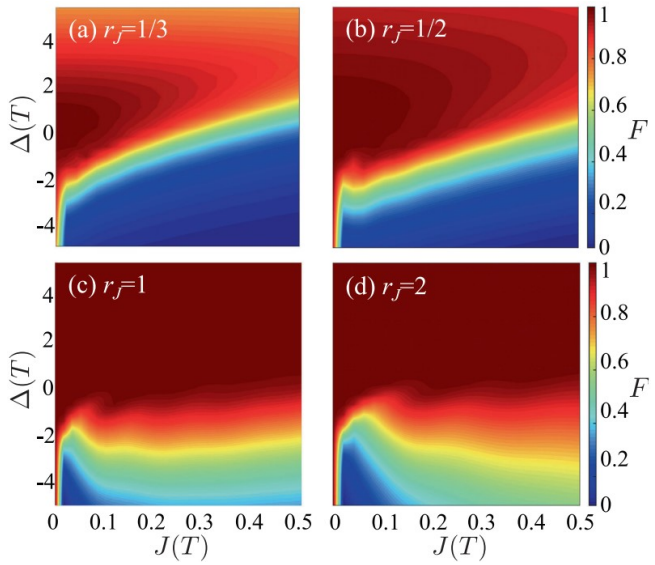

Figure 3.4: **Fidelity with MI initial state. a-d** Fidelity of the prepared state F vs target hopping rate $J(T)$ and target detuning $\Delta(T)$ for ramping index r_J given in the panel. Here $g(t) \equiv 1$, $J(0) = \Delta(0) = 0$, $r_\Delta/r_J = 1$, and $T = 15\pi/g$.

index in the intermediate regimes of the parameter space, which also agrees with our analytical prediction.

Next we consider trajectories that starts from the deep SF phase with $g(0) = 0$, $g(T) = 1$, $J(0) = 0.5$, $J(T) = 0$, $\Delta(t) \equiv 0$, and the initial state Eq.(3.6). With both J and g being time-dependent, we can choose different ramping indices for them. As shown in Fig. 3.5a, the ramping trajectory in the parameter space of J and g depends on the ratio r_g/r_J, which affects the energy spectrum and the value of the energy gap. In Fig. 3.5c, we plot the energy spectrum of the lowest excited states vs the hopping rate J for $r_g/r_J = 1$, where the solid curve is the energy of the lowest symmetric state. The energy gap occurs at $J_{\rm gp} = 0.104$ with $E_{\rm gp} = 0.25$. The energy spectrum for $r_g/r_J \neq 1$ can be found in Supplementary Figure 3.1a. The sweeping rate of the Hamiltonian is $H'_{\rm gp} = J'_{\rm gp} I_J + g'_{\rm gp} I_g$ with $I_J = \langle \partial H/\partial J \rangle_{\rm gp}$, $I_g = \langle \partial H/\partial g \rangle_{\rm gp}$, $g'_{\rm gp}$ being the time derivative of the coupling g at the gap position. With Eq.(3.10)

and Eq.(3.11), it can be shown that

$$g'_{\rm gp} = \frac{r_g}{r_J}\frac{g_{\rm gp}}{J_{\rm gp} - J(0)}J'_{\rm gp}. \tag{3.14}$$

For a given ratio r_g/r_J, $g'_{\rm gp}/J'_{\rm gp}$ is a constant that does not depend on the specific value of r_J or r_g. The dependence of $H'_{\rm gp}$ on the ramping indices can hence be characterized by the dependence of $J'_{\rm gp}$ on r_J, which is shown in Fig. 3.5b. For $r_g/r_J = 1$, $J'_{\rm gp}$ has a minimum at $r_J^{(\rm min)} = 0.234$. In Fig. 3.5d, we plot the fidelity of the final state vs r_J from our numerical simulation, which indicates that the best fidelity can be achieved when $r_J \in (1/2, 1)$ at $T = 10\pi/g, 15\pi/g$ and when $r_J \in (1/3, 1/2)$ at $T = 5\pi/g$. This result confirms our analysis that the optimal ramping index for this trajectory will shift to a smaller value with $r_J^{(\rm min)} < 1$ in comparison to that of Fig. 3.3d. The discrepancy between the numerical and the estimated results of $r_J^{(\rm min)}$ could be owing to the small difference $|J_{\rm gp} - J(T)|$ between the gap position and the target parameter, which affects the accuracy of the Landau-Zener formula in adiabatic processes [95,96]. We also numerically simulate the ramping process for the target hopping rate $J(T) \in [0, 0.5]$ and obtain the fidelity of the final state vs $J(T)$ for several values of r_J, as plotted in Fig. 3.5e. The fidelity decreases as $J(T)$ becomes smaller, as $|J'_{\rm gp}|$ increases with the difference $|J(T) - J(0)|$. The fidelity vs r_J for $r_g/r_J \neq 1$ is given in Fig. 3.5f. It can be seen that the optimal ramping index $r_J^{(\rm min)}$ for different r_g/r_J can be quite different. This is due to the change of the ramping trajectory and the energy spectrum as r_g/r_J is varied. Detailed results on $E_{\rm gp}$, $J_{\rm gp}$, and $r_J^{(\rm min)}$ for different values of r_g/r_J can be found in Supplementary Figure 3.1b.
We present the fidelity of the final state vs the target parameters following the trajectory Eq.(3.10) with $g(0) = 0$, $g(T) = 1$, $J(0) = 0.5$, $\Delta(0) = 0$, $r_g/r_J = r_\Delta/r_J = 1$, and the SF initial state Eq.(3.6) for $r_J = 1/3$, $1/2$, 1, 2, respectively, in Fig. 3.6a-d. Our numerical result shows that the fidelity decreases quickly as the target parameters enter the MI phase and strongly depends on the ramping index in the intermediate regimes of the parameter space.

3.3 Discussions

We have shown that the fidelity of the prepared state in the intermediate regimes of the parameter space can be improved by choosing the optimal ramping index for a given trajectory and by increasing the total ramping time T. Another approach to increase the fidelity is by choosing a favorable trajectory for a given set of target parameters. When the target parameters are in the MI phase, it is better to start from an initial state in the deep MI regime such as Eq.(3.5) so that the adiabatic evolution does not need to cross a region with narrow energy gap to reach the target parameters so that diabatic transitions can be negligible. Similarly, when the target parameters are in the SF phase, we can choose the initial state to be in the deep SF regime such as Eq.(3.6). Combing the selection of the initial state with optimized nonlinear ramping can have dramatic impact on the fidelity of the prepared states. For illustration, in Fig. 3.7a, we plot the maximal fidelity among all eight sets of data in Fig. 3.4a-d and Fig. 3.6a-d for two initial states and various values of linear or nonlinear ramping index r_J. It can be seen that the maximal fidelity remains close to unity in almost the entire parameter space. For comparison, in Fig. 3.7b, we plot the maximal fidelity between the data for linear ramping ($r_J = 1$) in Fig. 3.4c and Fig. 3.6c. The result in Fig. 3.7a outperforms that of Fig. 3.7b, and both results are much better than the individual plots in Fig. 3.7 and Fig. 3.6. We expect that further improvement can be achieved by optimizing the trajectory, e.g., using optimized $r_g/r_J, r_\Delta/r_J$ or the optimal control technique.

An obvious approach to improve the fidelity of adiabatic processes is to increase the ramping time T, which can reduce the time derivatives of the parameters and the sweeping rate of the Hamiltonian. This can be seen from the numerical result in Fig. 3.3d and Fig. 3.5d. For quantum devices in the NISQ era, however, the decoherence times of qubits and cavity modes set a limitation on the evolution time. The many-body ground states studied here involve finite number of polariton excitations. In the presence of decoherence, excitations can decay in a timescale comparable to the decoherence times. The ramping time needs to be much shorter than the decoherence times. In experiments, superconducting resonator cavities with frequency $\omega_c/2\pi = 10$

GHz and quality factor $Q = 10^5$ can be readily realized, which corresponds to a decay time of $1.6\,\mu$s. Superconducting qubits can have a decoherence time of $\sim 100\,\mu$s [94]. With a typical coupling strength of $g/2\pi, \mathrm{J}/2\pi = 200$ MHz, the evolution time $T = 15\pi/\mathrm{g} \approx 37.5$ ns. The state initialization pulses can be completed within a few 10's of ns. These time scales are much shorter than the decoherence times. To quantitatively characterize the effect of dissipation, we utilize a phenomenological approach with a non-Hermitian Hamiltonian [100]: $\widetilde{H}_\mathrm{t} = H_\mathrm{t} - \mathrm{i}(\kappa/2)\sum_j a_j^\dagger a_j - \mathrm{i}(\gamma/2)\sum_j \sigma_{jz}$, where κ is the cavity damping rate and γ is the qubit decay rate. We numerically simulate the ramping process under the Hamiltonian $\widetilde{H}_\mathrm{t}$ and calculate the fidelity of the final state. For $r_J = 1$ and $T = 15\pi/g$ studied in Fig. 3.3d, with $Q = 5 \times 10^4$ ($\kappa/2\pi = 200$ kHz) and $\gamma/2\pi = 2$ kHz, the fidelity $F = 0.9737$. For comparison, $F = 0.9738$ when dissipation is not included. This result shows that the effect of dissipation with practical parameters is negligible at time scales of interest. Details of this result can be found in Supplementary Discussion and Supplementary Figure 2. Note that dissipation can be used for robust preparation and stabilization of entangled states, as studied in [83,84]. In addition, the qubit-cavity interaction in Eq.(3.2) has the form of JC coupling with the counter-rotating terms omitted. This is because we study the system in the strong-coupling regime with $g \ll \omega_\mathrm{c}, \omega_z$, where the effect of the counter-rotating terms can be neglected.

METHODS

We employ a method developed in our previous work [60] to conduct numerical simulation on the JC lattice studied in this work. This method allows us to efficiently solve the ground states and the dynamics of a finite-sized JC lattice with given number of polariton excitations. In a JC lattice, each unit cell contains a qubit and a cavity mode. If we choose the photon cutoff on each lattice site to be equal to the total number of excitations in the lattice N, then the total number of basis states for this lattice is $(2N+1)^L$, which depends exponentially on the size of the lattice L. For $N = L = 6$, the number of basis states is 4826809. This dependence sets a serious limitation on the computable size of JC lattices. In our method, we only

consider basis states that have exactly N excitations. We developed a code to find out such basis states. For $N = L = 6$, we find that the total number of basis states is 5336, which shows that this method can greatly reduce the demand on computing power. We also developed codes to derive the matrix elements for the Hamiltonian and other operators, such as the creation and annihilation operators of cavity modes, the Pauli operators of qubits, and the number operator of cavity modes, under these basis states. With these matrices, we can calculate the eigenstates and eigenenergies of a JC lattice using the exact diagonalization method. We also simulate the dynamical evolution of this system under time-dependent Hamiltonians. The matrices for the creation operators and the Pauli operators enable us to generate the initial state in the MI and the SF phases numerically. Our method can be applied to different types of JC lattices as it can be used regardless of the specific form of interaction between neighboring lattice sites.

DATA AVAILABILITY

The data that support the findings of this study are available from the authors upon reasonable request.

CODE AVAILABILITY

The codes that are used to produce the data presented in this study are available from the authors upon reasonable request.

ACKNOWLEDGEMENTS

This work is supported by the UC Multicampus-National Lab Collaborative Research and Training under Award No. LFR-17-477237. G.L.L. is supported by the National Natural Science Foundation of China under Grant No. 11974205 and No. 11774197. C.W.W. is also supported by NSF QII-TAQS-1936375, NSF 1919355, and

ONR N00014-15-1-2368. L.T. is also supported by UC Merced Faculty Research Grants 2017 and NSF awards No.1720501, No. 2006076, and No. 2037987.

AUTHOR CONTRIBUTIONS

K.C. and P.P. are co-first authors. K.C. and P.P. conducted numerical simulation, L.T. designed the project and conducted analytical derivation, K.C., P.P. and L.T. analyzed the numerical data and wrote the paper with inputs from G.-L.L. and C.W.W., all authors discussed the results and contributed to the final paper.

COMPETING INTERESTS

The authors declare that there are no competing interests.

ADDITIONAL INFORMATION

Supplementary information The online version contains supplementary material at t https://doi.org/10.1038/s41534-021-00433-y.

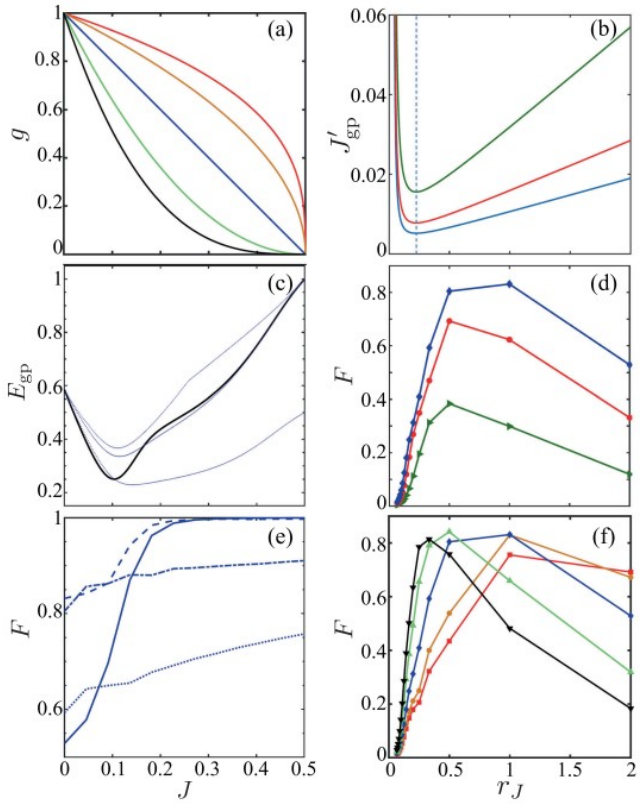

Figure 3.5: **Ramping from SF to MI phase.** **a** Ramping trajectory in the parameter space of J and g for $r_g/r_J = 1/3, 1/2, 1, 2, 3$ from top to bottom. **b** Time derivative $J'_{\rm gp}$ vs ramping index r_J at $r_g/r_J = 1$, $J(T) = 0$, and $T = 5\pi/g, 10\pi/g, 15\pi/g$ from top to bottom. **c** Energy spectrum of the lowest excited states vs hopping rate J for $r_g/r_J = 1$. Solid (dotted) curve is for the symmetric (asymmetric) state with the ground-state energy set to zero. **d** Fidelity F vs r_J at $r_g/r_J = 1$, $J(T) = 0$, and $T = 5\pi/g, 10\pi/g, 15\pi/g$ from bottom to top. **e** Fidelity F vs $J(T) = J$ for $r_J = 2$ (solid), 1 (dashed), 1/2 (dot-dashed), and 1/3 (dotted) at $r_g/r_J = 1$ and $T = 15\pi/g$. **f** Fidelity F vs r_J at $r_g/r_J = 1/3$ (square), 1/2 (circle), 1 (diamond), 2 (triangle), and 3 (inverted triangle), $J(T) = 0$, and $T = 15\pi/g$. In all plots, $g(0) = 0$, $g(T) = 1$, $J(0) = 0.5$, and $\Delta(t) \equiv 0$.

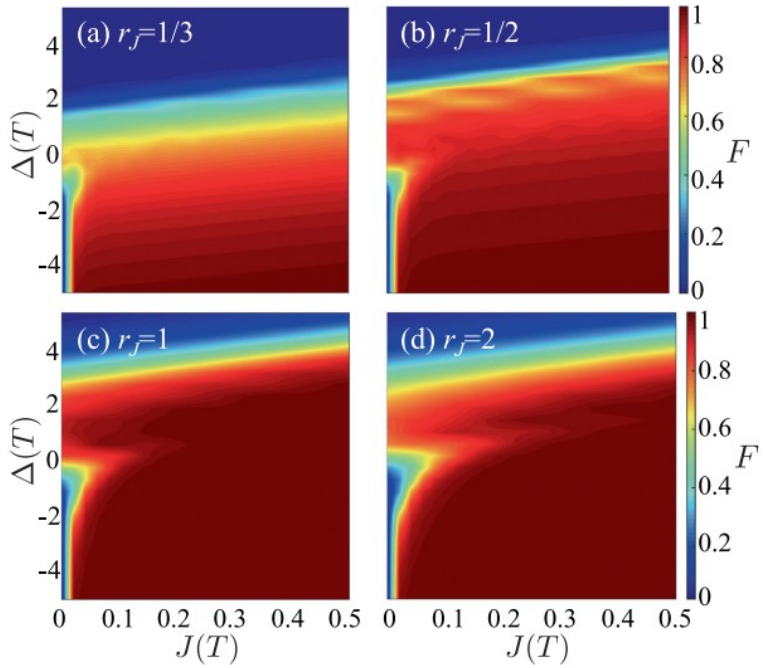

Figure 3.6: **Fidelity with SF initial state. a-d** Fidelity of the prepared state F vs target hopping rate $J(T)$ and target detuning $\Delta(T)$ for ramping index r_J given in the panel. Here $g(0) = 0$, $g(T) = 1$, $J(0) = 0.5$, $\Delta(0) = 0$, $r_g/r_J = r_\Delta/r_J = 1$, and $T = 15\pi/g$.

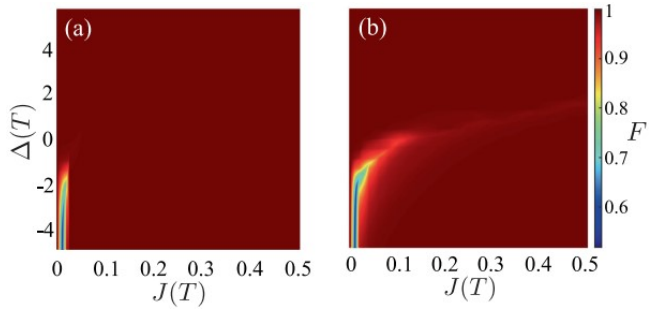

Figure 3.7: **Maximal fidelity with different ramping indices and trajectories.** Maximal fidelity of the prepared state F vs target hopping rate $J(T)$ and target detuning $\Delta(T)$: **a** among all data in Fig. 3.4a-d and Fig. 3.6a-d, and **b** between the linear ramping data in Fig. 3.4c and Fig. 3.6c.

Chapter 4

Shortcut to adiabaticity

This work was done in collaboration with Kang Cai. This work will be submitted for publication soon.

4.1 Introduction

Quantum simulation of complex quantum systems starts with the preparation of desired many-body ground states in a given quantum simulator. Preparing many-body ground states in the quantum simulator is not a trivial task due to decoherence and unwanted control errors in such devices. To mitigate such problem it is desirable to prepare a many-body ground state in a fast and efficient manner [9, 101]. Different many-body state preparation schemes have been developed for each analog, digital and hybrid quantum simulations [102–104]. One of the robust state preparation schemes in such simulators is the adiabatic state preparation which involves preparing a many-body ground state in experimentally feasible parameter regimes using quantum engineering and driving the prepared state to the target region following the adiabatic trajectory [95, 96, 105, 106]. However, the constraint imposed by the adiabatic criterion, that the total evolution time should be greater than inverse of the square of the energy gap between the ground state and first excited state, limits the applicability of adiabatic state preparation scheme to systems with long

coherence time. But currently available quantum simulators have very short coherence time [107]. In addition, the fact that the energy gap decreases as system size increases constrains the adiabatic state preparation scheme to systems having few qubits only. To circumvent these limitations imposed by the adiabatic criterion and to get the same final results as the adiabatic process gives in much shorter time, the shortcuts to adiabatic (STA) method was developed [9, 108].

The term STA was first coined in Chen, Ruschhaupt *et al.* [74] in the context of cooling down atoms in harmonic trap without phase-space compression. The STA method existed before Chen's work [109–111]. In particular, the systematic development of counterdiabatic(CD) driving paradigm by Demirplak and Rice [10–12] for the internal state transfer using control fields had been influential to control the dynamics of two- and three level systems at that time. Berry [13] later discovered the different but equivalent form of CD driving method as " transitionless tracking" method. After the work of Chen [74], many control schemes based on STA have been developed to speed up slow processes in different fields ranging from quantum transport, quantum thermodynamics to quantum information processing and quantum control. Some of the STA methods are CD driving, invariant-based inverse engineering, fast forward methods, parallel adiabatic transfer and variational methods. A comprehensive review of different STA methods can be found in Guéry-Odelin *et al.* [9].

In this chapter we discuss the transitionless tracking method to prepare a quantum many-body ground state in a JC lattices in an optimal time. Based on the energy uncertainty relation, there exists a fundamental speed limit with which a given quantum process can take place. This limit is called quantum speed limit(QSL) [112, 113]. In this context, STA helps to determine the QSL in a many-body state preparation process i.e. a minimum time to reach the target state with almost perfect fidelity [104, 114, 115].

4.2 Transitionless tracking method

Berry formulation

In the Transitionless tracking method, we add an auxiliary interaction to the reference Hamiltonian $H(t)$ which guides the dynamics to follow the approximate adiabatic evolution of $H(t)$ [9,13]. Let us consider a reference Hamiltonian $H(t)$. For simplicity, let us assume the eigenenergies are non-degenerate and eigenstates are discrete. We can express $H(t)$ in terms of eigenbasis and eigenenergy as ($\hbar = 1$):

$$H(t) = \sum_p E_p(t)|p(t)\rangle\langle p(t)| \tag{4.1}$$

where $E_p(t)$ is the instantaneous eigenenergy corresponding to the eigenstate $|p(t)\rangle$. If $|p(0)\rangle$ is the initial eigenstate of $H(0)$, the state will continue to be so with addition of the adiabatic phases $\alpha_p(t)$ under slow evolution of the system governed by the time-dependent Schrödinger equation i.e.

$$|\psi_p(t)\rangle = e^{i\alpha_p(t)}|p(t)\rangle \tag{4.2}$$

$$\alpha_p(t) = -\int_0^t dt^{'} E_p(t^{'}) + i\int_0^t dt^{'}\langle p(t^{'})|\partial_{t'} p(t^{'})\rangle \tag{4.3}$$

The job now for us is to find a Hamiltonian $H_{ST}(t)$ for which $|\psi_p(t)\rangle$ is the exact evolved state i.e.

$$\partial_t|\psi_p(t)\rangle = -iH_{ST}(t)|\psi_p(t)\rangle. \tag{4.4}$$

$H_{ST}(t)$ can be constructed from the unitary evolution operator $U(t)$ as

$$H_{ST} = i\dot{U}U^{\dagger}, \tag{4.5}$$

where, $U(t)$ is

$$U(t) = \sum_p e^{i\alpha_p(t)}|p(t)\rangle\langle p(0)|. \tag{4.6}$$

Here $U(t)$ obeys unitary dynamics, hence the evolution of an arbitrary state $|\phi(t)\rangle$ can be expressed as:

$$\phi(t)\rangle = \sum_p e^{i\alpha_p(t)}|p(t)\rangle\langle p(0)|\phi(0)\rangle. \tag{4.7}$$

Substituting Eq.(4.6) into Eq.(4.5), we get the expression for $H_{ST}(t)$ as:

$$H_{ST}(t) = H(t) + H_{cd}(t) \tag{4.8}$$

with auxiliary Hamiltonian

$$H_{cd} = i\sum_p \left[|\partial_t p(t)\rangle\langle p(t)| - \langle p(t)|\partial_t p(t)\rangle|p(t)\rangle\langle p(t)|\right] \tag{4.9}$$

which is called counterdiabatic (CD) Hamiltonian. An alternating form of H_{cd} can be derived by differentiating $H(t)|p(t)\rangle = E_p(t)|p(t)\rangle$,

$$H_{cd}(t) = i\sum_{q\neq p}\sum_p \frac{|q(t)\rangle\langle q(t)|\partial_t H(t)|p(t)\rangle\langle p(t)|}{E_p(t) - E_q(t)} \tag{4.10}$$

4.3 Counter-diabatic driving in many-body state preparation in JC lattices

4.3.1 Analytical Results

In this section we derive the analytical expression of counterdiabatic Hamiltonian $H_{cd}(t)$ for the JC lattices. Let us consider a JC lattices with N sites having N excitations and the excitation number is conserved in the system. The Hamiltonian in rotating frame can be written as [15]

$$H = \Delta\sum_{j=1}^{N} a_j^\dagger a_j + g\sum_{j=1}^{N}(a_j^\dagger\sigma_j^- + a_j\sigma_j^+) - J\sum_{j=1}^{N}(a_j^\dagger a_{j+1} + a_j a_{j+1}^\dagger) \tag{4.11}$$

Here, Δ, g and J are detuning beetween cavity frequency and qubit frequency, coupling strength, and hopping strength respectively. $a_j^\dagger(a_j)$ and $\sigma_j^+(\sigma_j^-)$ are cavity excitation creation (annihilation) operator and atomic excitation creation (annihilation) operator respectively. Since the system is invariant under translation, momentum is also conserved [106].
In order to find the CD Hamiltonian, let us define collective operators:

$$a_j = \frac{1}{\sqrt{N}}\sum_k a_k exp(-ik.r_j); a_k = \frac{1}{\sqrt{N}}\sum_j a_j exp(ik.r_j) \tag{4.12}$$

$$\sigma_j^- = \frac{1}{\sqrt{N}}\sum_k \sigma_k^- exp(-ik.r_j); \sigma_k^- = \frac{1}{\sqrt{N}}\sum_j \sigma_j^- exp(ik.r_j) \tag{4.13}$$

where $k = 2\pi n/N$ with $n = 0, 1, ..., N-1$. After substituting the momentum operators in Eq.(4.11), we get (see appendix A)

$$H = \sum_k \big[\Delta - 2Jcos(kR)\big] a_k^\dagger a_k + g\sum_k (a_k^\dagger \sigma_k^- + a_k \sigma_k^+) \tag{4.14}$$

where R is the separation between two sites. Based on collective operators $a_k^\dagger$ and σ_k^+, we can define two kind of states:

$$|1, g\rangle_k = a_k^\dagger |vac\rangle \tag{4.15}$$

$$|0, e\rangle_k = \sigma_k^+ |vac\rangle \tag{4.16}$$

In space of $\{|1, g\rangle_k, |0, e\rangle_k\}$, eigenvalues of each mode k are

$$E_{(1,\pm)} = \frac{(\Delta - 2Jcos(kR)) \pm \chi(1)}{2} \tag{4.17}$$

with $\chi(1) = \sqrt{(\Delta - 2Jcos(kR))^2 + 4g^2}$. The corresponding eigenstates are:

$$|1, -\rangle_k = sin(\theta/2)|1, g\rangle_k - cos(\theta/2)|0, e\rangle_k \tag{4.18}$$

$$|1, +\rangle_k = cos(\theta/2)|1, g\rangle_k + sin(\theta/2)|0, e\rangle_k \tag{4.19}$$

where $sin(\theta_k) = \sqrt{(1-(\Delta - 2Jcos(kR)))/\chi(1)}$ and
$cos(\theta_k) = \sqrt{(1+(\Delta - 2Jcos(kR)))/\chi(1)}$.

When hopping rate J depends on time

In CD driving, the auxiliary Hamiltonian i.e. CD Hamiltonian prevents the system to excite in the symmetric higher states. The general expression of CD Hamiltonian is Eq.(4.10)

$$H_{cd}(t) = i\sum_{m\neq n}\sum_{n}\frac{|m(t)\rangle\langle m(t)|\partial_t H(t)|n(t)\rangle\langle n(t)|}{E_n(t)-E_m(t)} \tag{4.20}$$

Conservation of momentum in the system implies system can excites to the states which has same momentum k only.

$$\langle 1,-|\sum(a_i^\dagger a_j + a_i a_j^\dagger)|1,+\rangle_k \tag{4.21}$$

$$= \langle 1,g|\sum(a_i^\dagger a_j + a_i a_j^\dagger)|1,g\rangle_k$$

$$= cos(kR)sin(\theta_k/2)cos(\theta_k/2) \tag{4.22}$$

$$= cos(kR)\frac{\sqrt{\chi(1)^2 - 4k^2cos^2(kR)}}{\chi(1)} \tag{4.23}$$

We can change the number operator to physical operator as:

$$|1,-\rangle_k\langle 1,+| - |1,+\rangle_k\langle 1,-| \tag{4.24}$$

$$= [sin(\theta/2)|1,g\rangle_k - cos(\theta/2)|0,e\rangle_k] \tag{4.25}$$

$$[cos(\theta/2)\langle 1,g|_k + sin(\theta/2)\langle 0,e|_k] - h.c.$$

$$= [sin^2(\theta/2) + cos^2(\theta/2)](|1,g\rangle_k\langle 0,e| - h.c) \tag{4.26}$$

$$= |1,g\rangle_k\langle 0,e| - h.c. \tag{4.27}$$

$$= a_k^\dagger\sigma_k^- - h.c. \tag{4.28}$$

For the zero-th momentum state i.e. $k = k_0 = 0$ the CD Hamiltonian has the form

$$H_{cd} = -icos(k_0R)\frac{\sqrt{\chi(1)^2 - 4J^2cos^2(k_0R)}}{\chi(1)^2}\frac{\partial J}{\partial t}(a_{k_0}^\dagger\sigma_{k_0}^- - h.c.) \tag{4.29}$$

Since momentum k is conserved, we can generalize the CD Hamiltonian to

$$H_{cd} = -icos(k_0R)\frac{\sqrt{\chi(1)^2 - 4J^2cos^2(k_0R)}}{\chi(1)^2}\frac{\partial J}{\partial t}\sum_k(a_k^\dagger\sigma_k^- - h.c.) \tag{4.30}$$

$$= -icos(k_0R)\frac{\sqrt{\chi(1)^2 - 4J^2cos^2(k_0R)}}{\chi(1)^2}\frac{\partial J}{\partial t}\sum_j(a_j^\dagger\sigma_j^- - h.c.) \tag{4.31}$$

When coupling strength g depends on time

For the time dependent coupling strength g:

$$\langle 1,-|\sum(a_i^\dagger a_j + a_i a_j^\dagger)|1,+\rangle_k \tag{4.32}$$

$$= -cos^2(\theta_{k_0}/2)\langle 0,e|\sum_j a_j\sigma_j^+|1,g\rangle_{k_0}$$

$$+ sin^2(\theta_{k_0}/2)\langle 1,g|\sum_j a_j^\dagger\sigma_j^-|0,e\rangle_{k_0}$$

$$= sin^2(\theta_{k_0}/2) - cos^2(\theta_{k_0}/2) \tag{4.33}$$

$$= -\frac{\Delta - 2Jcos(k_0R)}{\chi(1)} \tag{4.34}$$

Hence, if we consider the excitation in k_0 space, the CD Hamiltonian is:

$$H_{cd} = -i\frac{\Delta - 2Jcos(k_0R)}{\chi(1)^2}\frac{\partial g(t)}{\partial t}(a_{k_0}^\dagger\sigma_{k_0}^- - h.c.) \tag{4.35}$$

since momentum is conserved, we can generalize Eq.(4.35) to

$$H_{cd} = -i\frac{\Delta - 2Jcos(k_0R)}{\chi(1)^2}\frac{\partial g(t)}{\partial t}\sum_k(a_k^\dagger\sigma_k^- - h.c.) \tag{4.36}$$

$$= -i\frac{\Delta - 2Jcos(k_0R)}{\chi(1)^2}\frac{\partial g(t)}{\partial t}\sum_j(a_j^\dagger\sigma_j^- - h.c.) \tag{4.37}$$

4.3.2 Numerical Results

Two sites with one excitation

Let us consider a JC latttices with two sites having two excitations. The Hamiltonian of the system can be written as:

$$H(t) = \Delta \sum_{j=1}^{2} a_j^\dagger a_j + g \sum_{j=1}^{2} (a_j^\dagger \sigma_j^- + a_j \sigma_j^+) - J(t)(a_j^\dagger a_{j+1} + a_j a_{j+1}^\dagger) \tag{4.38}$$

Here, the time dependent term is the hopping strength i.e. $J(t)$. The Hamiltonian $H(t)$ in terms of the basis $\{|1,g,0,g\rangle, |0,e,0,g\rangle, |0,g,1,g\rangle, |0,g,0,e\rangle\}$ can be written as:

$$H(t) = \begin{bmatrix} \Delta & g & -J & 0 \\ g & 0 & 0 & 0 \\ -J & 0 & \Delta & g \\ 0 & 0 & g & 0 \end{bmatrix} \tag{4.39}$$

THe eigenstates and eigenvalues of $H(t)$ are:

$$v_1 = \frac{1}{2} \begin{bmatrix} -\sqrt{\frac{\chi_J^- - \Delta_J^-}{\chi_j^-}} \\ \sqrt{\frac{\chi_J^- + \Delta_J^-}{\chi_j^-}} \\ -\sqrt{\frac{\chi_J^- - \Delta_J^-}{\chi_j^-}} \\ \sqrt{\frac{\chi_J^- + \Delta_J^-}{\chi_j^-}} \end{bmatrix}, E_1 = \frac{1}{2}(\Delta_J^- - \chi_J^-) \tag{4.40}$$

$$v_2 = \frac{1}{2} \begin{bmatrix} \sqrt{\frac{\chi_J^- + \Delta_J^-}{\chi_j^-}} \\ \sqrt{\frac{\chi_J^- - \Delta_J^-}{\chi_j^-}} \\ \sqrt{\frac{\chi_J^- + \Delta_J^-}{\chi_j^-}} \\ \sqrt{\frac{\chi_J^- - \Delta_J^-}{\chi_j^-}} \end{bmatrix}, E_2 = \frac{1}{2}(\Delta_J^- + \chi_J^-) \tag{4.41}$$

$$v_3 = \frac{1}{2}\begin{bmatrix} \sqrt{\frac{\chi_J^+ - \Delta_J^+}{\chi_j^+}} \\ -\sqrt{\frac{\chi_J^+ + \Delta_J^+}{\chi_j^+}} \\ -\sqrt{\frac{\chi_J^+ - \Delta_J^+}{\chi_j^+}} \\ \sqrt{\frac{\chi_J^+ + \Delta_J^+}{\chi_j^+}} \end{bmatrix}, E_3 = \frac{1}{2}(\Delta_J^+ - \chi_J^+) \tag{4.42}$$

$$v_4 = \frac{1}{2}\begin{bmatrix} -\sqrt{\frac{\chi_J^+ + \Delta_J^+}{\chi_j^+}} \\ -\sqrt{\frac{\chi_J^+ - \Delta_J^+}{\chi_j^+}} \\ \sqrt{\frac{\chi_J^+ + \Delta_J^+}{\chi_j^+}} \\ \sqrt{\frac{\chi_J^+ - \Delta_J^+}{\chi_j^+}} \end{bmatrix}, E_4 = \frac{1}{2}(\Delta_J^+ + \chi_J^+) \tag{4.43}$$

where, $\Delta_J^{\pm} = \Delta \pm J$ and $\chi_J^{\pm} = \sqrt{(\Delta_J^{\pm})^2 + 4g^2}$. We want to constrain the system to remain in the ground state during the evolution. For this, we need to find the CD Hamiltonian H_{cd} i.e.

$$H_{cd}(t) = i \sum_{m \neq n} \sum_{n} \frac{|m(t)\rangle\langle m(t)|\partial_t H(t)|n(t)\rangle\langle n(t)|}{E_n(t) - E_m(t)} \tag{4.44}$$

With the addition of the CD Hamiltonian,the system evolves under the Hamiltonian:

$$H_{ST} = H(t) + H_{cd}(t) \tag{4.45}$$

$H(t)$ depends on time due to the parameter $J(t)$. Hence, $\partial_t H(t) = -\partial_t J(t)(a_1^\dagger a_2 + a_1 a_2^\dagger)$. The hopping terms can be calculated as:

$$\begin{aligned}
\langle v_1|(a_1^\dagger a_2 + a_1 a_2^\dagger)|v_2\rangle = -\frac{g}{\chi_J^-}; \langle v_1|(a_1^\dagger a_2 + a_1 a_2^\dagger)|v_3\rangle = 0; \\
\langle v_1|(a_1^\dagger a_2 + a_1 a_2^\dagger)|v_4\rangle = 0; \langle v_2|(a_1^\dagger a_2 + a_1 a_2^\dagger)|v_1\rangle = -\frac{g}{\chi_J^-}; \\
\langle v_2|(a_1^\dagger a_2 + a_1 a_2^\dagger)|v_3\rangle = 0; \langle v_2|(a_1^\dagger a_2 + a_1 a_2^\dagger)|v_4\rangle = 0; \\
\langle v_3|(a_1^\dagger a_2 + a_1 a_2^\dagger)|v_1\rangle = 0; \langle v_3|(a_1^\dagger a_2 + a_1 a_2^\dagger)|v_2\rangle = 0; \\
\langle v_3|(a_1^\dagger a_2 + a_1 a_2^\dagger)|v_4\rangle = \frac{g}{\chi_J^+}; \langle v_4|(a_1^\dagger a_2 + a_1 a_2^\dagger)|v_1\rangle = 0; \\
\langle v_4|(a_1^\dagger a_2 + a_1 a_2^\dagger)|v_3\rangle = \frac{g}{\chi_J^+}; \langle v_4|(a_1^\dagger a_2 + a_1 a_2^\dagger)|v_2\rangle = 0;
\end{aligned}$$

Hence, the CD Hamiltonian H_{cd} has the form:

$$H_{cd}(t) = i\frac{g}{(\chi_J^-)^2}\partial_t J(|v_1\rangle\langle v_2| - |v_2\rangle\langle v_1|) - i\frac{g}{(\chi_J^+)^2}\partial_t J(|v_3\rangle\langle v_4| - |v_4\rangle\langle v_3|) \tag{4.46}$$

Since $|v_1\rangle$ and $|v_2\rangle$ have same symmetry, and $|v_3\rangle$ and $|v_4\rangle$ have same symmetry, excitations can be exchanged only between $|v_1\rangle$ and $|v_2\rangle$, and between v_3 and $|v_4\rangle$. In occupation number basis, the concrete form of different states can be written as:

$$\begin{aligned}
|v_1\rangle &= -\frac{1}{2}\sqrt{\frac{\chi_J^- - \Delta_J^-}{\chi_J^-}}(|1,g,0,g\rangle + |0,g,1,g\rangle) + \frac{1}{2}\sqrt{\frac{\chi_J^- + \Delta_J^-}{\chi_J^-}}(|0,e,0,g\rangle + |0,g,0,e\rangle) \\
|v_2\rangle &= \frac{1}{2}\sqrt{\frac{\chi_J^- - \Delta_J^-}{\chi_J^-}}(|1,g,0,g\rangle + |0,g,1,g\rangle) + \frac{1}{2}\sqrt{\frac{\chi_J^- + \Delta_J^-}{\chi_J^-}}(|0,e,0,g\rangle + |0,g,0,e\rangle) \\
|v_3\rangle &= \frac{1}{2}\sqrt{\frac{\chi_J^+ - \Delta_J^+}{\chi_J^+}}(|1,g,0,g\rangle - |0,g,1,g\rangle) + \frac{1}{2}\sqrt{\frac{\chi_J^+ + \Delta_J^+}{\chi_J^+}}(|0,e,0,g\rangle - |0,g,0,e\rangle) \\
|v_4\rangle &= -\frac{1}{2}\sqrt{\frac{\chi_J^+ - \Delta_J^+}{\chi_J^+}}(|1,g,0,g\rangle - |0,g,1,g\rangle) + \frac{1}{2}\sqrt{\frac{\chi_J^+ + \Delta_J^+}{\chi_J^+}}(|0,e,0,g\rangle - |0,g,0,e\rangle)
\end{aligned}$$

This clearly shows that the sign of $|v_1\rangle$ and $|v_2\rangle$ does not change when we exchange the state of two sites but $|v_3\rangle$ and $|v_4\rangle$ gains a negative sign when we exchange the state of two sites. Parity is conserved in the system. We use this property to convert

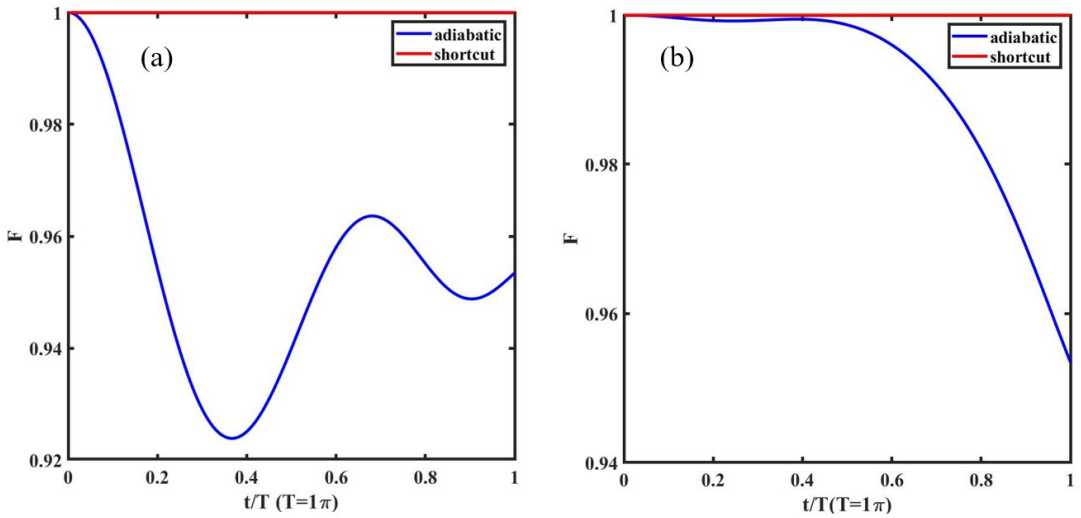

Figure 4.1: **Comparison of fidelity between adiabatic method and STA method with time dependent hopping strength** J a. at $\Delta = 0$,$g = 1$, $J_{init} = 0.00001$ and $J_{final} = 5$. b. at $\Delta = 5$,$g = 1$, $J_{init} = 0.00001$ and $J_{final} = 5$

the non-physical Hamiltonian into a physical Hamiltonian.

One of the important steps in implementing the CD Hamiltonian in an actual experiment is to map the basis projectors to physical operators. We have defined $a_1^\dagger\sigma_1^- = |1,g,0,g\rangle\langle 0,e,0,g|$, $a_1^\dagger a_2 = |1,g,0,g\rangle\langle 0,g,1,g|$,$\sigma_2^+\sigma_1^- = |0,g,0,e\rangle\langle 0,e,0,g|$... . With this transformation:

$$|v_1\rangle\langle v_2| - |v_2\rangle\langle v_1| = \frac{1}{2}[(a_1 + a_2)(\sigma_1^\dagger + \sigma_2^\dagger) - (a_1^\dagger + a_2^\dagger)(\sigma_1^- + \sigma_2^-)] \tag{4.47}$$

$$|v_3\rangle\langle v_4| - |v_4\rangle\langle v_3| = \frac{1}{2}[(a_1 - a_2)(\sigma_1^\dagger - \sigma_2^\dagger) - (a_1^\dagger - a_2^\dagger)(\sigma_1^- - \sigma_2^-)] \tag{4.48}$$

The Eq.(4.47) and Eq.(4.48) are symmetric and antisymmetric respectively. With this, the CD Hamiltonian can be written as:

$$\begin{aligned} H_{cd}(t) =& i\frac{g}{2(\chi_J^-)^2}\partial_t J\left[(a_1 + a_2)(\sigma_1^+ + \sigma_2^+) - (a_1^\dagger + a_2^\dagger)(\sigma_1^- + \sigma_2^-)\right] \\ & -i\frac{g}{2(\chi_J^+)^2}\partial_t J\left[(a_1 - a_2)(\sigma_1^+ - \sigma_2^+) - (a_1^\dagger - a_2^\dagger)(\sigma_1^- - \sigma_2^-)\right] \end{aligned} \tag{4.49}$$

Suppose we want to confine the evolution of the system in symmetric subspace. This means only the first term of Eq.(4.49) control the dynamics of the system, the second anti-symmetric term has no influence in the evolution. The first term of Eq.(4.49) has non-local terms like $a_1^\dagger \sigma_2^-$ which are extremely hard to implement in experiments. Since anti-symmetric term of Eq.(4.49) has no effect in evolution, we combine symmetric and anti-symmetric terms to construct the physical Hamiltonian. Since

$$\begin{aligned} a_1\sigma_1^+ + a_2\sigma_2^+ - a_1^\dagger\sigma_1^- - a_2^\dagger\sigma_2^- & \\ =&\frac{1}{2}[(a_1+a_2)(\sigma_1^+ + \sigma_2^+) - (a_1^\dagger + a_2^\dagger)(\sigma_1^- + \sigma_2^+)] \\ +&\frac{1}{2}[(a_1-a_2)(\sigma_1^+ - \sigma_2^+) - (a_1^\dagger - a_2^\dagger)(\sigma_1^- - \sigma_2^+)], \end{aligned} \tag{4.50}$$

we can obtain physical the CD Hamiltonian as:

$$\begin{aligned} H_{cd}^{ph}(t) =& i\frac{g}{2(\chi_J^-)^2}\partial_t J\left[(a_1+a_2)(\sigma_1^+ + \sigma_2^+) - (a_1^\dagger + a_2^\dagger)(\sigma_1^- + \sigma_2^-)\right] \\ &-i\frac{g}{2(\chi_J^-)^2}\partial_t J\left[(a_1-a_2)(\sigma_1^+ - \sigma_2^+) - (a_1^\dagger - a_2^\dagger)(\sigma_1^- - \sigma_2^-)\right] \\ =& i\frac{g}{(\chi_J^-)^2}\partial_t J\left[a_1\sigma_1^+ + a_2\sigma_2^+ - a_1^\dagger\sigma_1^- - a_2^\dagger\sigma_2^-\right] \end{aligned} \tag{4.51}$$

In matrix form, Eq.(4.51) can be written as:

$$H_{cd}^{ph}(t) = i\frac{g}{(\chi_J^-)^2}\partial_t J \begin{bmatrix} 0 & -1 & 0 & 0 \\ 1 & 0 & 0 & 0 \\ 0 & 0 & 0 & -1 \\ 0 & 0 & 1 & 0 \end{bmatrix} \tag{4.52}$$

With the CD Hamiltonian given by Eq.(4.51), the exact Hamiltonian of the system can be written as:

$$H_{ST}(t) = H(t) + H_{cd}^{ph}(t) \tag{4.53}$$

In Fig.(4.1) we have compared the fidelity obtained with the STA method and with the adiabatic method for the time dependent hopping strength J. The figure shows

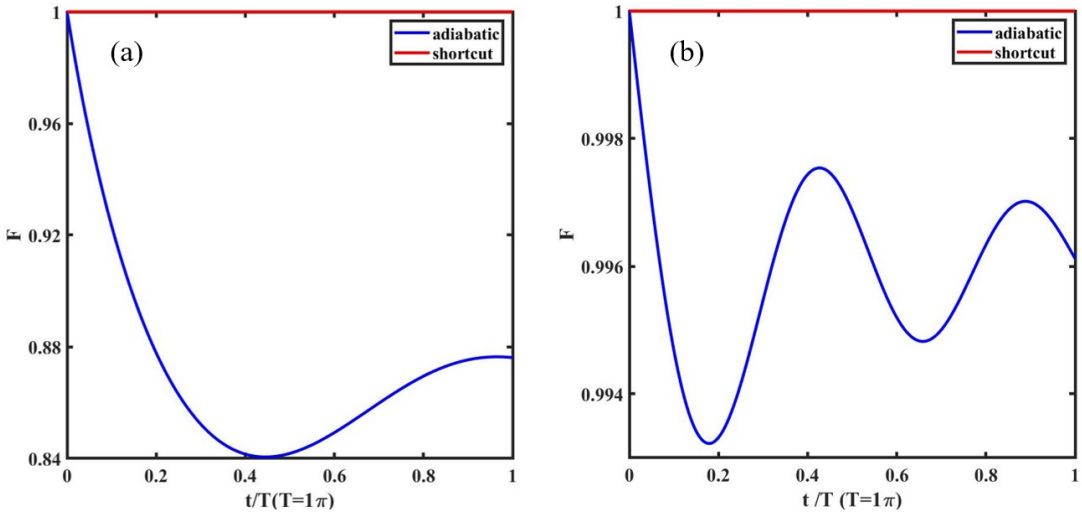

Figure 4.2: **Comparison of fidelity between the adiabatic method and STA method with time dependent coupling strength** g. a. at $\Delta = 0$,$J = 1$, $g_{init} = 0.00001$ and $g_{final} = 1$. b. at $\Delta = 5$,$J = 1$, $g_{init} = 0.00001$ and $g_{final} = 1$

that application of the STA gives the fidelity 1 even for a small evolution time whereas the fidelity is very low for the adiabatic process during such small evolution time. If the hopping strength is fixed but the coupling between cavity and qubit is time dependent, the Hamiltonian can be expressed as:

$$H(t) = \Delta \sum_{j=1}^{2} a_j^\dagger a_j + g(t) \sum_{j=1}^{2} (a_j^\dagger \sigma_j^- + a_j \sigma_j^+) - J(a_j^\dagger a_{j+1} + a_j a_{j+1}^\dagger) \tag{4.54}$$

The CD Hamiltonian (see appendix A) corresponding to Eq.(4.54) has the form

$$\begin{aligned} H_{cd}(t) =& i\frac{\Delta_J^-}{2(\chi_J^-)^2}\partial_t g \left[(a_1 + a_2)(\sigma_1^+ + \sigma_2^+) - (a_1^\dagger + a_2^\dagger)(\sigma_1^- + \sigma_2^-)\right] \\ & -i\frac{\Delta_J^+}{2(\chi_J^+)^2}\partial_t g \left[(a_1 - a_2)(\sigma_1^+ - \sigma_2^+) - (a_1^\dagger - a_2^\dagger)(\sigma_1^- - \sigma_2^-)\right] \end{aligned} \tag{4.55}$$

We can use parity symmetry to convert $H_{cd}(t)$ to physical Hamiltonian i.e.

$$\begin{aligned} H_{cd}^{ph}(t) =& i\frac{\Delta_J^-}{2(\chi_J^-)^2}\partial_t g\left[(a_1+a_2)(\sigma_1^+ + \sigma_2^+) - (a_1^\dagger + a_2^\dagger)(\sigma_1^- + \sigma_2^-)\right] \\ &+ i\frac{\Delta_J^-}{2(\chi_J^-)^2}\partial_t g\left[(a_1-a_2)(\sigma_1^+ - \sigma_2^+) - (a_1^\dagger - a_2^\dagger)(\sigma_1^- - \sigma_2^-)\right] \\ =& i\frac{\Delta_J^-}{(\chi_J^-)^2}\partial_t g\left[a_1\sigma_1^+ + a_2\sigma_2^+ - a_1^\dagger\sigma_1^- - a_2^\dagger\sigma_2^-\right] \end{aligned} \tag{4.56}$$

The total Hamiltonian of the system now includes original Hamiltonian and CD Hamiltonian i.e.

$$\begin{aligned} H_{ST}(t) &= H(t) + H_{cd}^{ph}(t) \\ &= \Delta\sum_{j=1}^{2} a_j^\dagger a_j + \left[g(t) + i\frac{\Delta_J^-}{(\chi_J^-)^2}\partial_t g\right]\sum_{j=1}^{2}(a_j^\dagger\sigma_j^- + a_j\sigma_j^+) - J(a_j^\dagger a_{j+1} + a_j a_{j+1}^\dagger) \end{aligned} \tag{4.57}$$

In Fig.(4.2) we have compared the fidelity obtained with the STA method and with the adiabatic method for the time dependent coupling strength g. It shows that application of the STA gives the fidelity 1 even for a small evolution time but the fidelity is very low for the adiabatic process during such small evolution time.
The time dependent coupling strength $g(t)$ induces non-adiabatic excitations which can be stop by changing the coupling strength. This is also called self-correction. Experimental implementation of the self correction term is extremely challenging.

4.4 Summary

In this chapter we have applied the shortcuts to adiabaticity method with CD driving for the fast many-body state preparation in JC lattices. We have considered two different scenarios: i) time dependent hopping and ii) time dependent cavity-qubit coupling and derived the analytical form of the CD Hamiltonian. To verify our analytical result, we considered a case of two sites with single excitation and numerically verified the analytical result. We have compared the fidelity of state preparation given by the STA method and by the adiabatic method. The result clearly showed that STA gives very high fidelity in relatively small evolution time compared with

the adiabatic method. We also use the parity symmetry to convert the non-local Hamiltonian to the local Hamiltonian.

Chapter 5

Quantum optimal control

This chapter is the central part of my dissertation.

5.1 Introduction

Quantum optimal control (QOC) is a numerical technique which helps to design optimal pulses to steer the dynamics of quantum systems in a controlled manner satisfying a given set of constrains [116–118]. The QOC theory was introduced in the late 1980s [118] to design strategies to control the electromagnetic field profiles. Different and sophisticated strategies have been developed thereafter to control and manipulate the dynamics of quantum systems. One important example is the Krotov method, which was developed by Tannor and coworkers based on Krotov's initial work, which was later introduced as Krotov algorithm by Sklarz *et al.* [119]. This method is still an active field of research. In the initial period, QOC theory was mainly concerned with optimization of state transfer and optimization of the expectation value of an operator. However, after the 2000s, with rapid progress in quantum information science and unprecedented success in controlling and manipulating individual quantum systems, applications of QOC theory have been ranging from quantum state preparation, quantum simulation, quantum sensing to controlling chemical reactions [120, 121]. In recent years, people have developed QOC theory to control dynamics of an open quantum systems and are actively exploring applicability

of QOC theory for quantum error correction [122–126].
Different conditions have to be satisfied to achieve a QOC solution. For example, for a finite energy control pulse, a unitary transformation can not be achieved arbitrarily fast. The time-energy uncertainty bound, known as quantum speed limit(QSL), constrains the speed of the process [127–129, 133, 134]. Similarly, information contained in the control pulse should be sufficient to steer the dynamics of the quantum system to the target state. From an experimental prospective, the control pulses should be smooth (i.e. bandwidth limited) for to be implemented in experiments [130–132]. This gives rise to different sophisticated QOC algorithms to make a band-width limited few parameter ansatz for the solution. The comprehensive review of QOC methods can be found in these references [117, 124, 132].

5.2 Controllability of quantum system

The controllability of quantum systems is a fundamental issue in most of the control problems. The controllability is associated with the reachability to the target state. This problem has fundamental importance because of its close connection to the universality of quantum computation and the possibility of achieving atomic or molecular scale transformations [135]. There are different notions of controllability such as pure state controllability, operator controllability, and eigenstate controllability. For a finite dimensional quantum system, the controllability criteria can be expressed in terms of the structure and the rank of the corresponding dynamical Lie group and Lie algebra [117]. Finding rank of a dynamical Lie group and Lie algebra is a difficult task for an infinite dimensional and open quantum system. The basic introduction of the Lie group and Lie algebra is given in appendix B.
For a controllable quantum system, developing good control strategies is essential to accomplish a given control tasks. For a coherent quantum system, different open-loop coherent control strategies based on applying semi-classical potentials have been developed to preserve coherence in the system. Examples range from the application of open-loop control strategies to achieve a given objective in physical chemistry [136,137], to improve sensitivity of multidimensional nuclear magnetic resonance

(NMR) [138–140]. Similarly, closed-loop control based on the application of control algorithms in actual experiment has also been developed [141, 142]. This method involves the application of laser pulses to the sample and the subsequent observation of its impact. The laser pulses are then optimize by analyzing the output of the experiment. A good closed-loop control strategy requires to be insensitive to the initial trials and the process should converge to achieve a given control objective [141, 142]. In control problems, the control objective is usually formulated in terms of an optimal control problem by converting the problem into a problem of optimizing a functional of the quantum states, control inputs, control time, and the problem is solved iteratively using different algorithms.

5.3 Formulation of QOC problem

QOC problems are formulated in terms of extremization of a cost functional J which maps the resulting state trajectory of a system driven by a control pulse $u(t)$ to $\mathbb{R}^1$. In most of the cases, the initial state is given and the cost functional J would be the functional of the final state. QOC starts with separating the given Hamiltonian into two parts: time independent drift part and time dependent control part [117,134]. We cannot control the drift part and different control algorithms are applied to optimize the time dependent parameter of the control Hamiltonian i.e.

$$H(t) = H_0 + u(t)H_1 \tag{5.1}$$

here H_0 is the drift Hamiltonian, and H_1 is the control Hamiltonian which depends on time via the time dependent parameter $u(t)$.

State to state transfer problem

In state to state transfer control problems, the goal is to drive the initial state $|\psi_0\rangle$ to the target state $|\psi_t\rangle$ in a minimal time T with fidelity closed to one [117,143]. The

closed quantum system evolves according to the Schrödinger equation ($\hbar = 1$) i.e.

$$\frac{\partial}{\partial t}|\psi(t)\rangle = -iH(t)|\psi(t)\rangle, \qquad |\psi(t=0)\rangle = |\psi_0\rangle. \tag{5.2}$$

The control problem is formulated as a maximization of fidelity i.e. $\mathbb{J}$:

$$\underset{u(.)}{max} \;\; \mathbb{J} = |\langle\psi(T)|\psi_t\rangle|^2 \tag{5.3}$$

This is also equivalent to minimization of infidelity $\mathbb{I}((1 - |\langle\psi(T)|\psi_t\rangle|^2))$

$$\underset{u(.)}{min} \;\; \mathbb{I} = (1 - \langle\psi(T)|\psi_t\rangle|^2) \tag{5.4}$$

Observable optimization problem

In this kind of optimization problems, the expectation value of some observable O is formulated in terms of the cost functional $\mathbb{J}$. The cost functional can be evaluated either at the final time or averaged over the whole time interval $[0, T]$ i.e.

$$\begin{aligned} \mathbb{J} &= \langle\psi(T)|O|\psi(T)\rangle \\ \mathbb{J} &= \frac{1}{T}\int_0^T \langle\psi(T)|O|\psi(T)\rangle dt \end{aligned} \tag{5.5}$$

and optimization is performed using different optimization algorithms [144].

Unitary gate optimization problem

Due to decoherence and control errors in current quantum devices, performing the unitary evolution in a faster and more efficient manner is essential. Different approaches to define the cost functional and its optimization have been developed [144–146]. Two

common approaches to define the cost functional are

$$\begin{aligned} \mathbb{J} &= \frac{1}{N} Re\{Tr(V^\dagger U(T))\} \\ \mathbb{J} &= \frac{1}{N^2} |\sum_{i=1}^{N} \langle \xi_i | V^\dagger | \psi_i(T) \rangle|^2. \end{aligned} \tag{5.6}$$

Here V is the target Unitary and $U(T)$ is the time evolved unitary. N represents the number of basis states. $|\xi_i\rangle$ and $|\psi_i(T)\rangle$ are the initial and the final states which are connected by the unitary operator $U(T)$.

Entanglement maximization problem

Quantum entanglement is associate with the inseparability of two or more systems into local subsystems [21, 147]. There are different notions of entanglement measurement and all such measurements need to be invariant with respect to local transformations. For a mixed state ρ with fraction ω_i in the pure state $|\psi_i\rangle$ defining an ensemble, we quantify an entanglement by the von Neumann entropy

$$S(\rho) = -\sum_i \omega_i log(\omega_i) = -tr(\rho log(\rho)). \tag{5.7}$$

To achieve the control objective, the cost function is defined as $\mathbb{J} = S(\rho(T))$ and the optimization is performed using different algorithms.

5.4 Different QOC algorithms

To obtain an optimal pulse $u^*(t)$ which satisfies a given constraint and is robust to noise in the system, different iterative numerical algorithms have been developed. We have mentioned some leading algorithms in this section.

5.4.1 GRAPE algorithm

Gradient Ascent Pulse Engineering (GRAPE) is the simplest optimal control algorithm based on the steepest ascent method [148]. In this method, fidelity is defined as a cost function i.e.

$$\mathbb{J}(\vec{u}) = |\langle\psi_t|\psi(T)\rangle|^2 \tag{5.8}$$

In the first step, the control pulse $u(t)$ is discretized into M time steps i.e.

$$\begin{aligned} \vec{u} =&(u(t_1), u(t_2), ..., u(t_M)) = (u_1, ..., u_j, ...u_M) \\ & j \in [1:1:length(t)]. \end{aligned} \tag{5.9}$$

Since the Hamiltonian of the system is $H(t) = H_0 + u(t)H_1$, the evolution operator at each t_j can be written as:

$$\hat{\mathbb{U}}_j \equiv \hat{\mathbb{U}}(u(t_j)) = e^{-i(H_0+u(t_j)H_1)\Delta t} \tag{5.10}$$

The gradient of the fidelity is calculated as:

$$\nabla_{\vec{u}}\mathbb{J}(\vec{u}) = \begin{pmatrix} \frac{\partial}{\partial u_1} \\ . \\ . \\ \frac{\partial}{\partial u_j}. \\ . \\ . \\ \frac{\partial}{\partial u_M} \end{pmatrix} \mathbb{J}(\vec{u}). \quad j \in [1:1:length(\vec{t})]. \tag{5.11}$$

With the following definitions and identities

1. Define $c \equiv \langle\psi_t|\psi(T)\rangle \implies \mathbb{J} = c^*c$
2. Define $\langle\chi(T)| \equiv -i\langle\psi(T)|\psi_t\rangle.\langle\psi_t|$
3. Forward evolution $|\psi(t_j)\rangle = \Pi_{j'=1}^{j}\hat{\mathbb{U}}_{j'}|\psi(0)\rangle$
4. Backward evolution: $|\psi(t_j)\rangle = \Pi_{j'=M-1}^{j}\hat{\mathbb{U}}_{j'}^{\dagger}|\psi(T)\rangle$

and some algebra we can get

$$\frac{\partial}{\partial u_j}\mathbb{J}(\vec{u}) = 2\Delta t Re(\langle\chi(t_j)|\frac{\partial H(u_j)}{\partial u_j}|\psi(t_j)\rangle) \tag{5.12}$$

The full gradient $\nabla_{\vec{u}}\mathbb{J}(\vec{u})$ can be calculated using the following steps:

1. Starting from $|\psi(0)\rangle = |\psi_{init}\rangle$, calculate $|\psi(t_j)\rangle$ by forward propagating over the current $\vec{u}$

2. Starting from $|\chi(T)\rangle = i\langle\psi(T)|\psi_t\rangle|\psi_t\rangle$, calculate all $|\chi(t_j)\rangle$ by backward propagation over the current $\vec{u}$

3. Calculate $\frac{\partial H(u)}{\partial u}$ analytically and evaluate its value for every element in current $\vec{u}$

Once the gradient is calculated efficiently, next step is to optimize the parameters by using steepest ascent with linesearch [143, 144] i.e. at iteration k calculate the local gradient $\nabla_{\vec{u}}\mathbb{J}(\vec{u}_k)$ and find the best stepsize α_k

$$\vec{u}_{k+1} = \vec{u}_k + \alpha_k \nabla_{\vec{u}}\mathbb{J}(\vec{u}_k) \tag{5.13}$$

such that

$$\mathbb{J}(\vec{u}_{k+1}) \geq \mathbb{J}(\vec{u}_k) \tag{5.14}$$

under the boundary condition

$$\begin{aligned} u(0) =& u_{init} && \text{(fixed)} \\ u(T) =& u_{final} && \text{(fixed)} \\ |\psi(0)\rangle =& |\psi_{init}\rangle && \text{(fixed)} \\ |\chi(T)\rangle =& i\langle\psi(T)|\psi_t\rangle|\psi_t\rangle && (|\psi(T)\rangle \quad \text{produce by} \quad \vec{u}). \end{aligned} \tag{5.15}$$

To deal with the limited computing time, we can use several stopping criteria for the optimization algorithm. Some of them are

- $\mathbb{J}(\vec{u}_k) > \mathbb{J}_{\text{threshold}}$

- Iteration number k exceeds maximum number of iterations
- Norm of gradient is very small
- Difference of fidelity between iteration $k+1$ and k is too small

The rigorous derivation of the GRAPE algorithm and its implementation in QOC problems can be found in these references [133, 134, 148].

5.4.2 Krotov algorithm

The Krotov method is based on a variational principle [133, 134, 146]. The two main branches of Krotov algorithms for the QOC were developed by Tannor *et al.* [149] and by Zhu and Rabitz [150]. The design principle of Tannor *et al.* is to sweep forward in time by updating the control $u(t)$ and state trajectory $|\psi(t)\rangle$ simultaneously. Controls are updated by

$$u^{(k+1)}(t) = u^{(k)}(t) + \alpha S(t) Re\{\langle \chi^k(t)| \frac{\partial H}{\partial u^k} |\psi^{(k+1)}(t)\rangle\}. \tag{5.16}$$

Here, k represents the number of iterations. $|\chi^k(t)\rangle$ is the costate at k^{th} the iteration obtained by backward propagation of the Schrödinger equation. The parameter α is the search length parameter, which directly affects the convergence speed. Similarly, $S(t)$ is the shape function $0 \leq S(t) \leq 1$, which allows for smooth turning on and off at the boundaries. Zhu and Rabitz principle is different from Tannor *et al.* in a sense that they applied the sweeping procedure for backward propagation too [149, 151]. The gradient of H with respect to u is calculated like in the GRAPE method.
In the Krotov method, regularization term R is added in the cost functional to achieve a monotonic convergence of the cost functional. One widely used regularization term is:

$$R = -\frac{\gamma}{2} \int_0^T u^2(t) dt \tag{5.17}$$

where the parameter $\gamma > 0$ balances the trade off between the small control amplitudes and high fidelity values. Similarly, an alternative regularization term is:

$$R = -\frac{\gamma}{2}\int_0^T (u^k(t) - u^{(k-1)}(t))^2 dt \tag{5.18}$$

which is based on the difference of pulse amplitudes between successive iterations. A proof of monotonic convergence can be found in [152]. The rigorous derivation of the Krotov method and its implementation in QOC problems can be found in these references [134, 149–151].

5.4.3 Machine learning inspired QOC algorithms

In recent years, inspired by unprecedented success of machine learning algorithms in different fields, different QOC methods based on machine learning algorithms have been developed [153–157]. Most of these QOC methods are based on reinforcement learning (RL) in which an agent dynamically interacts with an environment with the goal of performing certain task. Based on the nature of the problem, a discrete set of interactions between the agent and the environment is assumed. During each interaction, an agent observes the state of the environment and performs a certain action. The state of the environment for the next interaction is determined by the performance of the agent to complete an assign task. The reward is provided to the agent based on the performance, which helps to update the behavior of the agent to improve its performance [154]. Different algorithms have been developed to teach the RL agent to find the optimal protocol. Some examples are action critic algorithm [158], Q-learning algorithm [159], policy gradient [154] algorithm.

5.4.4 Chopped random basis algorithms

The Chopped random basis (CRAB) algorithm was initially developed by P. Doria *et al.* in the context of controlling the dynamics of nonintegrable quantum many-body systems [132, 160, 161]. In this method, the admissible controls are parameterized by a set of smooth functions i.e. we expand the control field in a suitable, truncated

orthogonal function basis $\{f_i(t)\}$

$$u(t) = \sum_{i=1}^{N_{cut}} c_i f_i(t). \tag{5.19}$$

Here, the c_i are real coefficients subjected to optimization and N_{cut} is the cut off value of the truncated orthogonal function basis. This algorithm has advantages over the GRAPE and the Krotov algorithm in that it can solve both open-and close- loop control problems without requiring analytical computation beforehand and does not require to do backward propagation. This method is inspired by the fact that in most of the control problems the high quality solutions often lie in low dimensional subspace inside the space of admissible controls, hence, a proper lower dimensional parametrization of control space have no effect on quality of optimal solution [162]. In the CRAB algorithm, the optimization is performed using standard direct search algorithms like the Nelder-Mead simplex algorithm [163], Powell's method [164], parallel simplex [165], Monte Carlo optimization [166] or by gradient based algorithms like gradient optimization of analytic controls (GOAT) [167], gradient optimization using parametrization (GROUP) [168].

5.5 Quantum optimal control on JC lattices

5.5.1 CRAB algorithm in JC lattices

The time dependent Hamiltonian representing the JC lattices in the rotating wave approximation can be written as ($\hbar = 1$):

$$H(t) = \Delta H_{\mathrm{d}} + g(t) H_{\mathrm{g}} - J(t) H_{\mathrm{J}}. \tag{5.20}$$

Here, an uncontrollable drift part of H(t) is

$$H_{\mathrm{d}} = \sum_{i=1}^{N} a_{\mathrm{i}}^{\dagger} a_{\mathrm{i}}$$

and the time dependent control parts of H(t) are

$$H_{\mathrm{g}} = \sum_{i=1}^{N}(a_{\mathrm{i}}^{\dagger}\sigma_{\mathrm{i}}^{-} + a_{\mathrm{i}}\sigma_{\mathrm{i}}^{+}); H_{\mathrm{J}} = \sum_{i=1}^{N}(a_{\mathrm{i}}^{\dagger}a_{\mathrm{i+1}} + a_{\mathrm{i+1}}^{\dagger}a_{\mathrm{i}}).$$

Δ is the detuning between the cavity mode(ω_{c}) and the qubit(ω_{q}) i.e. $\Delta = \omega_{\mathrm{c}} - \omega_{\mathrm{q}}$. $a_{\mathrm{i}}^{\dagger}(a_{\mathrm{i}})$ is the creation(annihilation) operator of the i^{th} cavity and $\sigma_{\mathrm{i}}^{+}(\sigma_{\mathrm{i}}^{-})$ is the raising (lowering) operator of Pauli matrices of i^{th} qubit. The qubit is coupled to the cavity via electric dipole coupling with coupling strength $g(t)$ and adjacent cavities are connected by photon hopping with hopping strength $J(t)$. The parameters $g(t)$ and $J(t)$ are time dependent control parameters. The competition between onsite interaction $g(t)$ and photon hopping $J(t)$ leads to second order quantum phase transition between the Mott Insulator (MI) and Superfluid phases.The different phases in the system is characterized by spatial correlation which is measured by the single particle density matrix

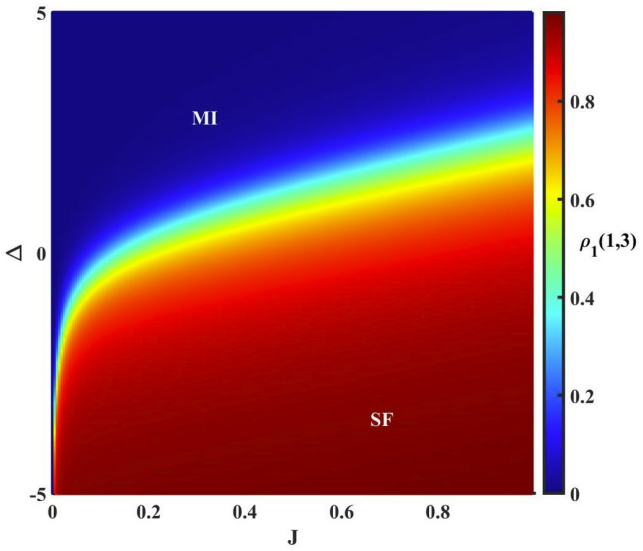

Figure 5.1: **Single particle density matrix $\rho_1(1,3)$ vs hopping rate J**

$$\rho_1(i,j) = \langle GS|a_i^{\dagger}a_j|GS\rangle / \langle GS|a_i^{\dagger}a_i|GS\rangle \tag{5.21}$$

with $|GS\rangle$ representing the many-body ground state. The spatial correlation decreases algebraically and exponentially with the spatial separation $|i-j|$ in the SF and MI phases respectively. In this section we focus on the many-body ground state preparation of JC lattice in targeted region using quantum optimal control with the CRAB algorithm.

The many-body state preparation process starts with preparing an initial state $|\psi(0)\rangle$ in the deep superfluid region using quantum engineering. The detail engineering process is discussed in chapter 3 or can be found in this paper [106]. Once the initial state is prepared, the goal is to prepare the many-body ground state in the targeted region by driving the initial state to the target region using control parameters $g(t)$ and $J(t)$. For a numerical simulation, we define the target state $|\psi_t\rangle$ in the Mott insulating region. Our goal is to reach the target state in a minimum evolution time T_{Th} with the fidelity above 0.99. Since we need to pass through the critical region during this process, the fidelity of the state preparation would be very low for a small evolution time. Fidelity gets improved for a longer evolution time. However, from experimental perspective, a long evolution time adds noises in the system which eventually decreases the fidelity. In this scenario, to find the optimal control pulses for the state preparation, we formulate the state preparation in terms of a numerical optimization problem. For this, we define cost functional $\mathbb{F} = |\langle\psi(t=T)|\psi_{\mathrm{t}}\rangle|^2$ and the goal is to maximize it i.e.

$$\max_{g(.),J(.)} \mathbb{F} = |\langle\psi(t=T)|\psi_{\mathrm{t}}\rangle|^2 \tag{5.22}$$

This is also equivalent to minimizing

$$\min_{g(.),J(.)} \mathbb{I} = (1-\mathbb{F}) \tag{5.23}$$

where $\mathbb{I}$ is called the infidelity. To achieve this goal, we expand the control pulses $g(t)$

and $J(t)$ in the truncated Fourier basis by keeping upto 8^{th} harmonics:

$$\begin{aligned} g(t) &= g_0(t) + S(t)\sum_{\mathrm{k=1}}^{\mathrm{K=8}}\{c_{\mathrm{k},1}cos[k(1+\omega_{1,\mathrm{k}})t/T] + c_{\mathrm{k},2}sin[k(1+\omega_{1,\mathrm{k}})t/T]\} \\ J(t) &= J_0(t) + S(t)\sum_{\mathrm{k=1}}^{\mathrm{K=8}}\{d_{\mathrm{k},1}cos[k(1+\omega_{2,\mathrm{k}})t/T] + d_{\mathrm{k},2}sin[k(1+\omega_{2,\mathrm{k}})t/T]\} \end{aligned} \tag{5.24}$$

Here $g_0(t)$ and $J_0(t)$ are the adiabatic trajectories, which are defined as:

$$\begin{aligned} g_0(t) &= g(0) + [(g(T) - g(0))t/T] \\ J_0(t) &= J(0) + [(J(T) - J(0))t/T]. \end{aligned} \tag{5.25}$$

$g(0)(J(0))$ and $g(T)(J(T))$ are the initial and the target value of the parameter g(t)(J(t)). Similarly, $S(t)$ is the shape function defined as $S(t) = [1 - cos(2t/n)]$ which is zero at $t = 0$ and $t = T = n\pi$. $c_{\mathrm{k},1}(d_{\mathrm{k},1})$ and $c_{\mathrm{k},2}(d_{\mathrm{k},2})$ are Fourier amplitudes corresponding to the cosine and sine components of the k^{th} harmonics of $g(t)(J(t))$. $(1+\omega_{1,k})((1+\omega_{2,k}))$ are the k^{th} base frequencies corresponding to $g(t)(J(t))$. In order to bound the control parameters, the parameters are restricted by applying constraints

$$g(t) = \begin{cases} g(t) & \text{if } |g(t)| < g_{\max} \\ sign[g(t)]g_{\max} & \text{if } |g(t)| \geq g_{\max} \end{cases} \tag{5.26}$$

$$J(t) = \begin{cases} J(t) & \text{if } |J(t)| < J_{\max} \\ sign[J(t)]J_{\max} & \text{if } |J(t)| \geq J_{\max} \end{cases} \tag{5.27}$$

The algorithmic flow diagram is shown in the Fig.(5.2).

5.5.2 Numerical Results

For a numerical simulation, we consider JC lattices with four sites having four polariton excitations. The JC lattices undergo second order quantum phase transitions

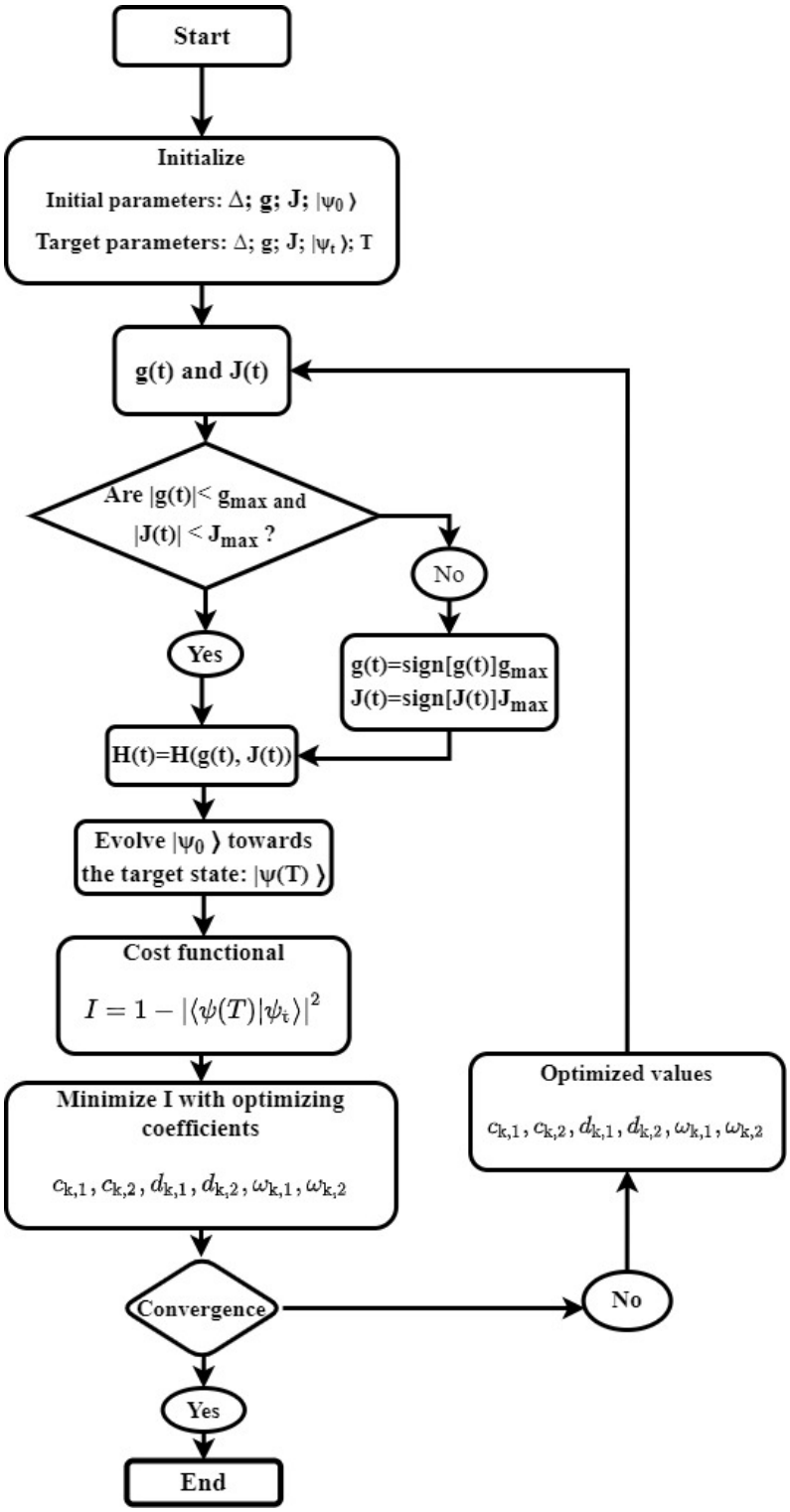

Figure 5.2: **Optimization of time dependent parameters using the CRAB algorithm**

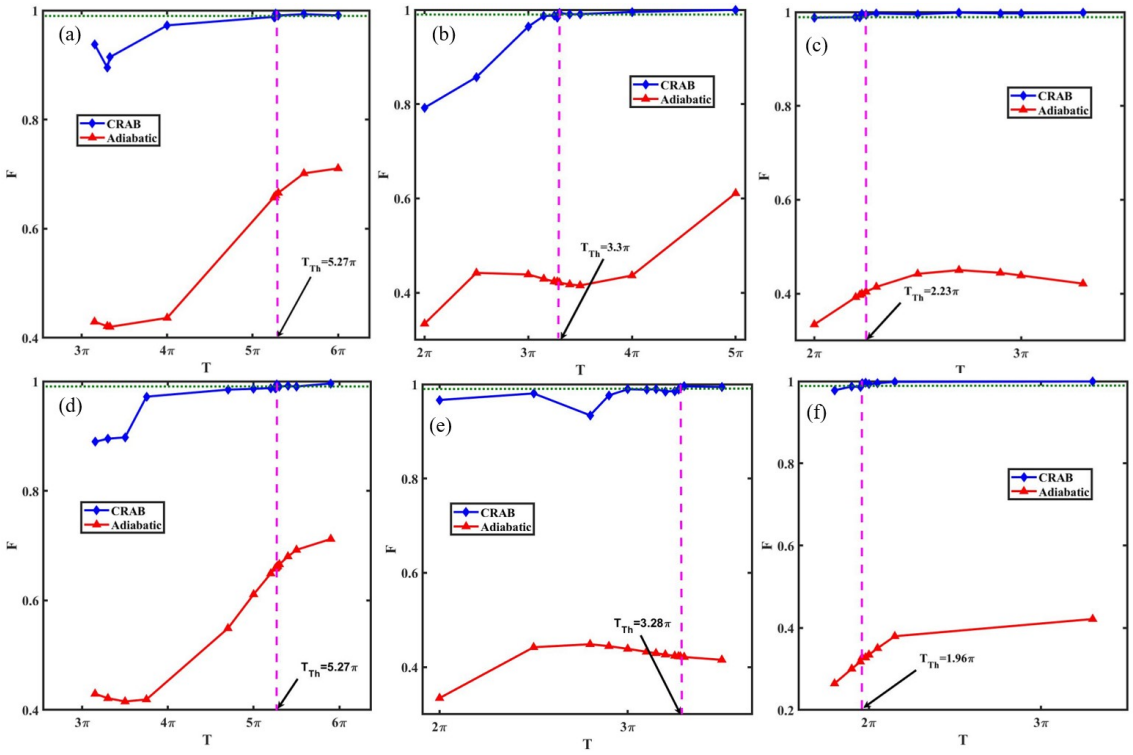

Figure 5.3: **Fidelity corresponding to the CRAB algorithm and the adiabatic algorithm for different evolution times and for different sets of constraints with a.** $g_{\max}=1, J_{\max}=1$. **b.**$g_{\max}=2, J_{\max}=1$. **c.**$g_{\max}=4, J_{\max}=1$.**d.** $g_{\max}=1, J_{\max}=2$. **e.** $g_{\max}=2, J_{\max}=2$. **f.** $g_{\max}=4, J_{\max}=2$. Green dotted line represents the fidelity 0.99.

between the Mott Insulating phase and the Superfluid (SF) phase at integer fillings. To start the simulation, we prepare an initial state $|\psi_0\rangle$ as a ground state in the deep SF phase with parameters $\Delta=0$, $g(0)=0$, $J(0)=0.5$, and define the target state $|\psi_t\rangle$ in the deep MI phase with parameters $\Delta=0$, $g(T)=1$, $J(T)=0.02$. The system is driven along the trajectory defined by the evolution of the control pulses defined in Eq.((5.24)). The cost functional i.e. infidelity (defined in Eq.((5.23))) is minimized with respect to the Fourier amplitudes and base frequencies i.e. $c_{k,1}$, $c_{k,2}$, $d_{k,1}$, $d_{k,2}$, and, $\omega_{1,k}$ and $\omega_{2,k}$. The optimization is performed using a standard optimization software package developed by MathWorks.

To achieve high fidelity state preparation in an optimal time, we optimize infidelity

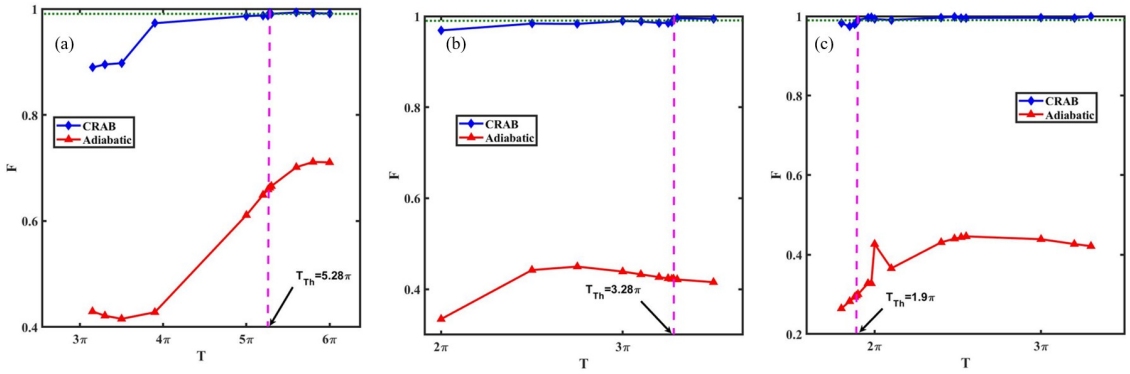

Figure 5.4: **Fidelity corresponding to the CRAB algorithm and the adiabatic algorithm for different evolution times and for different sets of constraints a.** $g_{\max} = 1, J_{\max} = 4$. **b.**$g_{\max} = 2, J_{\max} = 4$. **c.**$g_{\max} = 4, J_{\max} = 4$.Green dotted line represents the fidelity 0.99.

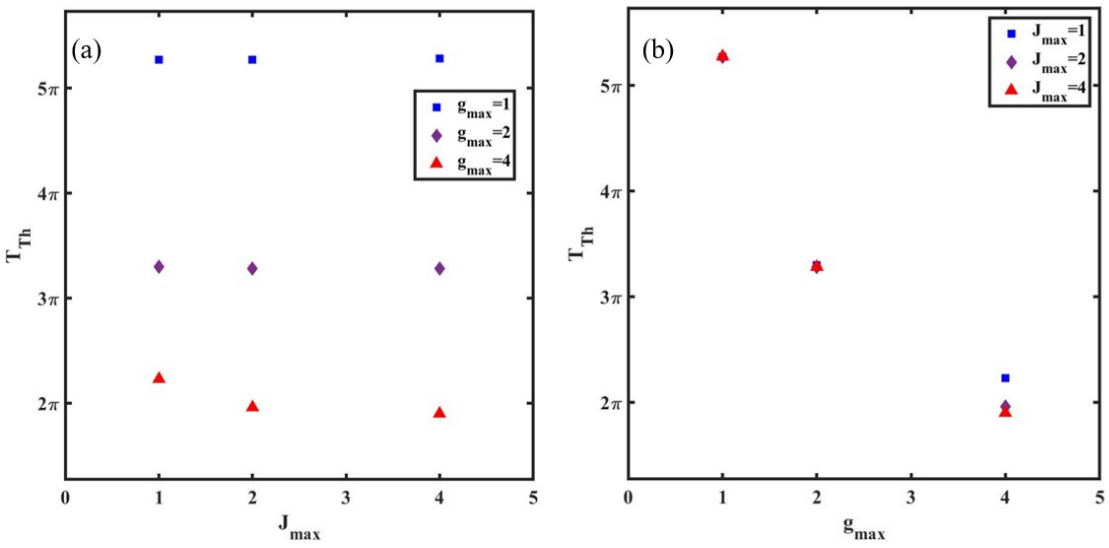

Figure 5.5: **Plot of threshold time for different set of constraintsa.**T_{Th} vs $J_{\max}$. **b.**T_{Th} vs $g_{\max}$

.

Table 5.1: Minimal time to reach a fidelity greater than 0.99 with the CRAB algorithm and the corresponding fidelity without CRAB algorithm

Constraints	T_{Th}	**With CRAB**	**without CRAB**
$J_{\max}=1, g_{\max}=1$	5.27π	0.9944	0.6610
$J_{\max}=1, g_{\max}=2$	3.30π	0.9932	0.4213
$J_{\max}=1, g_{\max}=4$	2.23π	0.9963	0.3995
$J_{\max}=2, g_{\max}=1$	5.27π	0.9944	0.6610
$J_{\max}=2, g_{\max}=2$	3.28π	0.9927	0.4223
$J_{\max}=2, g_{\max}=4$	1.96π	0.9954	0.3276
$J_{\max}=4, g_{\max}=1$	5.28π	0.9925	0.6626
$J_{\max}=4, g_{\max}=2$	3.28π	0.9927	0.4223
$J_{\max}=4, g_{\max}=4$	1.90π	0.9904	0.3001

with different values of total evolution time T and find the minimal time T_{Th} to reach infidelity below 0.01. We fix the tolerance of the function value to 10^{-10}, the tolerance of the input variables to 10^{-10} and the maximum number of allowed iterations to 150000. We bound the amplitude of control pulses by applying a set of constraints. Fig.(5.3) and Fig.(5.4) represents a plot of fidelity (F) as a function of evolution time (T). The blue curve represents the fidelity corresponding to the CRAB algorithm with a different set of constraints. Similarly, the red curve represents the fidelity corresponding to the adiabatic algorithm [106]. The plots show that the CRAB algorithm gives high fidelity compared to the adiabatic algorithm for a small evolution time. For example, when $g_{\max}=2$ and $J_{\max}=1$, the fidelity is greater than 0.99 for the CRAB algorithm when the minimal evolution time is $T_{\mathrm{Th}}=3.30\pi$. In a meantime, the fidelity is 0.4213 at $T_{\mathrm{Th}}=3.30\pi$ for the adiabatic algorithm. Fig.(5.5) is the plot of minimum (threshold) time for different sets of constraints. The plot shows that the threshold time is sensitive to $g_{\max}$.

Fig.(5.6) represents the optimization path of the Fourier coefficients $c_{\mathrm{k},1}$, $c_{\mathrm{k},2}$, $d_{\mathrm{k},1}$, $d_{\mathrm{k},2}$, $\omega_{1,\mathrm{k}}$, and $\omega_{2,\mathrm{k}}$ at $T_{\mathrm{Th}}=3.30\pi$ for a set of constraints $g_{\max}=2$ and $J_{\max}=1$. The Fourier parameters are optimized after 43194 iterations. The optimized values of parameters are used to calculate the instantaneous fidelity for the CRAB method and they are compared with the instantaneous fidelity given by the adiabatic method.

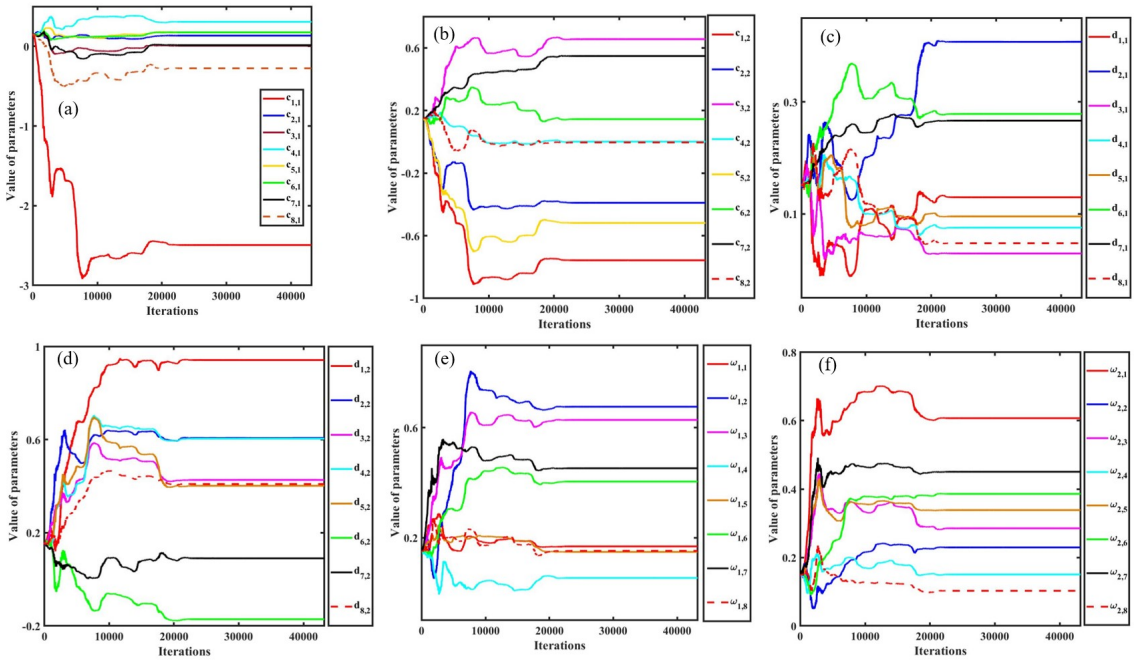

Figure 5.6: **Optimization of time dependent parameters using the CRAB algorithm for $g_{\max} = 2$ and $J_{\max} = 1$ at $T_{\text{Th}} = 3.3\pi$. a.**$c_{\text{k},1}$. **b.**$c_{\text{k},2}$. **c.**$d_{\text{k},1}$. **d.**$d_{\text{k},2}$. **e.**$\omega_{1,\text{k}}$. **f.**$\omega_{2,\text{k}}$

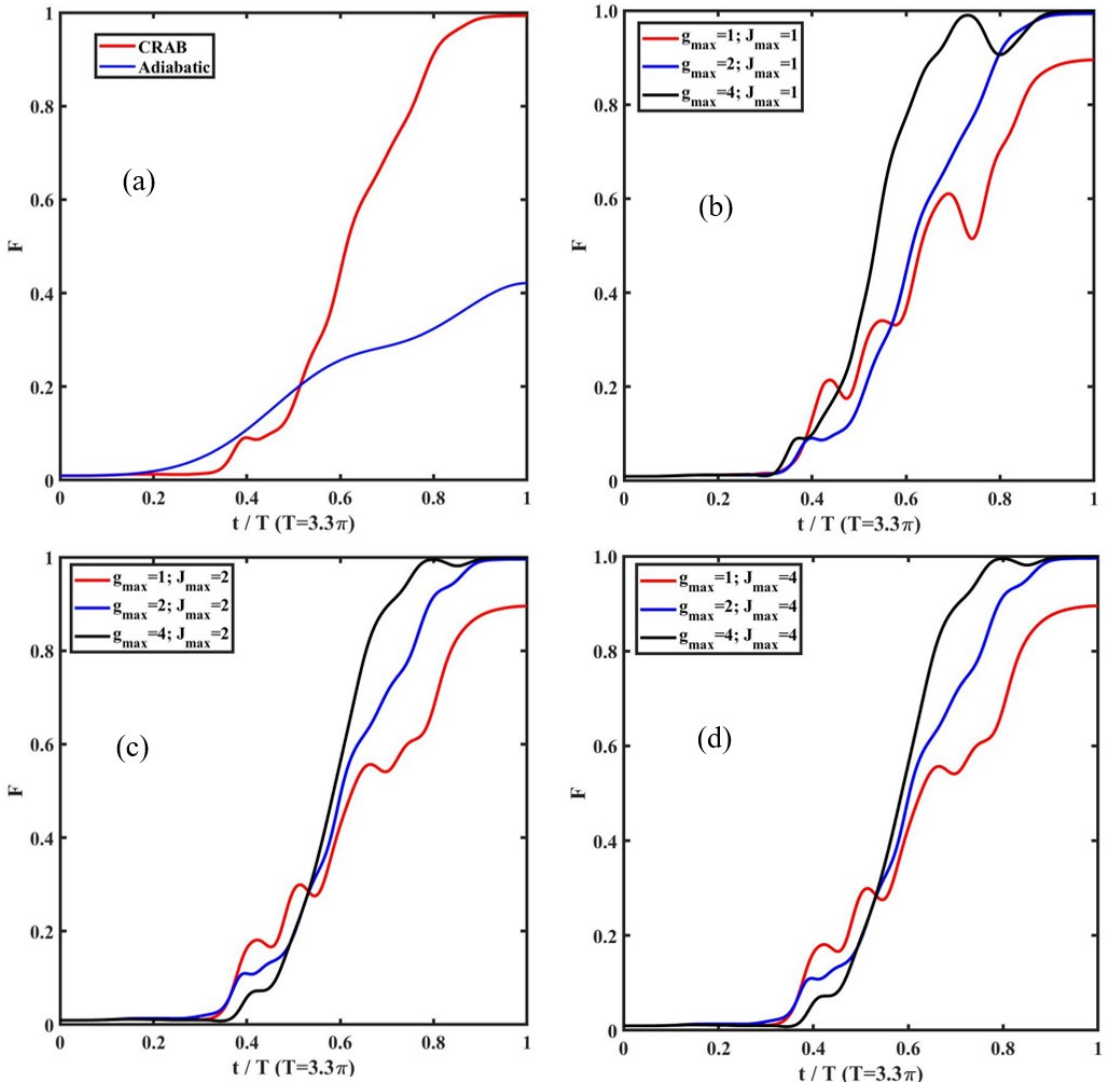

Figure 5.7: **Fidelity vs time $T = 3.3\pi$ for different set of constraints**. **a.** Comparison of instantaneous fidelity for CRAB algorithm and adiabatic algorithm when $g_{\max} = 2$ and $J_{\max} = 1$. **b.** Instantaneous fidelity for $J_{\max} = 1$ and $g_{\max} = 1, 2, 4$. **c.** Instantaneous fidelity for $J_{\max} = 2$ and $g_{\max} = 1, 2, 4$. **d.** Instantaneous fidelity for $J_{\max} = 4$ and $g_{\max} = 1, 2, 4$

Fig.(5.7) is a plot of the instantaneous fidelity for different sets of constraints at fixed evolution time $T = 3.30\pi$. Fig.(5.7(a)) is a plot of the instantaneous fidelity with time for a set of constraints $g_{\max} = 2$ and $J_{\max} = 1$. It shows that initially there is no improvement in the fidelity with the CRAB algorithm as compared to the adiabatic algorithm but after $0.5T$ the fidelity increases rapidly and attains the value 0.9932 at $T = 3.30\pi$. Fig.(5.7(b – d)), shows that T_{Th} depends on the relative strength of constraints $g_{\max}$ and $J_{\max}$. For a small value of $g_{\max}$ compared to $J_{\max}$, the time required to reach a fidelity above 0.99 is longer. Similarly, for a larger value of $g_{\max}$ compared to $J_{\max}$, it is smaller. In order to get insight into how T_{Th} depends on constraints, we evaluate minimal time required to reach the fidelity$\geq$ 0.99 for a given set of constraints with the CRAB algorithm and compare the results with the fidelity corresponding to the time obtained with the adiabatic protocols. The result is summarized in the Table 5.1.

Fig.(5.8) and Fig.(5.9) represents the evolution of the control parameters $g(t)$ and $J(t)$ with a given set of constraints $g_{\max}$ and $J_{\max}$ at fixed $T = 3.30\pi$. The plots show that the value of control parameters decreases and gains negative values in the initial phase but increases sharply in the region $0.3T$ - $0.5T$ to gain the maximum positive value. The value of control parameters decreases in the end phase. The maximum positive value of $g(t)$ is greater than the maximum positive value of $J(t)$ when the evolution time T is equal or greater than T_{Th} for the given set of constraints. However, if the evolution time T is small than T_{Th} for the given set of constraints, maximum positive value of $J(t)$ is larger or equal to the maximum positive value of $g(t)$.

Fig. 5.10 represents a plot of the instantaneous energy gap between the ground state and the first symmetric excited state for the evolution time $T = 3.30\pi$ in the presence of the given set of constraints to the control parameters. The plots show that for the same value of $J_{\max}$ but different values of $g_{\max}$, the minimum value of the energy gap in the beginning phase is small for a larger $g_{\max}$. Energy gap increases after attaining the minimum value. In the interval $0.3T$ - $0.5T$, the energy gap increases sharply to the maximum value. The maximum value of the energy gap depends on the value of $g_{\max}$. If $g_{\max}$ is large, the maximum value of the energy gap is large. The increase in energy gap is consistent with the increase in value of control parameters. After

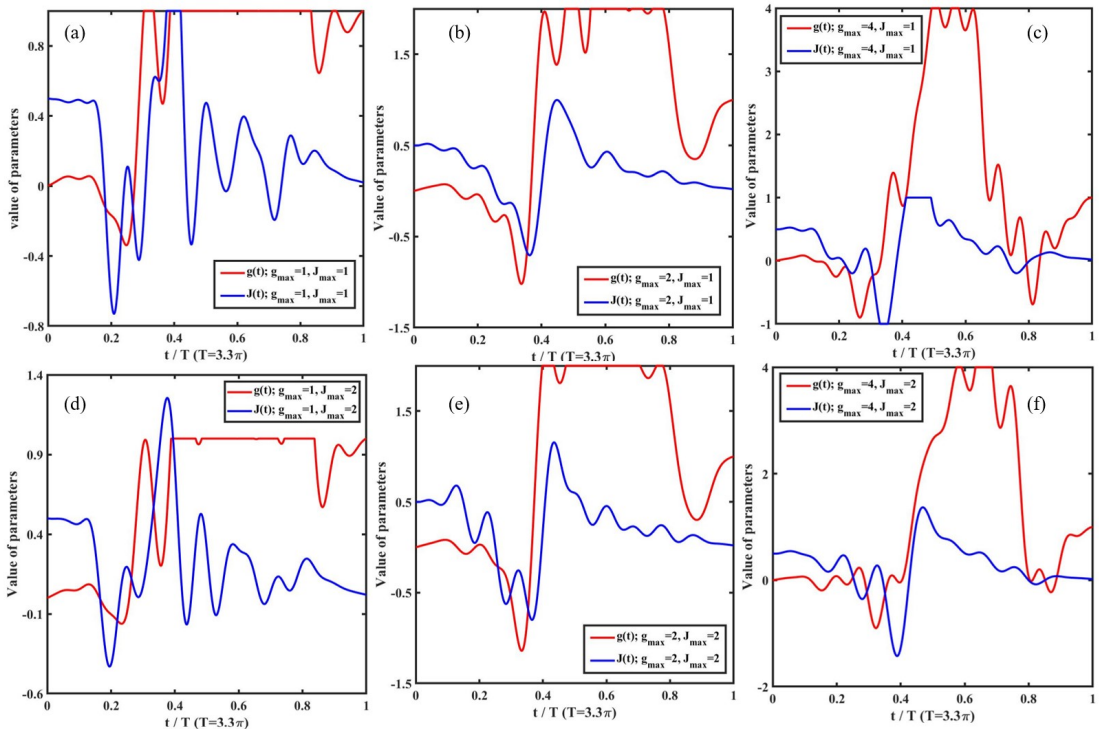

Figure 5.8: **Evolution of control parameters** $g(t)$ **and** $J(t)$. **a.** $g_{\max} = 1, J_{\max} = 1$. **b.** $g_{\max} = 2, J_{\max} = 1$. **c.** $g_{\max} = 4, J_{\max} = 1$. **d.** $g_{\max} = 1, J_{\max} = 2$. **e.** $g_{\max} = 2, J_{\max} = 2$. **f.** $g_{\max} = 4, J_{\max} = 2$

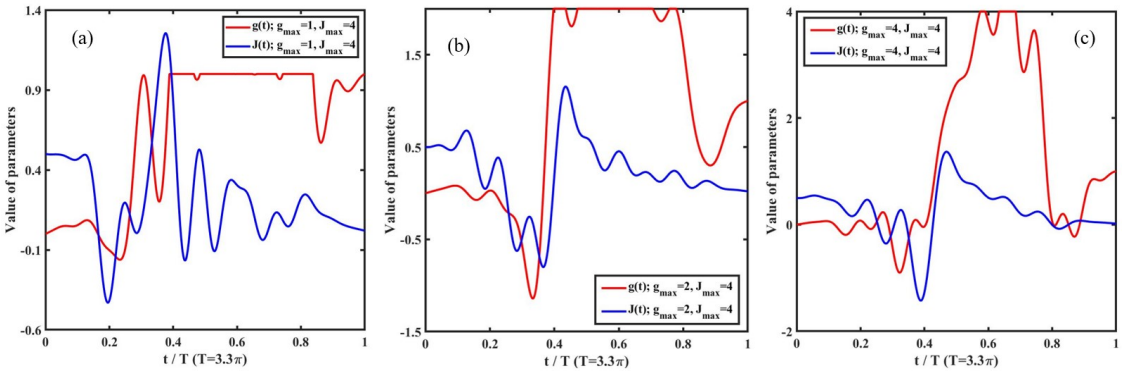

Figure 5.9: **Evolution of control parameters** $g(t)$ **and** $J(t)$. **a.** $g_{\max} = 1, J_{\max} = 4$. **b.** $g_{\max} = 2, J_{\max} = 4$. **c.** $g_{\max} = 4, J_{\max} = 4$.

attaining the maximum value the energy gap decreases and reach to the minimum value in the interval $0.7T$ - $0.9T$. The energy gap then increases for the remaining time interval $0.9T$ - $1T$. Fig. 5.10(d) represents the instantaneous energy gap for the same set of constraints at their corresponding optimal time T_{Th}. Occurrence of minimum energy gap between the ground state and first symmetric excited state at the beginning and end phases of the evolution can be explained based on diabatic excitation [169, 170]. In a pure state transfer for a driven quantum system, there exists several state trajectories which connects the initial state and the target state. How fast the state changes occurs along the state trajectory can be characterized by the rate of change of Wotter's distance [171–173]

$$\theta(|\psi_0\rangle, |\psi_{\mathrm{t}}\rangle) = 2arccos(\sqrt{F}) \tag{5.28}$$

i.e.

$$\frac{d\theta}{dt} = 2\Delta E \tag{5.29}$$

Here, $F = |\langle\psi_{\mathrm{t}}|\psi_0\rangle|^2$ is the fidelity between the initial state and the target state. Eq. 5.29 is equivalent to expressing the Fubini-Study metric on the projective Hilbert space [174] which implies that instantaneous energy uncertainty bounds the rate of change of quantum state. To transfer the initial state $|\psi_0\rangle$ at $t = 0$ to the target state $|\psi_{\mathrm{t}}\rangle$ at minimal time $t = T_{\mathrm{Th}}$, time step Δt should be large at all time. However, $\Delta E \to 0$ at $t \to 0$ and $T_{\mathrm{Th}} \to 0$ which opposes the criteria mentioned above. In order to satisfy above two criterion, optimal control pulses initially go through strong excitations creating a high ΔE to facilitating rapid motion in Hilbert space towards the target state. The occurrence of minimal energy gap at the beginning stage facilitates creation of excitations in higher symmetric excited states. Excitations uses information from the higher excited state to determine a shortest trajectory to reach the target state. Afterwards, when approaching target state Δt decreases to deexcite the state rapidly. This point is further explained by the fig. 5.10. This figure shows that when final time T is smaller, the system explore more deeper region in the Hilbert space to find the target state. This gives rise to the higher values of the Fourier amplitudes and base frequencies in the control pulses. One important point is

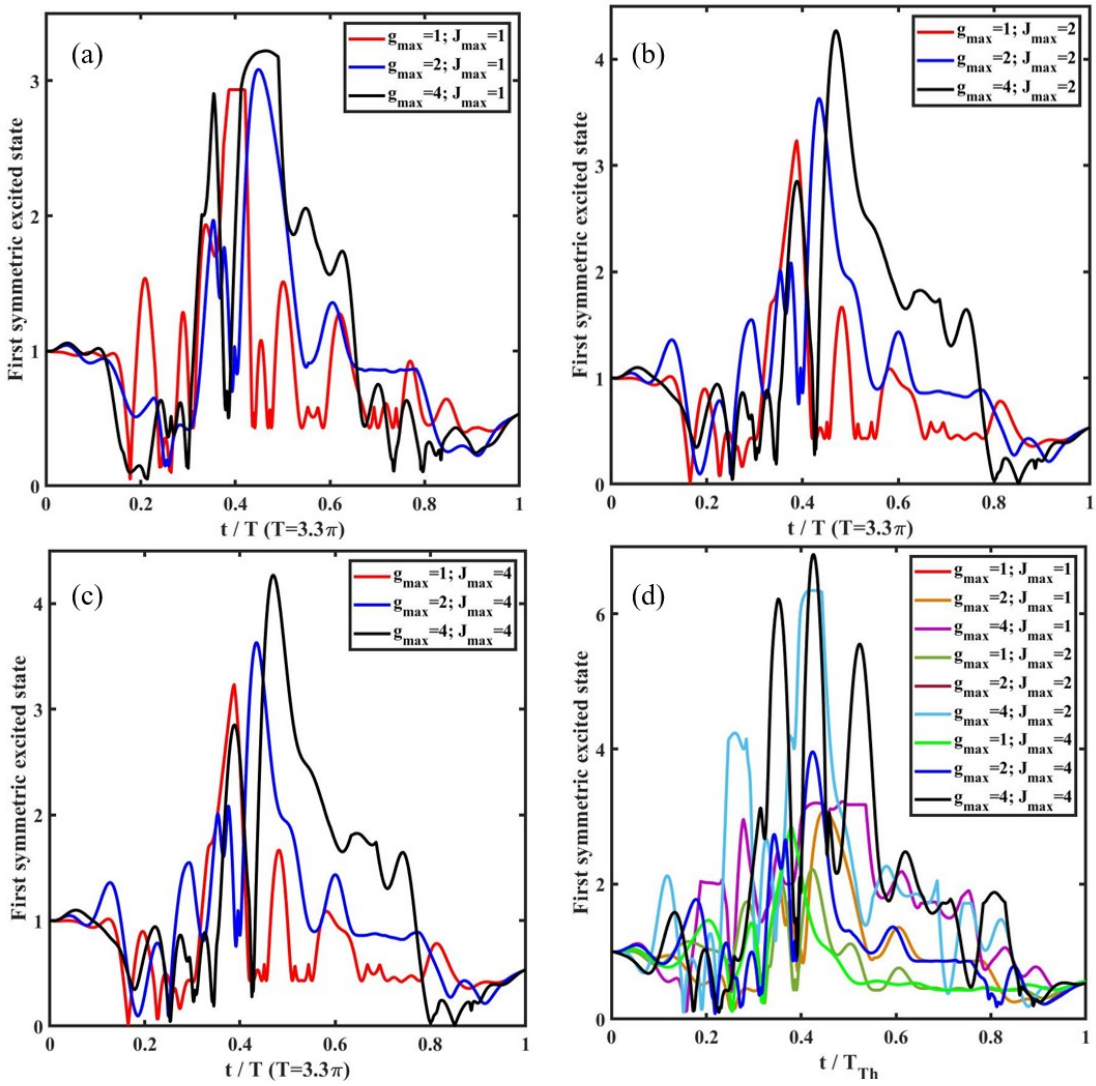

Figure 5.10: **Instantaneous first symmetric excited state vs time for different set of constraints. a-d**. **a.** $J_{\max} = 1$ and $g_{\max} = 1, 2, 4$ at $T = 3.3\pi$. **b.** $J_{\max} = 2$ and $g_{\max} = 1, 2, 4$ at $T = 3.3\pi$. **c.** $J_{\max} = 4$ and $g_{\max} = 1, 2, 4$ at $T = 3.3\pi$. **d.** Instantaneous first symmetric excited state for each set of constraints vs corresponding T_{Th}.

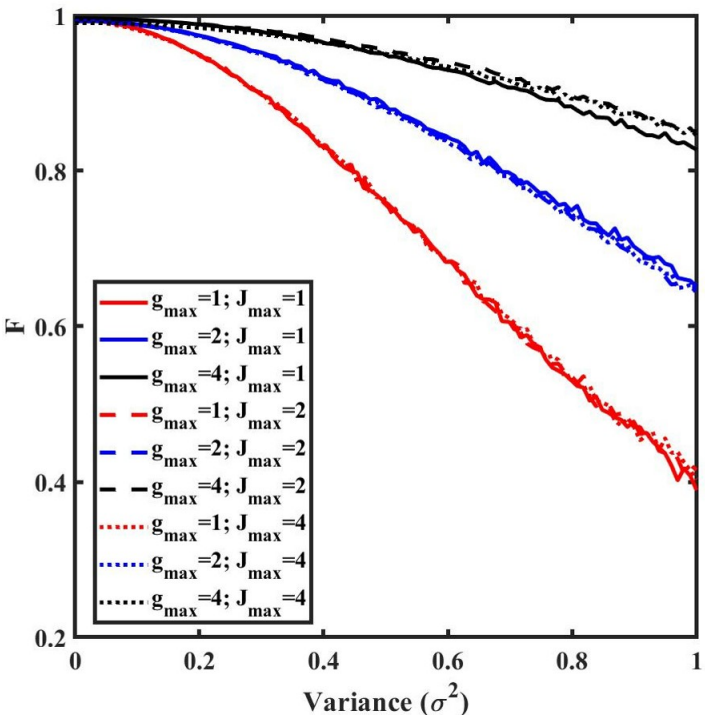

Figure 5.11: **Fidelity vs variance of Gaussian noise in control parameters for different set of constraints**

that each state trajectory has its own quantum speed limit not related to the optimal time.

5.5.3 Gaussian noise

To address the robustness of the CRAB algorithm to noises in the system due to control errors, we have added the time dependent Gaussian noise on the time dependent control pulses $g(t)$ and $J(t)$ i.e.

$$\begin{aligned} g(t) &= g(t) + \delta_1(t) \\ J(t) &= J(t) + \delta_2(t). \end{aligned} \tag{5.30}$$

$\delta_1(t)$ and $\delta_2(t)$ are random numbers obtained from a probability distribution function of the Gaussian distribution. We have defined a range of variances of the Gaussian

distribution from 0 to 1 to analyze the change in fidelity with variance at T_{Th} for different sets of constraints. In each value of variance, we perform 1000 trails and calculated the average value of the fidelity. Fig.(5.11) shows that, for the same value of $g_{\max}$, the fidelity decreases at the same rate for different values of $J_{\max}$ when the variance changes from 0 to 1. Similarly, for a different value of $g_{\max}$ with the same value of $J_{\max}$, the rate is different. This can be explained based on the optimal time T_{Th}. When the optimal time is small, fidelity decreases with a smaller rate.

5.5.4 Conclusion

We have applied a QOC technique with the CRAB algorithm to prepare a many-body ground state at the targeted region in the JC lattices. Our results showed that the evolution time to reach the fidelity above 0.99 decreases significantly with the CRAB algorithm as compared to the adiabatic algorithm. To bound the amplitude of control parameters with in experimental range, we have applied different set of constraints in the amplitude and calculated the optimal time corresponding to each set of constraints. Fig.(5.3) and Fig.(5.4) shows a comparison of the fidelity with CRAB and adiabatic algorithms for a different set of constraints. In Fig.(5.6), we showed the optimization of the Fourier parameters. To understand how the fidelity changes with different sets of constraints at the same evolution time, we considered an evolution time of $T = 3.3\pi$ and plotted the fidelity vs time plot. We also plotted the time evolution of the control parameters in Fig.(5.8) and Fig.(5.9). Fig.(5.10) shows that the system uses higher symmetric states to explore the Hilbert space faster in order to reach the target state.

In NISQ era, the decoherence times of qubits and cavities set a limitation on the evolution time of the system. Our state preparation method consists of a finite number of polariton excitations and these excitations can decay in a time scale comparable to the decoherence times. For a superconducting resonator cavity, a cavity frequency of $\omega_{\mathrm{c}}/2\pi = 10\mathrm{GHz}$ and the quality factor of $Q = 10^5$ can be realized efficiently [106]. This sets the limit to the cavity decay time to 1.6μs. Similarly, superconducting qubits can have decoherence times of 100μs. The coupling strengths i.e. $g/2\pi$ and

$J/2\pi$ typically are of the order of 2×10^2MHz. Hence, the evolution time $T_{\text{Th}} = 5.27\pi$ corresponds to 13.2ns. Similarly, $T_{\text{Th}} = 3.30\pi$, $T_{\text{Th}} = 2.23\pi$, $T_{\text{Th}} = 3.28\pi$, $T_{\text{Th}} = 1.96\pi$, $T_{\text{Th}} = 5.28\pi$, $T_{\text{Th}} = 1.90\pi$ corresponds to 8.3ns, 5.6ns, 8.2ns, 4.9ns, 13.2ns, and 4.8ns, respectively. This means state initialization pulses can be completed below 10ns in most of the cases. These time scales are much shorter than the decoherence time of superconducting cavities and qubits.

5.6 Summary

We have presented an application of the quantum optimal control technique with the CRAB algorithm to prepare a many-body ground state in the JC lattices. We have started the chapter by giving a basic introduction of the quantum optimal control theory and the controllability criterion for a quantum system. We have briefly introduced leading quantum optimal control algorithms like GRAPE, Krotov, chopped random basis algorithms(CRAB), and references were given for machine learning inspired QOC algorithms. The section 5.5 is the main part of this dissertation which corresponds to application of the CRAB algorithm in the JC lattices. The method we developed here is applicable in actual experiments and the results we got show that very fast and efficient many body state preparation is possible in JC lattices. This method is very simple and can be generalized to prepare many-body states in other quantum simulators and quantum computers.

Finding tight lower bounds for the quantum speed limit and searching for quantum advantages in quantum many-body state preparation remains to be explored in the future.

Chapter 6

Conclusion

6.1 Summary of the thesis

Many-body ground state preparation is the initial step in studying quantum systems in quantum simulators or quantum computers. In this NISQ era, due to decoherence in quantum hardware, computation tasks should be performed in fast and efficient ways to avoid unwanted noises in the system. In this regard, advent of an efficient many-body state preparation method is essential. Our main goal in this study is to understand the many-body correlations in quantum simulators and their impact in quantum information science. In chapter 1, we began by giving a basic introduction of quantum mechanics and quantum information science which was then followed by an overview of the thesis. In chapter 2, we introduced the idea of quantum simulation. We discussed different types of quantum simulations and different quantum simulation platforms. In chapter 3, we considered the JC lattices as a model system and develop a many-body ground state preparation method using nonlinear adiabatic ramping. We used a quantum engineering approach to prepare many-body ground states in the deep Mott insulating and deep superfluid regions and used the nonlinear ramping method to prepare many-body ground states in targeted regions. By using both, a analytical and a numerical approach, we concluded that high fidelity many-body ground states can be prepared in the JC lattices by combining quantum engineering and nonlinear ramping. In chapter 4.11, we presented the "shortcuts

to adiabaticity"(STA) approach to prepare many body ground state in the JC lattices. Using STA, we can prepare high fidelity many-body ground states very fast and efficient. We used transitionless tracking approach in our study and presented analytical and numerical results showing superiority of STA method over adiabatic method. One of the major challenges to implement STA method is that we need to know the instantaneous eigenstates and eigenenergies of the system to derive shortcut Hamiltonian which is very costly. In chapter 5, based on quantum optimal control theory, we transformed the state preparation problem into an optimization problem. We implemented chopped random basis algorithm to optimize the fidelity of the state preparation. To constrain the control parameters within an experimentally relevant range, we used hard wall constraints. Our results reveal that the system uses higher symmetric states to explore the Hilbert space faster to figure out the fastest high fidelity trajectory connecting the initial state to the target state. This result shed some light on finding quantum advantages in quantum simulation, especially in the context of adiabatic quantum computing.

6.2 Future Work

In research, new ideas develop based on old ideas. In this section, I will discuss a few project ideas which are not pursued further by me for this dissertation due to lack of time or technical difficulties that I ran into.

STA using approximate adiabatic gauge potential

The adiabatic gauge potential(AGP) is the generator of adiabatic deformations between quantum eignestates and it characterizes the distance between nearby eigenstates, i.e., the so called Fubini-Study metric. It has deep connections to a range of topics, including quantum state preparation, quantum computing, efficient quantum heat engines, quantum speed limits, quantum chaos and quantum computational complexity [181]. In the context of the STA, getting analytical expressions for the CD Hamiltonian is fundamentally important. The analytical form of the CD Hamiltonian

is comprised of the AGP term. There are some issues associated with the derivation of the many-body CD Hamiltonian. One issue is that instantaneous eigenbasis and eigenenergies are necessary to construct the CD Hamiltonian. This requires exact diagonalization of the Hamiltonian of the system. This is very difficult once the size of the system increases. The second issue is that the energy difference between eigenstates decreases exponentially with the increase in system size. This leads to ill-defined adiabatic gauge potentials in the thermodynamic limit [175–177]. In this context, addition of a regularization term in the gauge potential can be handy. For example, the CD Hamiltonian can be realized as an effective Floquet Hamiltonian by the oscillating original Hamiltonian term and the auxiliary Hamiltonian term. I will explore this topic in the context of many-body ground state preparation in future.

Many-body state preparation in JC lattice using reinforcement learning

In recent years, the application of machine learning techniques in quantum information science has gained huge interest because of its success in the characterization of different phases of quantum matter, high fidelity many-body state preparation, high fidelity quantum gates synthesis, and efficient quantum many-body control [155, 158, 159, 180]. Quantum many-body control is a milestone en route to harnessing quantum technologies. Since the dimension of the Hilbert space grows exponentially with the increase in system size, devising a novel framework to efficiently control the dynamics of the quantum-many body system using the traditional classical algorithm is impossible. For 1-dimensional systems, matrix product states(MPS) provide a compressed representation of the many-body wavefunctions as resources scale only linearly with the system size. Combining the MPS and deep reinforcement learning frameworks provides a new platform to control large 1-dimensional interacting systems using tensor network architecture. I have started to work on this project.

Appendix A

JCH Hamiltonian in momentum space

The Hamiltonian corresponding to the JC lattices is the JCH Hamiltonian:

$$H = \Delta \sum_{j=1}^{N} a_j^{\dagger} a_j + g \sum_{j=1}^{N} (a_j^{\dagger} \sigma_j^{-} + a_j \sigma_j^{+}) - J \sum_{j=1}^{N} (a_j^{\dagger} a_{j+1} + a_j a_{j+1}^{\dagger}) \tag{A.1}$$

The collective operators in momentum space can be defined as:

$$a_j = \frac{1}{\sqrt{N}} \sum_k a_k exp(-ik.r_j); a_k = \frac{1}{\sqrt{N}} \sum_j a_j exp(ik.r_j) \tag{A.2}$$

$$\sigma_j^{-} = \frac{1}{\sqrt{N}} \sum_k \sigma_k^{-} exp(-ik.r_j); \sigma_k^{-} = \frac{1}{\sqrt{N}} \sum_j \sigma_j^{-} exp(ik.r_j) \tag{A.3}$$

where $k = 2n\pi/N$, with $n = 0, 1, .., N-1$.

$$\begin{aligned}
\sum_{<i,j>} a_i^\dagger a_j &= \frac{1}{N} \sum_{<i,j>} \sum_{k,k'} a_k^\dagger a_{k'} exp(ik.r_i) exp(-ik^{'}.r_j) \\
&= \sum_{k,k'} a_k^\dagger a - k^{'} \frac{1}{N} \sum_i exp(i(k-k^{'}).r_i) \sum_{\delta=\pm R} exp(-ik^{'}.\delta) \\
&= \sum_{k,k'} a_k^\dagger a_{k'} \delta_{k,k'} \sum_{\delta=\pm R} exp(-ik^{'}.\delta) \\
&= \sum_k \sum_{\delta=\pm R} exp(-ik.\delta) a_k^\dagger a_k \\
&= 2 \sum_k cos(kR) a_k^\dagger a_k
\end{aligned} \tag{A.4}$$

here, R is the separation between neighboring sites. Similarly,

$$\begin{aligned}
\sum_j a_j^\dagger \sigma_j^- &= \frac{1}{N} \sum_j \sum_{k,k'} a_k^\dagger \sigma_{k'}^- exp(ik.r_j) exp(-ik^{'}.r_j) \\
&= \sum_{k,k'} a_k^\dagger \sigma_{k'}^- \frac{1}{N} \sum_j exp(i(k-k^{'}).r_j) \\
&= \sum_{k,k'} a_k^\dagger \sigma_{k'}^- \delta_{k,k'} \\
&= \sum_k a_k^\dagger \sigma_k^-
\end{aligned} \tag{A.5}$$

With this, the Hamiltonian of the JC lattices can be written as:

$$H = \sum_k \big[\Delta - 2Jcos(kR)\big] a_k^\dagger a_k + g \sum_k (a_k^\dagger \sigma_k^- + a_k \sigma_k^+). \tag{A.6}$$

which is the same as in Eq.(4.14)

Appendix B

Controllability

Definitions and other concepts about Lie algebra and Lie group presented here are adapted from [117].

B.1 Lie algebra

Definition: A Lie algebra $\mathcal{L}$ over a field $\mathcal{F}$ is a vector space over $\mathcal{F}$ with an additional binary operation $\mathcal{L} \times \mathcal{L} \to \mathcal{L}$. This operation associates with an ordered pair of elements $\{x, y\}$ in $\mathcal{L}$ and element $[x, y]$. It is called the *Lie bracket* or *commutator* and it is required to satisfy the following axioms:

1. Bilinearity:

$$\begin{aligned} [x+y, z] = [x, z] + [y, z], \qquad & [x, y+z] = [x, y] + [x, z], \\ [\beta x, y] = \beta [x, y], \qquad & \forall \beta \in \mathcal{F}. \end{aligned} \tag{B.1}$$

2.

$$[x, x] = 0 \qquad \forall x \in \mathcal{L}. \tag{B.2}$$

3. Jacobi identity:

$$[x, [y, z]] + [y, [z, x]] + [z, [x, y]] = 0 \tag{B.3}$$

In quantum physics, the Field $\mathcal{F}$ is a set of complex numbers $\mathcal{C}$ and the condition B.2 is replaced by the *skew-symmetry condition* $[x, y] = -[y, x]$. The commutation relations on a basis determines the structure of the Lie algebra because they determine the value of the commutator of any pair of elements in the Lie algebra.

Subalgebras: Given a Lie algebra $\mathcal{L}$, suppose a subspace $\mathcal{B} \subseteq \mathcal{L}$. If $\mathcal{B}$ with the commutator defined on $\mathcal{L}$ is a Lie algebra, then $\mathcal{B}$ is called subalgebra of $\mathcal{L}$.

Lie algebra generated by a set of elements : Given a set of a Lie algebra $\mathcal{L}$, $\{x_1, ..., x_n\}$, the set of all commutators of $\{x_1, ..., x_n\}$ spans a subalgebra of $\mathcal{L}$ which is called the Lie algebra generated by $\{x_1, ..., x_n\}$.

B.2 Lie group

Definition: A Lie group is a group which is an analytic differentiable manifold and in such a way that the group operations, $\{x, y\} \rightarrow xy$, and $x \rightarrow x^{-1}$, are analytic.
The Lie algebra of the group is obtained by constructing a group of elements that are reachable from the identity $\mathbb{I}$ by an infinitesimal tangent vector. Unitary representation of the group can be obtained by constructing generators from the element of the Lie algebra. Various methods of obtaining the generators of the Lie algebra have been discussed in reference [178].

B.3 Complete controllability of a quantum system

A quantum system $H = H_0 + \sum_{i=1}^{M} u_{i(t)} H_i$ is completely controllable if every unitary operator U is accessible from the identity operator $\mathbb{I}$ via a path $\gamma(t) = U(t, t_0)$ where $i\partial_t U(t, t_0) = HU(t, t_0)$. From [179], the criterion for a complete controllability of a quantum system H is that the Lie algebra L_0 should have the dimension N^2, where N is the dimension of the system. The Lie group L_0 is generated from the skew-Hermitian operators $\{iH_0, iH_1, ..., iH_M\}$.

Bibliography

[1] Nouredine Zettili. *Quantum mechanics: concepts and applications*. American Association of Physics Teachers, 2003.

[2] J. I. Cirac and P. Zoller. Quantum computations with cold trapped ions. *Phys. Rev. Lett.*, 74:4091–4094, May 1995.

[3] D. Jaksch, C. Bruder, J. I. Cirac, C. W. Gardiner, and P. Zoller. Cold bosonic atoms in optical lattices. *Phys. Rev. Lett.*, 81:3108–3111, Oct 1998.

[4] I. Georgescu, S. Ashhab, and F. Nori. Quantum simulation. *Rev. Mod. Phys.*, 86:153–185, Mar 2014.

[5] R. Feynman. Quantum simulation. *Int. J. Theor. Phys*, 21:467–488, June 1982.

[6] S. Lloyd. Universal quantum simulators. *Science*, 273:1073–1078, August 1996.

[7] K. J. Satzinger, Y.-J Liu, A. Smith, C. Knapp, M. Newman, C. Jones, Z. Chen, C. Quintana, X. Mi, A. Dunsworth, C. Gidney, I. Aleiner, F. Arute, K. Arya, J. Atalaya, R. Babbush, J. C. Bardin, R. Barends, J. Basso, A. Bengtsson, A. Bilmes, M. Broughton, B. B. Buckley, D. A. Buell, B. Burkett, N. Bushnell, B. Chiaro, R. Collins, W. Courtney, S. Demura, A. R. Derk, D. Eppens, C. Erickson, L. Faoro, E. Farhi, A. G. Fowler, B. Foxen, M. Giustina, A. Greene, J. A. Gross, M. P. Harrigan, S. D. Harrington, J. Hilton, S. Hong, T. Huang, W. J. Huggins, L. B. Ioffe, S. V. Isakov, E. Jeffrey, Z. Jiang, D. Kafri, K. Kechedzhi, T. Khattar, S. Kim, P. V. Klimov, A. N. Korotkov, F. Kostritsa, D. Landhuis, P. Laptev, A. Locharla, E. Lucero, O. Martin, J. R. McClean, M. McEwen,

K. C. Miao, M. Mohseni, S. Montazeri, W. Mruczkiewicz, J. Mutus, O. Naaman, M. Neeley, C. Neill, M. Y. Niu, T. E. O'Brien, A. Opremcak, B. Pató, A. Petukhov, N. C. Rubin, D. Sank, V. Shvarts, D. Strain, M. Szalay, B. Villalonga, T. C. White, Z. Yao, P. Yeh, J. Yoo, A. Zalcman, H. Neven, S. Boixo, A. Megrant, Y. Chen, J. Kelly, V. Smelyanskiy, A. Kitaev, M. Knap, F. Pollmann, and P. Roushan. Realizing topologically ordered states on a quantum processor. *Science*, 374(6572):1237–1241, 2021.

[8] G. Semeghini, H. Levine, A. Keesling, S. Ebadi, T. T. Wang, D. Bluvstein, R. Verresen, H. Pichler, M. Kalinowski, R. Samajdar, A. Omran, S. Sachdev, A. Vishwanath, M. Greiner, V. Vuletić, and M. D. Lukin. Probing topological spin liquids on a programmable quantum simulator. *Science*, 374(6572):1242–1247, 2021.

[9] D. Guéry-Odelin, A. Ruschhaupt, A. Kiely, E. Torrontegui, S. Martínez-Garaot, and J. G. Muga. Shortcuts to adiabaticity: Concepts, methods, and applications. *Rev. Mod. Phys.*, 91:045001, Oct 2019.

[10] Mustafa Demirplak and Stuart A. Rice. On the consistency, extremal, and global properties of counterdiabatic fields. *The Journal of Chemical Physics*, 129(15):154111, 2008.

[11] Mustafa Demirplak and Stuart A. Rice. Assisted adiabatic passage revisited. *The Journal of Physical Chemistry B*, 109(14):6838–6844, 2005. PMID: 16851769.

[12] Mustafa Demirplak and Stuart A. Rice. On the consistency, extremal, and global properties of counterdiabatic fields. *The Journal of Chemical Physics*, 129(15):154111, 2008.

[13] M V Berry. Transitionless quantum driving. *Journal of Physics A: Mathematical and Theoretical*, 42(36):365303, aug 2009.

[14] P. Forn-Díaz, L. Lamata, E. Rico, J. Kono, and E. Solano. Ultrastrong coupling regimes of light-matter interaction. *Rev. Mod. Phys.*, 91:025005, Jun 2019.

[15] E.T. Jaynes and F.W. Cummings. Comparison of quantum and semiclassical radiation theories with application to the beam maser. *Proceedings of the IEEE*, 51(1):89–109, 1963.

[16] I. M. Georgescu, S. Ashhab, and Franco Nori. Quantum simulation. *Rev. Mod. Phys.*, 86:153–185, Mar 2014.

[17] David P DiVincenzo and Daniel Loss. Quantum information is physical. *Superlattices and Microstructures*, 23(3-4):419–432, 1998.

[18] S. Somaroo, C. H. Tseng, T. F. Havel, R. Laflamme, and D. G. Cory. Quantum simulations on a quantum computer. *Phys. Rev. Lett.*, 82:5381–5384, Jun 1999.

[19] J. D. Biamonte, V. Bergholm, J. D. Whitfield, J. Fitzsimons, and A. Aspuru-Guzik. Adiabatic quantum simulators. *AIP Advances*, 1(2):022126, 2011.

[20] Ehud Altman, Kenneth R Brown, Giuseppe Carleo, Lincoln D Carr, Eugene Demler, Cheng Chin, Brian DeMarco, Sophia E Economou, Mark A Eriksson, Kai-Mei C Fu, et al. Quantum simulators: Architectures and opportunities. *PRX Quantum*, 2(1):017003, 2021.

[21] Michael A. Nielsen and Isaac L. Chuang. *Quantum Computation and Quantum Information: 10th Anniversary Edition*. Cambridge University Press, 2010.

[22] Kishor Bharti, Alba Cervera-Lierta, Thi Ha Kyaw, Tobias Haug, Sumner Alperin-Lea, Abhinav Anand, Matthias Degroote, Hermanni Heimonen, Jakob S. Kottmann, Tim Menke, Wai-Keong Mok, Sukin Sim, Leong-Chuan Kwek, and Alán Aspuru-Guzik. Noisy intermediate-scale quantum algorithms. *Rev. Mod. Phys.*, 94:015004, Feb 2022.

[23] Bela Bauer, Sergey Bravyi, Mario Motta, and Garnet Kin-Lic Chan. Quantum algorithms for quantum chemistry and quantum materials science. *Chemical Reviews*, 120(22):12685–12717, 2020. PMID: 33090772.

[24] M. Cerezo, Andrew Arrasmith, Ryan Babbush, Simon C. Benjamin, Suguru Endo, Keisuke Fujii, Jarrod R. McClean, Kosuke Mitarai, Xiao Yuan, Lukasz

Cincio, and et al. Variational quantum algorithms. *Nature Reviews Physics*, 3(9):625–644, 2021.

[25] G Wendin. Quantum information processing with superconducting circuits: a review. *Reports on Progress in Physics*, 80(10):106001, sep 2017.

[26] P. Krantz, M. Kjaergaard, F. Yan, T. P. Orlando, S. Gustavsson, and W. D. Oliver. A quantum engineer's guide to superconducting qubits. *Applied Physics Reviews*, 6(2):021318, 2019.

[27] Rainer Blatt and David Wineland. Entangled states of trapped atomic ions. *Nature News*, Jun 2008.

[28] Shi-Liang Zhu, C. Monroe, and L.-M. Duan. Trapped ion quantum computation with transverse phonon modes. *Phys. Rev. Lett.*, 97:050505, Aug 2006.

[29] Colin D. Bruzewicz, John Chiaverini, Robert McConnell, and Jeremy M. Sage. Trapped-ion quantum computing: Progress and challenges. *Applied Physics Reviews*, 6(2):021314, 2019.

[30] Pieter Kok, W. J. Munro, Kae Nemoto, T. C. Ralph, Jonathan P. Dowling, and G. J. Milburn. Linear optical quantum computing with photonic qubits. *Rev. Mod. Phys.*, 79:135–174, Jan 2007.

[31] Jianwei Wang, Fabio Sciarrino, Anthony Laing, and Mark G Thompson. Integrated photonic quantum technologies. *Nature Photonics*, 14(5):273–284, 2020.

[32] J. Eli Bourassa, Rafael N. Alexander, Michael Vasmer, Ashlesha Patil, Ilan Tzitrin, Takaya Matsuura, Daiqin Su, Ben Q. Baragiola, Saikat Guha, Guillaume Dauphinais, Krishna K. Sabapathy, Nicolas C. Menicucci, and Ish Dhand. Blueprint for a Scalable Photonic Fault-Tolerant Quantum Computer. *Quantum*, 5:392, February 2021.

[33] D. Jaksch, J. I. Cirac, P. Zoller, S. L. Rolston, R. Côté, and M. D. Lukin. Fast quantum gates for neutral atoms. *Phys. Rev. Lett.*, 85:2208–2211, Sep 2000.

[34] M. D. Lukin, M. Fleischhauer, R. Cote, L. M. Duan, D. Jaksch, J. I. Cirac, and P. Zoller. Dipole blockade and quantum information processing in mesoscopic atomic ensembles. *Phys. Rev. Lett.*, 87:037901, Jun 2001.

[35] M. Saffman, T. G. Walker, and K. Mølmer. Quantum information with rydberg atoms. *Rev. Mod. Phys.*, 82:2313–2363, Aug 2010.

[36] M. Morgado and S. Whitlock. Quantum simulation and computing with rydberg-interacting qubits. *AVS Quantum Science*, 3(2):023501, 2021.

[37] Dolev Bluvstein, Ahmed Omran, Harry Levine, Alexander Keesling, Giulia Semeghini, Sepehr Ebadi, Tout T Wang, Alexios A Michailidis, Nishad Maskara, Wen Wei Ho, et al. Controlling quantum many-body dynamics in driven rydberg atom arrays. *Science*, 371(6536):1355–1359, 2021.

[38] Dimitris G Angelakis. Quantum simulations with photons and polaritons. *Quantum Science and Technology (Springer, 2017)*, 134, 2017.

[39] Immanuel Bloch, Jean Dalibard, and Sylvain Nascimbene. Quantum simulations with ultracold quantum gases. *Nature Physics*, 8(4):267–276, 2012.

[40] Christian Gross and Immanuel Bloch. Quantum simulations with ultracold atoms in optical lattices. *Science*, 357(6355):995–1001, 2017.

[41] JR Weber, WF Koehl, JB Varley, A Janotti, BB Buckley, CG Van de Walle, and David D Awschalom. Quantum computing with defects. *Proceedings of the National Academy of Sciences*, 107(19):8513–8518, 2010.

[42] Lilian Childress and Ronald Hanson. Diamond nv centers for quantum computing and quantum networks. *MRS bulletin*, 38(2):134–138, 2013.

[43] Daniel Loss and David P DiVincenzo. Quantum computation with quantum dots. *Physical Review A*, 57(1):120, 1998.

[44] Ruoyu Li, Luca Petit, David P Franke, Juan Pablo Dehollain, Jonas Helsen, Mark Steudtner, Nicole K Thomas, Zachary R Yoscovits, Kanwal J Singh,

Stephanie Wehner, et al. A crossbar network for silicon quantum dot qubits. *Science advances*, 4(7):eaar3960, 2018.

[45] David G Cory, Amr F Fahmy, and Timothy F Havel. Ensemble quantum computing by nmr spectroscopy. *Proceedings of the National Academy of Sciences*, 94(5):1634–1639, 1997.

[46] Nabin K Raut, Jeffery Miller, Jacob Pate, Raymond Chiao, and Jay E Sharping. Meissner levitation of a millimeter-size neodymium magnet within a superconducting radio frequency cavity. *IEEE Transactions on Applied Superconductivity*, 31(5):1–4, 2021.

[47] Nabin K Raut, Jeffery Miller, Raymond Chiao, and Jay E Sharping. Demonstrating levitation within a microwave cavity. *arXiv preprint arXiv:2101.01309*, 2021.

[48] Leonardo Midolo, Albert Schliesser, and Andrea Fiore. Nano-opto-electro-mechanical systems. *Nature nanotechnology*, 13(1):11–18, 2018.

[49] Jean-Michel Raimond, M Brune, and Serge Haroche. Manipulating quantum entanglement with atoms and photons in a cavity. *Reviews of Modern Physics*, 73(3):565, 2001.

[50] SM Girvin. Lecture notes on strong light-matter coupling: From atoms to solid-state systems. 2013.

[51] Jian-Qiang You and Franco Nori. Atomic physics and quantum optics using superconducting circuits. *Nature*, 474(7353):589–597, 2011.

[52] Michael J Hartmann, Fernando GSL Brandao, and Martin B Plenio. Strongly interacting polaritons in coupled arrays of cavities. *Nature Physics*, 2(12):849–855, 2006.

[53] Andrew D Greentree, Charles Tahan, Jared H Cole, and Lloyd CL Hollenberg. Quantum phase transitions of light. *Nature Physics*, 2(12):856–861, 2006.

[54] Dimitris G Angelakis, Marcelo Franca Santos, and Sougato Bose. Photon-blockade-induced mott transitions and x y spin models in coupled cavity arrays. *Physical Review A*, 76(3):031805, 2007.

[55] Davide Rossini and Rosario Fazio. Mott-insulating and glassy phases of polaritons in 1d arrays of coupled cavities. *Physical Review Letters*, 99(18):186401, 2007.

[56] Neil Na, Shoko Utsunomiya, Lin Tian, and Yoshihisa Yamamoto. Strongly correlated polaritons in a two-dimensional array of photonic crystal microcavities. *Physical Review A*, 77(3):031803, 2008.

[57] Jens Koch and Karyn Le Hur. Superfluid–mott-insulator transition of light in the jaynes-cummings lattice. *Physical Review A*, 80(2):023811, 2009.

[58] Andrew A Houck, Hakan E Türeci, and Jens Koch. On-chip quantum simulation with superconducting circuits. *Nature Physics*, 8(4):292–299, 2012.

[59] Yong Hu and Lin Tian. Deterministic generation of entangled photons in superconducting resonator arrays. *Physical review letters*, 106(25):257002, 2011.

[60] Kangjun Seo and Lin Tian. Quantum phase transition in a multiconnected superconducting jaynes-cummings lattice. *Physical Review B*, 91(19):195439, 2015.

[61] Seo KangJun and Tian Lin. Mott insulator-superfluid phase transition in a detuned multi-connected jaynes-cummings lattice. *SCIENCE CHINA Physics, Mechanics & Astronomy*, 58(7):1–6, 2015.

[62] Jian Xue, Kangjun Seo, Lin Tian, and Tao Xiang. Quantum phase transition in a multiconnected jaynes-cummings lattice. *Physical Review B*, 96(17):174502, 2017.

[63] Anthony J Hoffman, Srikanth J Srinivasan, Sebastian Schmidt, Lafe Spietz, José Aumentado, Hakan E Türeci, and Andrew A Houck. Dispersive photon

blockade in a superconducting circuit. *Physical review letters*, 107(5):053602, 2011.

[64] Felix Nissen, Sebastian Schmidt, Matteo Biondi, Gianni Blatter, Hakan E Türeci, and Jonathan Keeling. Nonequilibrium dynamics of coupled qubit-cavity arrays. *Physical review letters*, 108(23):233603, 2012.

[65] Mattias Fitzpatrick, Neereja M Sundaresan, Andy CY Li, Jens Koch, and Andrew A Houck. Observation of a dissipative phase transition in a one-dimensional circuit qed lattice. *Physical Review X*, 7(1):011016, 2017.

[66] Marco Schiro, Mykola Bordyuh, B Öztop, and HE Türeci. Phase transition of light in cavity qed lattices. *Physical review letters*, 109(5):053601, 2012.

[67] Brijesh Kumar and Somenath Jalal. Quantum ising dynamics and majorana-like edge modes in the rabi lattice model. *Physical Review A*, 88(1):011802, 2013.

[68] Alán Aspuru-Guzik, Anthony D Dutoi, Peter J Love, and Martin Head-Gordon. Simulated quantum computation of molecular energies. *Science*, 309(5741):1704–1707, 2005.

[69] Edward Farhi, Jeffrey Goldstone, Sam Gutmann, and Michael Sipser. Quantum computation by adiabatic evolution. 2000.

[70] Tameem Albash and Daniel A Lidar. Adiabatic quantum computation. *Reviews of Modern Physics*, 90(1):015002, 2018.

[71] Edward Farhi, Jeffrey Goldstone, Sam Gutmann, Joshua Lapan, Andrew Lundgren, and Daniel Preda. A quantum adiabatic evolution algorithm applied to random instances of an np-complete problem. *Science*, 292(5516):472–475, 2001.

[72] Jérémie Roland and Nicolas J Cerf. Quantum search by local adiabatic evolution. *Physical Review A*, 65(4):042308, 2002.

[73] HT Quan and W Hm Zurek. Testing quantum adiabaticity with quench echo. *New Journal of Physics*, 12(9):093025, 2010.

[74] Xi Chen, I Lizuain, A Ruschhaupt, D Guéry-Odelin, and JG Muga. Shortcut to adiabatic passage in two-and three-level atoms. *Physical review letters*, 105(12):123003, 2010.

[75] Adolfo del Campo, Marek M Rams, and Wojciech H Zurek. Assisted finite-rate adiabatic passage across a quantum critical point: exact solution for the quantum ising model. *Physical review letters*, 109(11):115703, 2012.

[76] A.Yu.Kitaev. Quantum measurements and the abelian stabilizer problem. 1995.

[77] Daniel S Abrams and Seth Lloyd. Simulation of many-body fermi systems on a universal quantum computer. *Physical Review Letters*, 79(13):2586, 1997.

[78] Alberto Peruzzo, Jarrod McClean, Peter Shadbolt, Man-Hong Yung, Xiao-Qi Zhou, Peter J Love, Alán Aspuru-Guzik, and Jeremy L O'brien. A variational eigenvalue solver on a photonic quantum processor. *Nature communications*, 5(1):1–7, 2014.

[79] Eugene F Dumitrescu, Alex J McCaskey, Gaute Hagen, Gustav R Jansen, Titus D Morris, T Papenbrock, Raphael C Pooser, David Jarvis Dean, and Pavel Lougovski. Cloud quantum computing of an atomic nucleus. *Physical review letters*, 120(21):210501, 2018.

[80] Shijie Wei, Hang Li, and GuiLu Long. A full quantum eigensolver for quantum chemistry simulations. *Research*, 2020, 2020.

[81] Barbara Kraus, Hans P Büchler, Sebastian Diehl, Adrian Kantian, Andrea Micheli, and Peter Zoller. Preparation of entangled states by quantum markov processes. *Physical Review A*, 78(4):042307, 2008.

[82] Frank Verstraete, Michael M Wolf, and J Ignacio Cirac. Quantum computation and quantum-state engineering driven by dissipation. *Nature physics*, 5(9):633–636, 2009.

[83] Camille Aron, Manas Kulkarni, and Hakan E Türeci. Steady-state entanglement of spatially separated qubits via quantum bath engineering. *Physical Review A*, 90(6):062305, 2014.

[84] Camille Aron, Manas Kulkarni, and Hakan E Türeci. Photon-mediated interactions: a scalable tool to create and sustain entangled states of n atoms. *Physical Review X*, 6(1):011032, 2016.

[85] John Preskill. Quantum computing in the nisq era and beyond. *Quantum*, 2:79, 2018.

[86] Diptiman Sen, K Sengupta, and Shreyoshi Mondal. Defect production in nonlinear quench across a quantum critical point. *Physical Review Letters*, 101(1):016806, 2008.

[87] Shreyoshi Mondal, K Sengupta, and Diptiman Sen. Theory of defect production in nonlinear quench across a quantum critical point. *Physical Review B*, 79(4):045128, 2009.

[88] Roman Barankov and Anatoli Polkovnikov. Optimal nonlinear passage through a quantum critical point. *Physical review letters*, 101(7):076801, 2008.

[89] Chi K Law and Joseph H Eberly. Arbitrary control of a quantum electromagnetic field. *Physical review letters*, 76(7):1055, 1996.

[90] Charles Neill, Pedran Roushan, K Kechedzhi, Sergio Boixo, Sergei V Isakov, V Smelyanskiy, A Megrant, B Chiaro, A Dunsworth, K Arya, et al. A blueprint for demonstrating quantum supremacy with superconducting qubits. *Science*, 360(6385):195–199, 2018.

[91] Peng Zhao, Zhenchuan Jin, Peng Xu, Xinsheng Tan, Haifeng Yu, and Yang Yu. Two-photon driven kerr resonator for quantum annealing with three-dimensional circuit qed. *Physical Review Applied*, 10(2):024019, 2018.

[92] Michel H Devoret and Robert J Schoelkopf. Superconducting circuits for quantum information: an outlook. *Science*, 339(6124):1169–1174, 2013.

[93] Göran Wendin. Quantum information processing with superconducting circuits: a review. *Reports on Progress in Physics*, 80(10):106001, 2017.

[94] Philip Krantz, Morten Kjaergaard, Fei Yan, Terry P Orlando, Simon Gustavsson, and William D Oliver. A quantum engineer's guide to superconducting qubits. *Applied Physics Reviews*, 6(2):021318, 2019.

[95] Lev Davidovich Landau. Zur theorie der energieubertragung ii. *Z. Sowjetunion*, 2:46–51, 1932.

[96] Clarence Zener. Non-adiabatic crossing of energy levels. *Proceedings of the Royal Society of London. Series A, Containing Papers of a Mathematical and Physical Character*, 137(833):696–702, 1932.

[97] Feng Mei, Vladimir M Stojanović, Irfan Siddiqi, and Lin Tian. Analog superconducting quantum simulator for holstein polarons. *Physical Review B*, 88(22):224502, 2013.

[98] Oliver Penrose and Lars Onsager. Bose-einstein condensation and liquid helium. *Physical Review*, 104(3):576, 1956.

[99] Chen Ning Yang. Concept of off-diagonal long-range order and the quantum phases of liquid he and of superconductors. *Reviews of Modern Physics*, 34(4):694, 1962.

[100] Jean Dalibard, Yvan Castin, and Klaus Mølmer. Wave-function approach to dissipative processes in quantum optics. *Physical review letters*, 68(5):580, 1992.

[101] Erik Torrontegui, Sara Ibáñez, Sofia Martínez-Garaot, Michele Modugno, Adolfo del Campo, David Guéry-Odelin, Andreas Ruschhaupt, Xi Chen, and Juan Gonzalo Muga. Chapter 2 - shortcuts to adiabaticity. In Ennio Arimondo, Paul R. Berman, and Chun C. Lin, editors, *Advances in Atomic, Molecular, and Optical Physics*, volume 62 of *Advances In Atomic, Molecular, and Optical Physics*, pages 117–169. Academic Press, 2013.

[102] Keisuke Suzuki and Kazutaka Takahashi. Performance evaluation of adiabatic quantum computation via quantum speed limits and possible applications to many-body systems. *Physical Review Research*, 2(3):032016, 2020.

[103] Hamed Saberi, Tomáš Opatrnỳ, Klaus Mølmer, and Adolfo del Campo. Adiabatic tracking of quantum many-body dynamics. *Physical Review A*, 90(6):060301, 2014.

[104] Marin Bukov, Dries Sels, and Anatoli Polkovnikov. Geometric speed limit of accessible many-body state preparation. *Physical Review X*, 9(1):011034, 2019.

[105] Umer Farooq, Abolfazl Bayat, Stefano Mancini, and Sougato Bose. Adiabatic many-body state preparation and information transfer in quantum dot arrays. *Physical Review B*, 91(13):134303, 2015.

[106] Kang Cai, Prabin Parajuli, Guilu Long, Chee Wei Wong, and Lin Tian. Robust preparation of many-body ground states in jaynes–cummings lattices. *npj Quantum Information*, 7(1):1–9, 2021.

[107] Nathalie P de Leon, Kohei M Itoh, Dohun Kim, Karan K Mehta, Tracy E Northup, Hanhee Paik, BS Palmer, N Samarth, Sorawis Sangtawesin, and DW Steuerman. Materials challenges and opportunities for quantum computing hardware. *Science*, 372(6539):eabb2823, 2021.

[108] Tameem Albash and Daniel A. Lidar. Adiabatic quantum computation. *Rev. Mod. Phys.*, 90:015002, Jan 2018.

[109] R.G Unanyan, L.P Yatsenko, K Bergmann, and B.W Shore. Laser-induced adiabatic atomic reorientation with control of diabatic losses. *Optics Communications*, 139(1):48–54, 1997.

[110] A. Emmanouilidou, X.-G. Zhao, P. Ao, and Q. Niu. Steering an eigenstate to a destination. *Phys. Rev. Lett.*, 85:1626–1629, Aug 2000.

[111] A. Couvert, T. Kawalec, G. Reinaudi, and D. Guéry-Odelin. Optimal transport of ultracold atoms in the non-adiabatic regime. *EPL (Europhysics Letters)*, 83(1):13001, jun 2008.

[112] T. Caneva, M. Murphy, T. Calarco, R. Fazio, S. Montangero, V. Giovannetti, and G. E. Santoro. Optimal control at the quantum speed limit. *Phys. Rev. Lett.*, 103:240501, Dec 2009.

[113] Márcio M Taddei, Bruno M Escher, Luiz Davidovich, and Ruynet L de Matos Filho. Quantum speed limit for physical processes. *Physical review letters*, 110(5):050402, 2013.

[114] Keisuke Suzuki and Kazutaka Takahashi. Performance evaluation of adiabatic quantum computation via quantum speed limits and possible applications to many-body systems. *Physical Review Research*, 2(3):032016, 2020.

[115] Narendra N Hegade, Koushik Paul, Yongcheng Ding, Mikel Sanz, Francisco Albarrán-Arriagada, Enrique Solano, and Xi Chen. Shortcuts to adiabaticity in digitized adiabatic quantum computing. *Physical Review Applied*, 15(2):024038, 2021.

[116] Herschel A Rabitz, Michael M Hsieh, and Carey M Rosenthal. Quantum optimally controlled transition landscapes. *Science*, 303(5666):1998–2001, 2004.

[117] Domenico d'Alessandro. *Introduction to quantum control and dynamics*. Chapman and hall/CRC, 2021.

[118] Anthony P Peirce, Mohammed A Dahleh, and Herschel Rabitz. Optimal control of quantum-mechanical systems: Existence, numerical approximation, and applications. *Physical Review A*, 37(12):4950, 1988.

[119] Shlomo E Sklarz and David J Tannor. Loading a bose-einstein condensate onto an optical lattice: An application of optimal control theory to the nonlinear schrödinger equation. *Physical Review A*, 66(5):053619, 2002.

[120] Robert J Gordon and Stuart A Rice. Active control of the dynamics of atoms and molecules. *Annual review of physical chemistry*, 48(1):601–641, 1997.

[121] Marco Anderlini, Patricia J Lee, Benjamin L Brown, Jennifer Sebby-Strabley, William D Phillips, and James V Porto. Controlled exchange interaction between pairs of neutral atoms in an optical lattice. *Nature*, 448(7152):452–456, 2007.

[122] Paraj Titum, Kevin Schultz, Alireza Seif, Gregory Quiroz, and BD Clader. Optimal control for quantum detectors. *npj Quantum Information*, 7(1):1–8, 2021.

[123] Cosimo Lovecchio, Florian Schaefer, Shahid Cherukattil, M Alì Khan, Ivan Herrera, Francesco S Cataliotti, Tommaso Calarco, Simone Montangero, and Filippo Caruso. Optimal preparation of quantum states on an atom-chip device. *Physical Review A*, 93(1):010304, 2016.

[124] Alicia B Magann, Christian Arenz, Matthew D Grace, Tak-San Ho, Robert L Kosut, Jarrod R McClean, Herschel A Rabitz, and Mohan Sarovar. From pulses to circuits and back again: A quantum optimal control perspective on variational quantum algorithms. *PRX Quantum*, 2(1):010101, 2021.

[125] Jeffrey M Gertler, Brian Baker, Juliang Li, Shruti Shirol, Jens Koch, and Chen Wang. Protecting a bosonic qubit with autonomous quantum error correction. *Nature*, 590(7845):243–248, 2021.

[126] Arthur Larrouy, Sabrina Patsch, Rémi Richaud, Jean-Michel Raimond, Michel Brune, Christiane P Koch, and Sébastien Gleyzes. Fast navigation in a large hilbert space using quantum optimal control. *Physical Review. X*, 10(2), 2020.

[127] Kamal Bhattacharyya. Quantum decay and the mandelstam-tamm-energy inequality. *Journal of Physics A: Mathematical and General*, 16(13):2993, 1983.

[128] Peter Pfeifer. How fast can a quantum state change with time? *Physical review letters*, 70(22):3365, 1993.

[129] Sebastian Deffner and Steve Campbell. Quantum speed limits: from heisenberg's uncertainty principle to optimal quantum control. *Journal of Physics A: Mathematical and Theoretical*, 50(45):453001, 2017.

[130] J. J. W. H. Sørensen, M. O. Aranburu, T. Heinzel, and J. F. Sherson. Quantum optimal control in a chopped basis: Applications in control of bose-einstein condensates. *Phys. Rev. A*, 98:022119, Aug 2018.

[131] T. Caneva, A. Silva, R. Fazio, S. Lloyd, T. Calarco, and S. Montangero. Complexity of controlling quantum many-body dynamics. *Phys. Rev. A*, 89:042322, Apr 2014.

[132] Matthias M Müller, Ressa S Said, Fedor Jelezko, Tommaso Calarco, and Simone Montangero. One decade of quantum optimal control in the chopped random basis. *arXiv preprint arXiv:2104.07687*, 2021.

[133] Jacob Sherson. *Quantum Optimal Control of Ultracold Systems*. PhD thesis, 2018.

[134] Jonathan Emanuel Zoller. *Optimal Quantum Engineeering*. PhD thesis, 2018.

[135] Daoyi Dong and Ian R Petersen. Quantum control theory and applications: a survey. *IET control theory & applications*, 4(12):2651–2671, 2010.

[136] Anthony P Peirce, Mohammed A Dahleh, and Herschel Rabitz. Optimal control of quantum-mechanical systems: Existence, numerical approximation, and applications. *Physical Review A*, 37(12):4950, 1988.

[137] M Dahleh, AP Peirce, and H Rabitz. Optimal control of uncertain quantum systems. *Physical Review A*, 42(3):1065, 1990.

[138] Navin Khaneja, Burkhard Luy, and Steffen J Glaser. Boundary of quantum evolution under decoherence. *Proceedings of the National Academy of Sciences*, 100(23):13162–13166, 2003.

[139] Jiazhao Tian, Haibin Liu, Yu Liu, Pengcheng Yang, Ralf Betzholz, Ressa S. Said, Fedor Jelezko, and Jianming Cai. Quantum optimal control using phase-modulated driving fields. *Phys. Rev. A*, 102:043707, Oct 2020.

[140] Sebastian Zaiser, Torsten Rendler, Ingmar Jakobi, Thomas Wolf, Sang-Yun Lee, Samuel Wagner, Ville Bergholm, Thomas Schulte-Herbrüggen, Philipp Neumann, and Jörg Wrachtrup. Enhancing quantum sensing sensitivity by a quantum memory. *Nature communications*, 7(1):1–11, 2016.

[141] Herschel Rabitz, Regina de Vivie-Riedle, Marcus Motzkus, and Karl Kompa. Whither the future of controlling quantum phenomena? *Science*, 288(5467):824–828, 2000.

[142] Richard S Judson and Herschel Rabitz. Teaching lasers to control molecules. *Physical review letters*, 68(10):1500, 1992.

[143] Francesca Albertini and Domenico D'Alessandro. Notions of controllability for bilinear multilevel quantum systems. *IEEE Transactions on Automatic Control*, 48(8):1399–1403, 2003.

[144] Shai Machnes, Urgen Sander, Steffen J Glaser, Pierre de Fouquieres, Audrunas Gruslys, Sonia Schirmer, and Thomas Schulte-Herbrüggen. Comparing, optimizing, and benchmarking quantum-control algorithms in a unifying programming framework. *Physical Review A*, 84(2):022305, 2011.

[145] Bilal Riaz, Cong Shuang, and Shahid Qamar. Optimal control methods for quantum gate preparation: a comparative study. *Quantum Information Processing*, 18(4):1–26, 2019.

[146] Michael Goerz, Daniel Basilewitsch, Fernando Gago-Encinas, Matthias G Krauss, Karl P Horn, Daniel M Reich, and Christiane Koch. Krotov: A python implementation of krotov's method for quantum optimal control. *SciPost physics*, 7(6):080, 2019.

[147] Masanori Ohya and Dénes Petz. *Quantum entropy and its use*. Springer Science & Business Media, 2004.

[148] Navin Khaneja, Timo Reiss, Cindie Kehlet, Thomas Schulte-Herbrüggen, and Steffen J Glaser. Optimal control of coupled spin dynamics: design of nmr pulse sequences by gradient ascent algorithms. *Journal of magnetic resonance*, 172(2):296–305, 2005.

[149] David J Tannor, Vladimir Kazakov, and Vladimir Orlov. Control of photochemical branching: Novel procedures for finding optimal pulses and global upper bounds. In *Time-dependent quantum molecular dynamics*, pages 347–360. Springer, 1992.

[150] Wusheng Zhu and Herschel Rabitz. A rapid monotonically convergent iteration algorithm for quantum optimal control over the expectation value of a positive definite operator. *The Journal of Chemical Physics*, 109(2):385–391, 1998.

[151] Daniel M. Reich, Mamadou Ndong, and Christiane P. Koch. Monotonically convergent optimization in quantum control using krotov's method. *The Journal of Chemical Physics*, 136(10):104103, 2012.

[152] Christiane P Koch, José P Palao, Ronnie Kosloff, and Françoise Masnou-Seeuws. Stabilization of ultracold molecules using optimal control theory. *Physical Review A*, 70(1):013402, 2004.

[153] Davide Castaldo, Marta Rosa, and Stefano Corni. Quantum optimal control with quantum computers: A hybrid algorithm featuring machine learning optimization. *Physical Review A*, 103(2):022613, 2021.

[154] Zheng An, Hai-Jing Song, Qi-Kai He, and DL Zhou. Quantum optimal control of multilevel dissipative quantum systems with reinforcement learning. *Physical Review A*, 103(1):012404, 2021.

[155] Murphy Yuezhen Niu, Sergio Boixo, Vadim N Smelyanskiy, and Hartmut Neven. Universal quantum control through deep reinforcement learning. *npj Quantum Information*, 5(1):1–8, 2019.

[156] Ling Hu, Shu-Hao Wu, Weizhou Cai, Yuwei Ma, Xianghao Mu, Yuan Xu, Haiyan Wang, Yipu Song, Dong-Ling Deng, Chang-Ling Zou, et al. Quantum generative adversarial learning in a superconducting quantum circuit. *Science advances*, 5(1):eaav2761, 2019.

[157] Jinglei Cheng, Haoqing Deng, and Xuehai Qia. Accqoc: Accelerating quantum optimal control based pulse generation. In *2020 ACM/IEEE 47th Annual International Symposium on Computer Architecture (ISCA)*, pages 543–555. IEEE, 2020.

[158] Han Xu, Junning Li, Liqiang Liu, Yu Wang, Haidong Yuan, and Xin Wang. Generalizable control for quantum parameter estimation through reinforcement learning. *npj Quantum Information*, 5(1):1–8, 2019.

[159] Marin Bukov, Alexandre G. R. Day, Dries Sels, Phillip Weinberg, Anatoli Polkovnikov, and Pankaj Mehta. Reinforcement learning in different phases of quantum control. *Phys. Rev. X*, 8:031086, Sep 2018.

[160] Patrick Doria, Tommaso Calarco, and Simone Montangero. Optimal control technique for many-body quantum dynamics. *Phys. Rev. Lett.*, 106:190501, May 2011.

[161] Tommaso Caneva, Tommaso Calarco, and Simone Montangero. Chopped random-basis quantum optimization. *Phys. Rev. A*, 84:022326, Aug 2011.

[162] S. Lloyd and S. Montangero. Information theoretical analysis of quantum optimal control. *Phys. Rev. Lett.*, 113:010502, Jul 2014.

[163] Jeffrey C Lagarias, James A Reeds, Margaret H Wright, and Paul E Wright. Convergence properties of the nelder–mead simplex method in low dimensions. *SIAM Journal on optimization*, 9(1):112–147, 1998.

[164] Michael JD Powell. An efficient method for finding the minimum of a function of several variables without calculating derivatives. *The computer journal*, 7(2):155–162, 1964.

[165] Donghoon Lee and Matthew Wiswall. A parallel implementation of the simplex function minimization routine. *Computational Economics*, 30(2):171–187, 2007.

[166] Nicholas Metropolis, Arianna W Rosenbluth, Marshall N Rosenbluth, Augusta H Teller, and Edward Teller. Equation of state calculations by fast computing machines. *The journal of chemical physics*, 21(6):1087–1092, 1953.

[167] Shai Machnes, Elie Assémat, David Tannor, and Frank K Wilhelm. Tunable, flexible, and efficient optimization of control pulses for practical qubits. *Physical review letters*, 120(15):150401, 2018.

[168] JJWH Sørensen, MO Aranburu, Till Heinzel, and JF Sherson. Quantum optimal control in a chopped basis: Applications in control of bose-einstein condensates. *Physical Review A*, 98(2):022119, 2018.

[169] EJ Crosson and DA Lidar. Prospects for quantum enhancement with diabatic quantum annealing. *Nature Reviews Physics*, 3(7):466–489, 2021.

[170] Ahmed Omran, Harry Levine, Alexander Keesling, Giulia Semeghini, Tout T Wang, Sepehr Ebadi, Hannes Bernien, Alexander S Zibrov, Hannes Pichler, Soonwon Choi, et al. Generation and manipulation of schrödinger cat states in rydberg atom arrays. *Science*, 365(6453):570–574, 2019.

[171] W. K. Wootters. Statistical distance and hilbert space. *Phys. Rev. D*, 23:357–362, Jan 1981.

[172] Samuel L Braunstein and Carlton M Caves. Statistical distance and the geometry of quantum states. *Physical Review Letters*, 72(22):3439, 1994.

[173] Philip J. Jones and Pieter Kok. Geometric derivation of the quantum speed limit. *Phys. Rev. A*, 82:022107, Aug 2010.

[174] J Anandan and Yakir Aharonov. Geometry of quantum evolution. *Physical review letters*, 65(14):1697, 1990.

[175] Christopher Jarzynski. Geometric phases and anholonomy for a class of chaotic classical systems. *Physical review letters*, 74(10):1732, 1995.

[176] Christopher Jarzynski. Generating shortcuts to adiabaticity in quantum and classical dynamics. *Physical Review A*, 88(4):040101, 2013.

[177] Michael Kolodrubetz, Dries Sels, Pankaj Mehta, and Anatoli Polkovnikov. Geometry and non-adiabatic response in quantum and classical systems. *Physics Reports*, 697:1–87, 2017.

[178] D Lichtenberg. *Unitary symmetry and elementary particles*. Elsevier, 2012.

[179] Velimir Jurdjevic and Héctor J Sussmann. Control systems on lie groups. *Journal of Differential equations*, 12(2):313–329, 1972.

[180] Friederike Metz and Marin Bukov. Self-correcting quantum many-body control using reinforcement learning with tensor networks. *arXiv preprint arXiv:2201.11790*, 2022.

[181] Mohit Pandey. *Studies of non-equilibrium behavior of quantum many-body systems using the adiabatic eigenstate deformations*. PhD thesis, Boston University, 2021.